NSF/RA-760716

PB 274 820

THEORETICAL STUDY ON EARTHQUAKE RESPONSE OF A REINFORCED CONCRETE CHIMNEY

Prepared by

T. Y. Yang, L. C. Shiau, and Hsu Lo

School of Aeronautics and Astronautics
Purdue University
West Lafayette, Indiana

Submitted to

THE NATIONAL SCIENCE FOUNDATION

June 3, 1976

BIBLIOGRAPHIC DATA SHEET	1. Report No. NSF/RA-760716	2.	3. Recipient's Accession No.
4. Title and Subtitle Theoretical Study on Earthquake Response of a Reinforced Concrete Chimney			5. Report Date June 3, 1976 6.
7. Author(s) T. Y. Yang, L. C. Shiau, Hsu Lo			8. Performing Organization Rept. No.
9. Performing Organization Name and Address Purdue University School of Aeronautics and Astronautics West Lafayette, IN 47906			10. Project/Task/Work Unit No. 11. Contract/Grant No. GI41897
12. Sponsoring Organization Name and Address Research Applied to National Needs (RANN) National Science Foundation Washington, D.C. 20550			13. Type of Report & Period Covered 14.

15. Supplementary Notes

16. Abstracts

A detailed dynamic analysis, presented in a series of reports, was conducted on the seismic response and structural safety of key subsystems (steam generator, high pressure steam piping, coal handling equipment, cooling tower, chimney) of Unit #3 of TVA at Paradise, Kentucky in order to: (1) determine for the key components the natural frequencies below 50 Hz and the corresponding normal modes; (2) determine response of plant to seismic disturbances; (3) verify through full scale tests results obtained in (1) and determine estimates of damping needed in (2); (4) determine potential failure modes of major structural components; and (5) determine a spare parts policy for a power system so that outages due to damage from seismic disturbances are minimal. Analytical and experimental methods are used. Here, the chimney is modeled and its dynamic responses analyzed by modal superposition. Three assumed values of damping coefficients are applied to its two reinforced concrete shells, yielding data for various stress areas after application of 1940 El Centro earthquake parameters. Stress distribution around flue openings at the worst time is determined from quadrilateral sheet finite element data.

17. Key Words and Document Analysis. 17a. Descriptors

Earthquake resistant structures
Earthquakes
Earth movements
Safety
Hazard
Safety engineering
Chimneys

17b. Identifiers/Open-Ended Terms

17c. COSATI Field/Group

18. Availability Statement	19. Security Class (This Report)	21. No. of Pages
NTIS	UNCLASSIFIED	96
	20. Security Class (This Page) UNCLASSIFIED	22. Price PC A05 / MF A01

THEORETICAL STUDY ON EARTHQUAKE RESPONSE OF A REINFORCED CONCRETE CHIMNEY

By

T. Y. Yang, L. C. Shiau, and Hsu Lo

Summary Report

Prior to 1974 there has been no detailed dynamic analysis of the seismic structural response and safety of large fossil-fuel steam generating plants. In March, 1974, under NSF Grant GI41897, a detailed dynamical analysis was begun on the seismic response and structural safety of key subsystems

(steam generator,
high pressure steam piping,
coal handling equipment,
cooling tower,
chimney)

of Unit #3 of TVA at Paradise, Kentucky to accomplish the following objectives:

a) Determine for the key components the natural frequencies below 50 Hz and the corresponding normal modes.

b) Determine response of plant to seismic disturbances.

c) Verify through full scale tests, where possible, results obtained in a), and determine estimates of damping needed in b).

d) Determine potential failure modes of major structural components.

e) Determine a spare parts policy for a power system so that outage due to damage from seismic disturbances are minimal.

Analytical and experimental methods are used.

The attached Reports present what has been accomplished to date.

Before making a few summarizing remarks on the individual Reports, some comments must be made in order to provide perspective on the study.

Paradise, Unit #3 of TVA was selected for study because near-by mine operations provide excitation (due to blasting) for the plant, and TVA was willing to cooperate in the conduct of the study. It should be pointed out that this plant was not designed to resist earthquakes. However, it was felt that this disadvantage was outweighed by the experimental possibilities.

The key components selected for study are critical for operation of the plant and would cause significant outage if damaged. All components can be studied using similar types of analyses. These are the basic reasons for including in this study only the steam generator, high pressure piping, coal handling equipment, cooling tower, and chimney.

Basic data for the analyses were obtained from drawings provided by TVA and Babcock-Wilcox. In addition to these data, a number of assumptions had to be introduced into the analyses. These assumptions refer in the main to the nature of the connections among elements of known properties, the

fixity of columns, the properties of hanger elements, etc. Choices were made based on physical as well as computational reasons.

The analyses were confined to the linear range. After such a study, it is possible to assess at what level of excitation parts of the structure become nonlinear.

Structure-foundation interaction was neglected. Unit #3 of Paradise rests on excavations in limestone. It is assumed that there is little interaction. However, experimental studies will be made on this point.

It was decided at the start that all computations would be carried out with an existing computer program. SAP IV was chosen. Some program modifications have proved necessary, but these have been relatively minor. To obtain familiarity with the program it was necessary to study a number of special cases of the actual structure to ensure that it was functioning properly. For example, substructures within the steam generator support were considered seperately; assumed values of viscous damping coefficients were used in generating time histories*; etc. We found the program execution

* It should be noted that the magnitude of the response with zero damping must be interpreted with some caution as systems with slightly different frequencies can exhibit significantly different magnitudes of response.

time slow in some respects which indicates that some of its internal subroutines, such as eigen value solution, could be improved. It is beyond the scope of this project, however, to improve existing programs.

The experimental part of the study has proved much more difficult to conduct than anticipated. TVA has been most cooperative. However, the sheer physical size of the units, the weather, etc. have caused a number of difficulties that were not easy to foresee. Progress is gradually being achieved.

Interest in simple models stems from their possible use in design studies. It was decided to develop a methodology for constructing simple models. At present, our simple models are in the embryonic stage. It is hoped that after the study of two more plants a useful methodology can be obtained. Simple models developed could have been used for one component under study; however, timing made this impossible.

No recommendations will be made or conclusions drawn at this time, except in special situations. The partial examination of one plant does not provide a sufficient basis for such actions. At the completion of the study conclusions and recommendations will be presented.

A number of factors of some importance have not been considered so far. For example, the steam generator's internal elements can move with respect to it, the steam piping exerts dynamic forces on its supports, dynamic stresses in steam piping are just part of its stress system, many different seismic excitations are available, plus many more. Also a spare parts policy was not considered. As additional progress is made, we shall consider some of these problems. However, it must be recognized that it is possible to consider in this study only those factors of major importance. A spare parts policy involves economic considerations; it may not be possible to acquire the information needed to address this point.

Contact with industry in this country and Japan clearly indicates that the current detailed study is of great interest.

An Advisory Committee consisting of

Carl L. Canon	- Babcock & Wilcox Product Design Supervisor for Structural Steel and Design
William A. English	- Tennessee Valley Authority Head Civil Engineer
Clinton H. Gilkey	- Combustion Engineering, Inc. Manager, Engineering Science
Richard F. Hill	- Federal Power Commission Acting Director, Office of Energy Systems

R. Bruce Linderman	- Bechtel Power Corporation Engineering Specialist
D. P. Money	- Foster-Wheeler Corporation Supervisor of Stress Analysis
R. D. Sands	- Burns & McDonnell Chief Mechanical Engineer
Erwin P. Wollak	- Pacific Gas & Electric Company Supervisor, Civil Engineering Division

has been formed to provide a forum for an interchange of practical and conceptual views on various aspects of the study. The aim is to ensure that what is developed (in simple models) will be of practical use to industry. The Advisory Committee has met twice and reviewed plans and the progress of the investigation.

Contact is also maintained with the following firms:

Mitsubishi Heavy Industries
Babcock-Hitachi
Ishikawajima Harima Heavy Industries
Kawasaki Heavy Industries
Taiwan Power Company

The initial visit provided considerable information on the methods they have used in seismic response studies conducted by the research groups in each organization and plant experience under seismic disturbances.

Comments from the Advisory Committee and reviewers have been most helpful and encouraging. Many of the comments have been considered. However, it is not possible to take account in our studies of all points that have been brought to our attention.

Five professors, 8-10 graduate students, 2 technicians, and a secretary devoted part time to the study. A great deal of effort was devoted to acquiring information and equipment. The cooperation of TVA and Babcock-Wilcox was most helpful and deeply appreciated. Progress was excellent when it is remembered that education of students is a major function of a University.

This research project was sponsored by NSF through Grant No. GI41897.

The Reports in this series are as follows:

Dynamic Behavior of the Steam Generator and Support Structures of the 1200 MW Fossil Fuel Plant, Unit #3, Paradise, Kentucky, by T.Y. Yang, M.I. Baig, J.L. Bogdanoff.

The High Pressure Steam Pipe, by C.T. Sun, A.S. Ledger, H. Lo.

Coal Handling Equipment, by K.W. Kayser and J.A. Euler.

Theoretical Study of the Earthquake Response of the Paradise Cooling Tower, by T.Y. Yang, C.S. Gran, J.L. Bogdanoff.

Theoretical Study on Earthquake Response of a Reinforced Concrete Chimney, by T.Y. Yang, L.C. Shiau, H. Lo.

A Simple Continuum Model for Dynamic Analysis of Complex Plane Frame Structures, by C.T. Sun, H. Lo, N.C. Cheng, and J. L. Bogdanoff.

A Timoshenko Beam Model for Vibration of Plane Frames, by C.T. Sun, C.C. Chen, J.L. Bogdanoff, and H. Lo.

ABSTRACT

The 822 feet tall chimney is modeled using Bernoulli-Euler beam finite elements and its dynamic responses are analyzed using the method of modal superposition. The chimney includes two reinforced concrete shells, each with a pair of flue openings. Three assumed values of damping coefficients are considered. Results include time history plots of tip deflections, spacings between the two shells, bending moments, and shearing forces at the base, etc. of the responses from the horizontal and vertical components of El Centro 1940 earthquake. The diagrams for the distributions of moment, shear, and deflection at several instants are shown. The stress distributions around the openings due to the combined effects of axial force, shearing force, and bending moments at the worst time are found by using quadrilateral shell finite elements.

Introduction

The chimney of the TVA Steam Generating Power Plant, Unit 3, at Paradise, Kentucky is studied. The 832 feet tall chimney includes two reinforced concrete shells with a 4-1/2 feet minimum air space. The chimney is analyzed with the use of eight pipe-type finite elements formulated on the basis of Bernoulli-Euler assumptions. The stiffness coefficients for the particular element that includes the flue openings are obtained by the use of quadrilateral shell finite elements.

Natural frequencies for the inner and outer shells both with and without flue openings are found. The frequencies are then used to find the time-history responses due to the north-south horizontal as well as the vertical components of the El Centro earthquake for the first 30 seconds. The method of modal superposition is used. Six flexural modes

are used for the horizontal earthquake input and two vertical modes are used for the vertical input. The 30 seconds are divided into 1500 time steps. Several assumed values of damping coefficients are included in the analysis.

The results are represented by time history plots of the maximum deflection (at the top) and the maximum bending moment and shearing force (at the base). The time-history plots of the variation of the spacing between the outer and inner shells at the top is given. The effects of damping are shown by plots of tip deflections, base shearing force, and base bending moment versus the value of damping coefficient, respectively. The diagrams for the distributions of deflection, bending moment, and shearing force along the chimney at several instants are presented. The stress concentrations around the flue openings due to the combination of axial and shearing forces and bending moment at the worst time are found by the use of quadrilateral shell elements and represented in the form of contour plots of surface stresses.

Description of the System

The chimney is composed of two slender cylindrical reinforced concrete shells as shown in Fig. 1. The inner shell serves as a liner and has 2" fiber glass insulation on its outer surface. The inner shell also has a stainless steel cap at the top covering the gap between the inner and outer shells. However, there is no significant structural connection between them. There is a 4'-6" minimum air space between the two shells.

The top surface of the chimney foundation is at elevation 390 feet. The earth fill extends to the elevation of 422 feet. The height of the chimney is 832 feet above the foundation. The outer diameter for the outer shell varies from 71.8 feet at the base to 38.5 feet at the top.

The thicknesses for the two shells also vary with their maximum values around the flue openings.

Each of the two shells has a pair of side flue openings. They are rectangular in shape with dimensions of 28 feet by 14 feet. The base lines of the openings are 73.5 feet above the base. The circumferential distance between the center lines of the two openings is 50.0 feet for the outer shell and 38.0 feet for the inner shell. Each opening at the inner shell is connected to the opening at the outer shell by steel framed flue duct. The concrete around the openings are heavily reinforced.

Finite Elements

Two types of finite element are used for the analysis of the chimney: the beam element and the plate element.

The finite element used in the analysis of the gross chimney behavior is a three-dimensional beam finite element with constant hollow circular cross section. The element has six degrees of freedom at each node: three displacements in the three Cartesian coordinate directions and three rotations about the three axes. The Bernoulli-Euler assumptions for beam are used in the derivation of the stiffness matrix. The mass matrix is based on the lumped masses. Since the element is assumed to have constant cross section, this element can only provide a step representation of the tapered chimney.

For the local analysis of the chimney, a three-dimensional quadrilateral plate finite element is used. The element is composed of four triangular elements with the four common vertices met at near the centroid of the quadrilateral. Each triangular element is a superimposed version of a constant membrane strain element (Ref. 1) and an HCT

flexural plate element (Ref. 2).

The three-dimensional quadrilateral plate elements serve for two functions. They are first used to model the particular chimney beam finite element that has two flue openings so that the 12 influence stiffness coefficients for an equivalent homogeneous beam element can be found. After the end displacement and force vectors for each chimney beam element are found in the dynamic response analysis, the plate elements are used to find the detail distributions of stresses within the element, especially around the openings.

Assumptions

The following basic assumptions underlie this study:

(a) The base of the chimney is fixed against rotation and lateral displacement. The chimney foundation is buried into the excavated limestone rock.

(b) The base circles of the two shells have no relative movement during earthquake. The two shells are unconnected elsewhere.

(c) The Bernoulli-Euler beam theory is used. No shear deformation and rotatory inertia are considered.

(d) Thermal effect and wind effect are not considered in this study.

(e) The behavior of the chimney is linearly elastic.

Results and Discussions

As described previously, both inner and outer shells have two 28x14 square feet flue openings at 36.1 feet above the ground. It is of interest to know how these openings affect the dynamic behaviors of the two shells. For this reason, most of the present analyses are performed for

both cases--with and without the flue openings.

(1) Free Vibration Analysis Without Damping

Free vibration analysis is first performed for the outer shell without the effect of flue openings. To find out how many beam finite elements are sufficient to model the chimney, four different kinds of modeling are used: 4, 8, 12, and 16 elements, respectively. For each mode, the frequency ratio (the frequency value obtained by using n elements divided by the one obtained by using 16 elements) is plotted against the number of elements (n) as shown in Fig. 2. It is seen that the eight element modeling gives approximately 1.2, 1.8, 3.8, and 5.2 percent discrepancies as compared to the 16 element solutions for the first, second, third, and fourth modes, respectively. It appears that the eight element model is sufficiently accurate for the purpose of the present dynamic response analysis. It is thus determined to use eight elements to model both the outer and inner shells, with and without flue openings. The modeling is shown in Fig. 3.

For the case with flue openings, the first beam element in Fig. 3 must be modified to an equivalent homogeneous beam finite element. This is done by first modeling the element by 70 quadrilateral plate finite elements and then finding the equivalent axial area and moments of inertia for the equivalent beam element. This is a rather laborious process.

The results for the first 12 natural frequencies and periods are shown in Table 1 for the outer shell and in Table 2 for the inner shell. It is seen in both tables that the flue openings have little effect on the values of frequencies. It is noted that for the outer shell, the 5th, 8th, and 11th modes are longitudinal modes while the others are

flexural modes. For the inner shell, the longitudinal modes appear at 5th, 9th, and 11th modes.

To validate the present assumptions and method, the frequency values obtained must be evaluated. This is one of the purposes for which an experimental program is conducted in this research project. In the experiment, accelerometer assemblies are installed on the foundation and three upper levels of the outer shell to measure accelerations in the three space coordinate directions. The set up includes nine units, 17 transducers, and 14 data recording channels. Primary excitation is due to wind and blasting of a nearby coal mine. The experimental results are given in a separate report by K. W. Kayser who conducted the experiment. Three natural frequencies have been found so far and the comparison is given in Table 2. The agreement strongly supports that the present assumptions and method are sound.

The results for the first, second, and third mode shapes are plotted in Fig. 4. The fourth, fifth, and sixth mode shapes are plotted in Fig. 5.

(2) Response to the Horizontal Component of an Earthquake.

The record of El Centro earthquake occurred on May 18, 1940 is selected to analyze the time-history dynamic response of the chimney. The south-north horizontal component of the acceleration record is shown in Fig. 6. Since the magnitude of acceleration becomes considerably smaller after 30 seconds, only 30 seconds are considered here. The record in Fig. 6 shows that the acceleration oscillates at the frequency of approximately 3 to 7 cycles per second. The results in Tables 1 and 2 for natural frequencies show that the seventh frequency (sixth flexural

frequency) is approximately 9.25 Hertz for outer shell and 8 Hertz for the inner shell, respectively. Thus the first six flexural modes are used in the modal superposition to simulate the dynamic response of the chimney to the horizontal component of this earthquake.

The time interval for the modal analysis is set as 0.02 seconds which corresponds to 50 time points for each second and 1500 points for the 30 second period. The central processing time required by a CDC 6500 computer with the use of eight elements, six flexural modes, and 1500 time points is approximately 25 seconds. In this entire analysis, the results for the time history response are plotted by the computer with the time interval of 0.05 seconds. This means that each subsequent time history curve is connected among 600 points in the 30 second period.

i. Outer and inner shell with no flue opening.

The time history response for the deflection at the tip of the outer shell (with the assumption of no flue opening) is shown in Fig. 7. The maximum tip deflection is seen to be 47.7 inches at 26.6 seconds. The late arrival of the maximum tip deflection suggests the possibility of occurrence of an even larger tip deflection at after 30 seconds. The results for the bending moment and shearing force at the base are shown in Figs. 8 and 9, respectively. The maximum bending moment occurs at the time of 13.8 seconds with magnitude of 44.7×10^6 in-kips. If the concrete is assumed not to crack under tensile stress, this bending moment produces a maximum compressive stress of 4147 psi in concrete and a maximum tensile stress of 33.2 ksi in reinforced bar. If, however, the concrete is assumed to be incapable of carrying tensile stress, the maximum compressive stress in concrete becomes 16.53 ksi and the

maximum tensile stress in steel becomes 136 ksi. The maximum shearing force occurs at the time of 26.95 seconds with magnitude of 17.08×10^6 pounds. This results in a maximum shearing stress of 667.6 psi in the concrete.

After the outer shell with the assumption of no flue opening has been studied, the inner shell with no flue opening is investigated. The results for the time history responses of tip deflection,base bending moment, and base shearing force are shown in Figs. 10, 11, and 12, respectively. It is seen that the magnitudes in Figs. 10-12 for the inner shell are considerably smaller than those shown in Figs. 7-9 for the outer shell. The maximum tip deflection is seen to be -24.85 inches at 28.8 seconds. The maximum bending moment occurs at the time of 18.3 seconds with magnitudes of 10.15×10^6 in-kips. If the concrete is assumed not to crack under tensile stress, such bending moment produces a maximum compressive stress of 2220 psi in concrete and a maximum tensile stress of 17.8 ksi in reinforced bar. If, however, the concrete is assumed as incapable of carrying tensile stress, the maximum compressive stress in concrete becomes 8730 psi and the maximum tensile stress in reinforced bar becomes 72.5 ksi. The maximum shearing force occurs at the time of 18.3 seconds with magnitude of 4.75×10^6 pounds. This corresponds to a maximum shearing stress of 365.7 psi in concrete.

In view of the large magnitudes of deflection at the top of both outer and inner shells (with no flue openings), it is desirable to find how do the two shells approach each other at the top during a simultaneous response to the subject earthquake. The results for the tip deflections obtained in Figs. 7 and 10 are compared from point to point (for 600 points)

and the net differences are plotted in Fig. 13. It is noted that the minimum air space between the two shells is designed as 54 inches. Fig. 13 shows that the tip spacings are everywhere greater than zero. It is interesting to see that the spacings are quite close to zero at the time of 14.2 seconds and 21.7 seconds.

ii. Outer and Inner Shell with Flue Openings

As described earlier in the section of Description of the System, each shell has two openings. Their effect must be accounted for by modifying the stiffness and mass matrices of the first beam finite element that contains the openings. The equivalent homogeneous stiffness properties are obtained by first modeling the first beam finite element by 70 quadrilateral shell finite elements and then finding the influence stiffness coefficients through applying unit value of each degree of freedom at each nodal point of the equivalent element. The process is straightforward but laborious. The effect of the openings on the lumped mass matrix of the equivalent beam element is accounted for by simply neglecting the masses due to the cut-outs.

For the equivalent beam element, the bending rigidity is not the same in every direction. The weakest direction is along the diameter that passes through the midpoint between the centers of the two openings. The strongest direction is perpendicular to the weakest direction. In this study, the earthquake acceleration is assumed to move in the weakest direction of the chimney.

The time history responses for the tip deflection, base bending moment, and base shearing force for the outer shell with two flue openings are shown in Figs. 14-16, respectively. When comparing Fig. 14 with

Fig. 7, it is seen that the tip deflections for the outer shell with no opening are generally slightly larger than those for the outer shell with two openings. When comparing Figs. 15-16 with Figs. 8-9, it is seen that the magnitudes of bending moment and shearing force at the base for the outer shell with no openings are generally noticeably larger than those for the outer shell with no opening. Although the cut-outs decrease the stiffness of the first finite element, they decrease the mass too. It is interesting to see that the openings affect the gross dynamic behavior of the chimney noticeably.

The time history responses for the tip deflection, the base bending moment, and the base shearing force for the inner shell with two flue openings are shown in Figs. 17-19, respectively. The three sets of curves are almost identical to the ones for the inner shell with no opening. The effect of openings is thus seen to be insignificant.

The time history of the net differences in tip deflection between the inner and outer shells with openings is shown in Fig. 20. The results are quite similar to those for the shells with no opening.

The distributions of deflection, bending moment, and shearing force for the outer shell with openings are plotted in Figs. 21-23, respectively, at three different instances. The instances are chosen at 22.5 seconds when the maximum base shearing force occurs, 25.2 seconds when the maximum base bending moment occurs, and 28.3 seconds when the maximum tip deflection occurs. The distributions of deflection, bending moment, and shearing force for the inner shell with openings are plotted in Figs. 24-26, respectively, at three instances. The instances are chosen at 26.5, 28.8, and 29.9 seconds when the maximum base shearing force, maximum base bending moment, and maximum tip deflection occur, respectively.

For both shells, it is seen that the maximum base shearing force occurs first, the maximum base bending moment second, and the maximum tip deflection last.

(3) Damping Effect on Responses to Horizontal Component of Earthquake.

The effect of viscous damping is considered in this study. It is assumed that each of the six flexural modes has the same damping coefficient. When including the damping effect, only shells with flue openings are considered. Three different values of viscous damping coefficient are assumed: 4 percent, 7 percent and 10 percent of its critical value.

The time history responses for the tip deflection, base bending moment, and base shearing force for the outer shell with the three different damping coefficients are shown in Figs. 27-35. Similar presentations for the results for the inner shell are given in Fig. 36-44. It is seen that all the physical quantities reduce progressively as the damping coefficient increases.

The time history response for the spacing between the top of the two shells is shown in Figs. 45, 46, and 47 for the damping coefficient equal to 4 percent, 7 percent, and 10 percent of its critical value, respectively. It is seen that when the damping is included, the tops of the two chimneys are quite far apart at all times.

The effect of damping on the tip deflection, base bending moment, and base shearing force for both shells is summarized by the plots shown in Figs. 48, 49, and 50, respectively. It is seen that at 4 percent of critical damping the tip deflection, base bending moment, and base shearing force all reduce by more than 50 percent of their original undamped values. The further increase in damping coefficient does not seem to

decrease much the three physical quantities. Figs. 48-50 serve to provide a basis for interpolating the effect of damping for any given coefficient value.

(4) Response to the Vertical Component of an Earthquake.

The vertical component of the acceleration record of El Centro earthquake is shown in Fig. 51. Only 30 seconds of the record are considered simply because the acceleration nearly vanishes after then. The time interval of 0.02 seconds is used in the present modal analysis. The outputs of time history response are plotted at a time interval of 0.05 seconds.

The first three natural frequencies of vertical modes are given in Tables 1 and 2 as approximately 5.0, 10.5, and 17.4 Hertz for the outer shell and 4.5, 11.3, and 17.7 Hertz for the inner shell, respectively. Since the vertical component of the acceleration oscillates at the frequency of around 8 to 9 Hertz, it is felt that two vertical modes may be sufficient to simulate the response behaviors. Thus two modes are used.

The time history responses for the tip axial displacement and the base axial force for the outer shell with no openings are shown in Figs. 52 and 53, respectively. The magnitudes of both tip displacement and base axial force decrease after 15 seconds. The time history responses for the tip axial displacement and base axial force for the inner shell with no opening are shown in Figs. 54 and 55, respectively. Unlike in the case of outer shell, the magnitudes for the tip axial displacement and base axial force for the inner shell remain quite constant during the entire 30 second period.

For the case of outer shell with two flue openings, the results for tip axial displacement and base axial force are shown in Figs. 56 and 57,

respectively. The variations of tip axial displacement and base axial force are seen to be more steady in the case of shell with openings than in the case of shell without opening. For the case of inner shell with two flue openings, the results for tip axial displacement and base axial force are shown in Figs. 58 and 59, respectively. Both the tip displacement and the base axial force are seen to decrease slowly but steadily with increasing time.

(5) Stress Concentration Around Flue Openings.

The stress concentrations in the region around the two flue openings in each shell are studied by performing local analysis of the first beam finite element of each shell. The first beam finite element is modeled by 244 quadrilateral shell finite elements. Both ends are subjected to the simultaneous actions of bending moment, shearing force and axial force caused by both the horizontal and vertical components of the earthquake. An inspection of the results given in Figs. 15, 16, and 57 finds that for the outer shell the most critical time is at 25.2 seconds when the base bending moment = 32.05×10^6 in-kips; the base shearing force = 11,810 kips; and the base axial force = 217.7 kips. The results of the local analysis is shown in Fig. 60 by a contour plot of axial stress in the outer surface of the outer shell. Because of symmetry, only one half of the shell segment with one opening is shown. The iso-stress curves varies from -2500 psi to zero and then to 3000 psi along the circumference at the base. Such distribution shows the dominant effect of a bending moment. The stress concentrations due to the openings are clearly presented in the figure.

For the inner shell, the most critical time appears to be at 28.8

seconds when the base bending moment = 11.28×10^6 in-kips (see Fig. 18); the base shearing force = 4,557 kips (see Fig. 19); and the base axial force = 150.5 kips (see Fig. 59). The contour plots of the resulting axial stresses in the outer surface of the inner shell are shown in Fig. 61. The stress concentration around the opening and the dominant bending effect at the base are clearly seen. The patterns of stress distribution for both shells are quite similar.

Concluding Remarks

The south-north horizontal and vertical components of the El Centro earthquake are used to perform the time history response analyses of the subject chimney. The two 30-second acceleration records are each broken down into 1500 time points with a time interval of 0.02 seconds. The results are all plotted for 30 seconds by 600 time points with a time interval of 0.05 seconds.

A thorough investigation of many aspects of the dynamic responses of the subject chimney is carried out and the results are presented in over 50 figures. Besides providing the comprehensive information about the dynamic behaviors of the chimney, this study also suggests the following conclusions.

(1) A full scale experiment shows that the free vibration analysis based on the present method and assumptions is valid.

(2) The effect of the flue openings appears to reduce the magnitudes of tip deflection, base bending moment and base shear (see Figs. 7-9 and 14-16).

(3) The damping coefficient with 4 percent of its critical value reduces the maximum deflection, shearing force, and bending moment by more than 50 percent of their undamped values. The

effect due to the increase in damping beyond this value is, however, no longer so pronounced.

(4) The stress distribution in the chimney is dominated by the bending action. The effect due to vertical component of the El Centro earthquake is little.

(5) For the present design, the two shells do not collide with each other under the El Centro earthquake.

References

[1] Clough, R. W., "The Finite Element in Plane Stress Analysis," Proceedings of the 2nd ASCE Conference on Electronic Computation, Pittsburgh, Pa., Sept. 1960.

[2] Clough, R. W. and Tocher, J. L., "Finite Element Stiffness Matrices for the Analysis of Plate Bending," Proceedings of the First Conference on Matrix Methods in Structural Mechanics, Air Force Flight Dynamics Lab., TR-66-80, Dayton, Ohio, 1965.

Table 1. The Natural Frequencies and Periods for the Outer Shell With or Without Flue Openings.

Mode Number	Without Opening		With Openings	
	Frequency (rad./sec.)	Period (Seconds)	Frequency (rad./sec.)	Period (Seconds
1	2.003	3.1371	1.969	3.1911
2	7.149	0.8789	7.009	0.8965
3	16.775	0.3746	16.573	0.3791
4	29.184	0.2153	29.015	0.2166
5*	31.846	0.1973	31.387	0.2002
6	43.475	0.1445	43.430	0.1447
7	58.063	0.1082	58.119	0.1081
8*	66.298	0.0948	65.275	0.0963
9	71.364	0.0881	71.436	0.0880
10	81.740	0.0769	81.811	0.0768
11*	109.990	0.0571	109.300	0.0575
12	145.550	0.0432	145.750	0.0431

* Longitudinal modes

Table 2. The Natural Frequencies and Periods for the Inner Shell With or Without Flue Openings.

Mode	Without Opening		With Openings	
Number	Frequency (rad./sec.)	Period (Seconds)	Frequency (rad./sec.)	Period (Seconds)
1	1.296	4.8491	1.277	4.9223
2	5.719	1.0987	5.615	1.1190
3	13.766	0.4564	13.572	0.4629
4	24.477	0.2567	24.319	0.2584
5*	28.407	0.2212	28.034	0.2241
6	36.987	0.1699	36.975	0.1699
7	50.161	0.1253	50.252	0.1250
8	61.890	0.1015	61.980	0.1014
9*	71.445	0.0879	70.369	0.0893
10	72.901	0.0862	72.996	0.0861
11*	111.660	0.0563	110.860	0.0567
12	148.600	0.0423	148.850	0.0422

* Longitudinal modes

Table 3. Comparison of the First Three Natural Frequencies for the Outer Shell With Two Flue Openings.

Mode Number	First (rad./sec.)	Second (rad./sec.)	Third (rad./sec.)
8-finite element solution	1.969	7.009	16.573
Full Scale Experiment*	1.82	6.35	15.1

* Details are given in a separate report by K. W. Kayser.

Figure Captions

Fig. 1. Description of the Chimney in the TVA Steam Generating Power Plant at Paradise, Kentucky.

Fig. 2. The Convergence Evaluation for the First Four Natural Frequencies Obtained by Different Modelings for the Chimney Outer Shell.

Fig. 3 The Eight-Element Modeling of the Chimney.

Fig. 4. The First, Second, and Third Mode Shapes for the Chimney Outer Shell.

Fig. 5. The Fourth, Fifth, and Sixth Mode Shapes for the Chimney Outer Shell.

Fig. 6. The Record of the South-North Acceleration Component of the El Centro Earthquake on May 18, 1940.

Fig. 7. Tip Deflection vs. Time Curve for Outer Shell Without Opening.

Fig. 8. Bending Moment at the Base vs. Time Curve for Outer Shell Without Opening.

Fig. 9. Shearing Force at the Base vs. Time Curve for Outer Shell Without Opening.

Fig. 10. Tip Deflection vs. Time Curve for Inner Shell Without Opening.

Fig. 11. Bending Moment at the Base vs. Time Curve for Inner Shell Without Opening.

Fig. 12. Shearing Force at the Base vs. Time Curve for Inner Shell Without Opening.

Fig. 13. Time History Curve for the Spacing Between the Tops of Outer and Inner Shells, Both Without Openings.

Fig. 14. Tip Deflection vs. Time Curve for Outer Shell with Two Openings.

Fig. 15. Bending Moment at the Base vs. Time Curve for Outer Shell with Two Openings.

Fig. 57. Axial Force at Base vs. Time Curve for Outer Shell with Two Openings.

Fig. 58. Vertical Tip Displacement vs. Time Curve for Inner Shell with Two Openings.

Fig. 59. Axial Force at Base vs. Time Curve for Inner Shell with Two Openings.

Fig. 60. Contour Plot of the Axial Stress (ksi) in the Outer Surface of the Outer Shell Around one Flue Opening at the Most Critical Time (25.2 Seconds) with Bending Moment = 32.048×10^9 in-lbs; Shearing Force = 11.81×10^6 lbs; and Axial Compression = 21.77×10^4 lbs at the Base.

Fig. 61. Contour Plot of the Axial Stress (ksi) in the Outer Surface of the Inner Shell Around One Flue Opening at the Most Critical Time (28.8 Seconds) with Bending Moment = 11.28×10^9 in-lbs; Shearing Force = 45.57×10^5 lbs; and Axial Tension = 15.05×10^4 lbs at the Base.

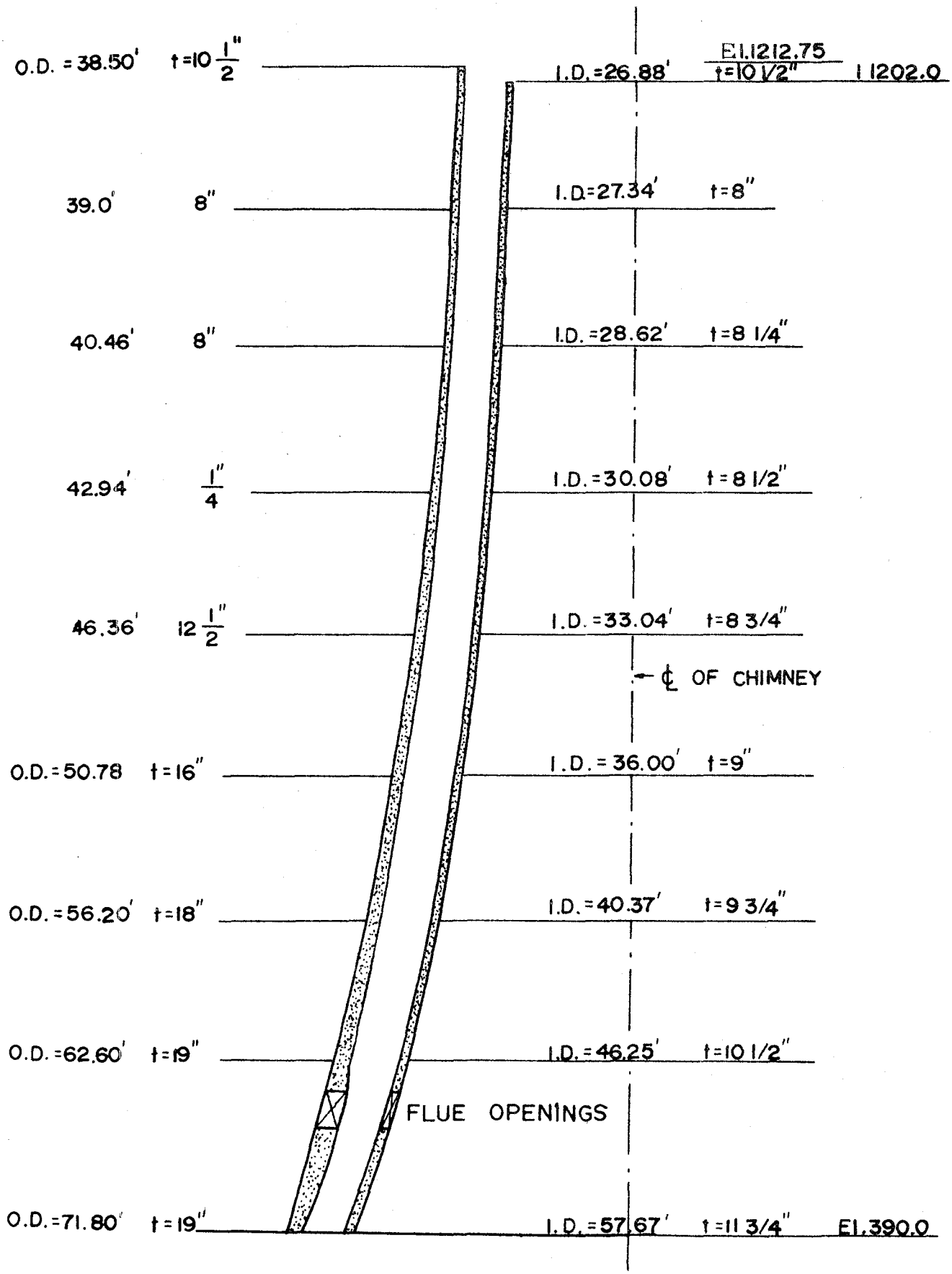

Fig. 1. Description of the Chimney in the TVA Steam Generating Power Plant at Paradise, Kentucky. (Not drawn to scale)

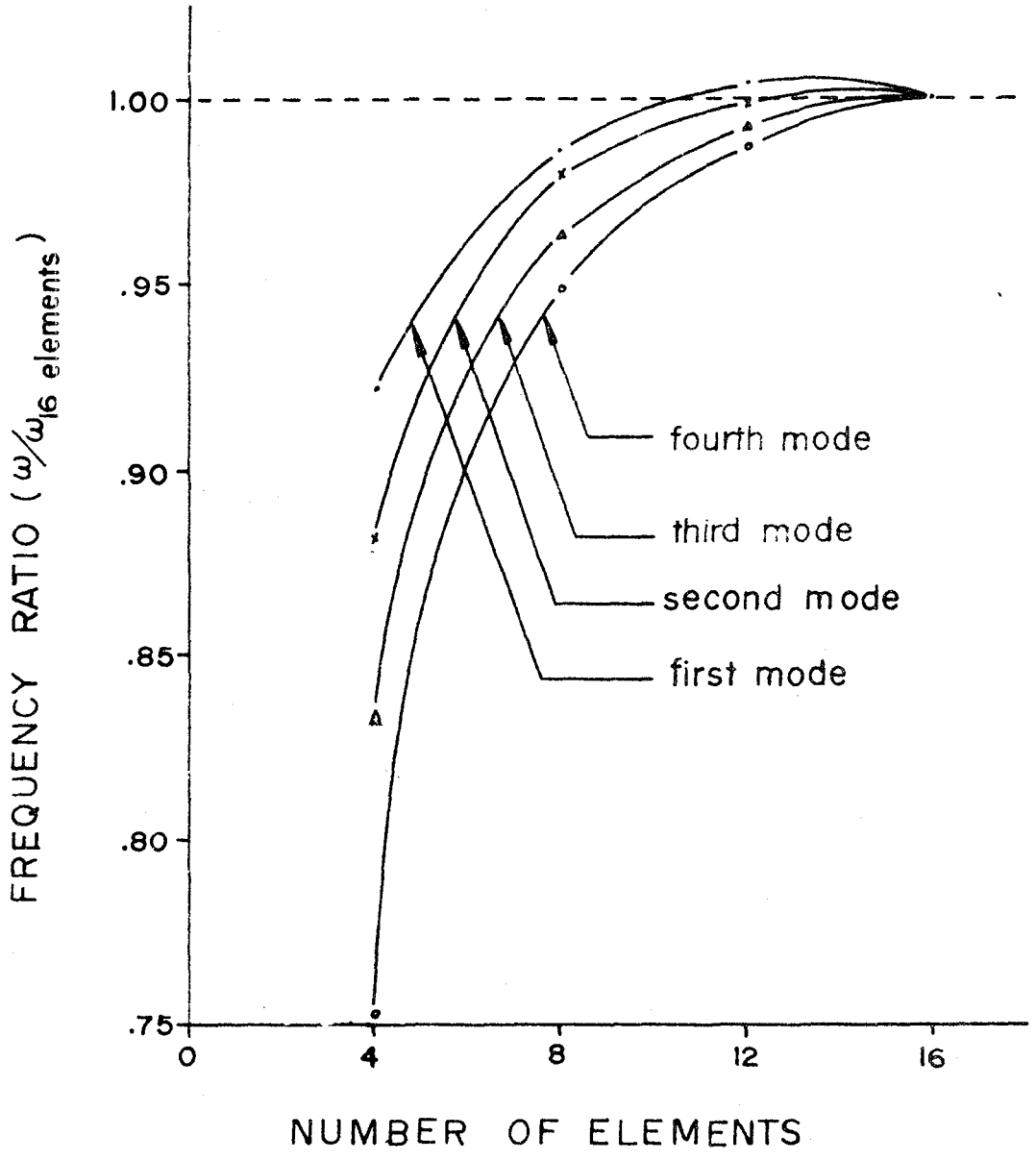

Fig. 2. The Convergence Evaluation for the First Four Natural Frequencies Obtained by Different Modelings for the Chimney Outer Shell.

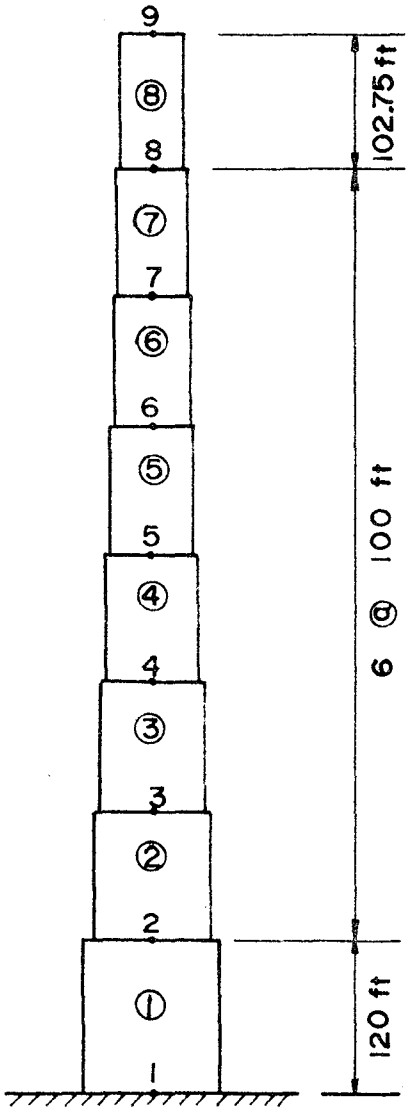

Fig. 3. The Eight-Element Modeling of the Chimney.

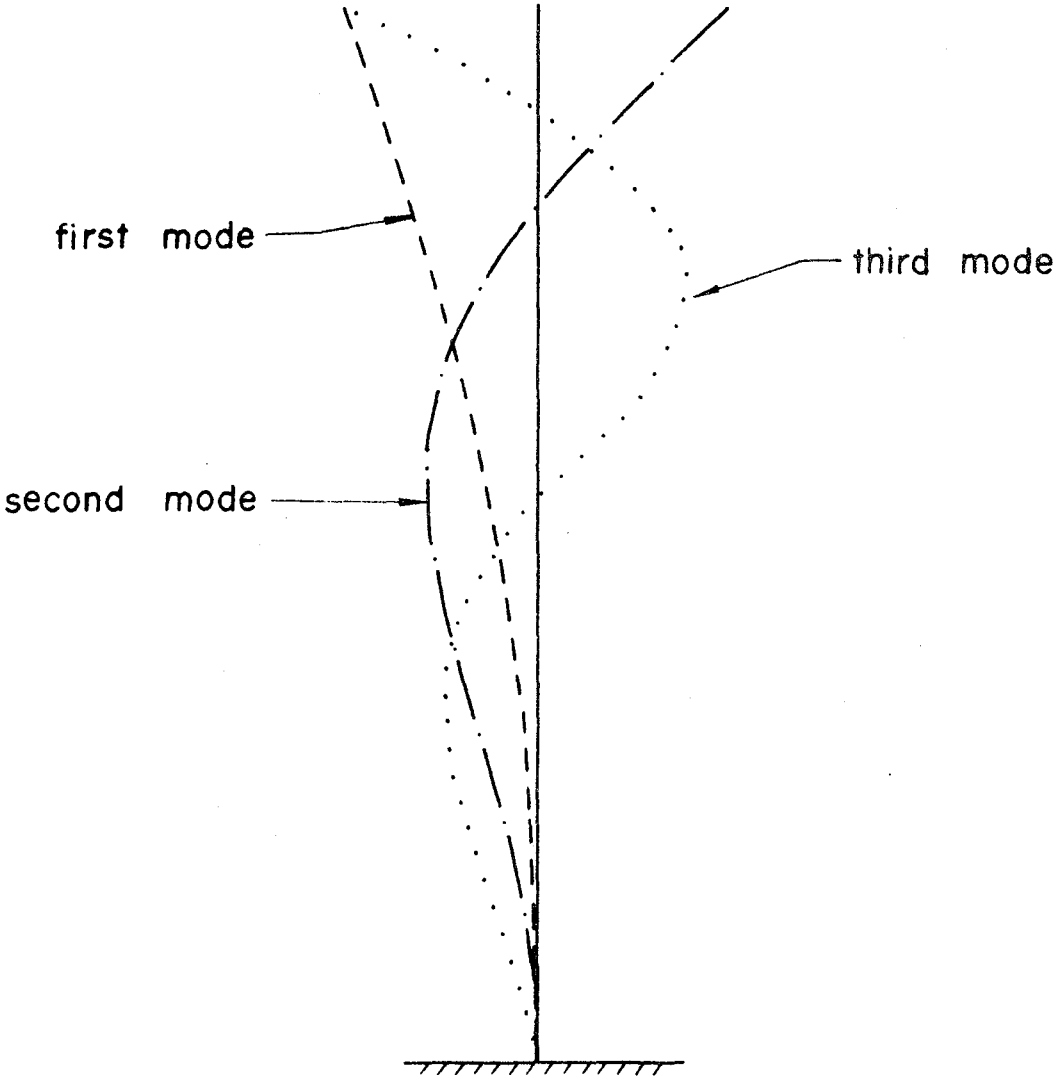

Fig. 4. The First, Second, and Third Mode Shapes for the Chimney Outer Shell.

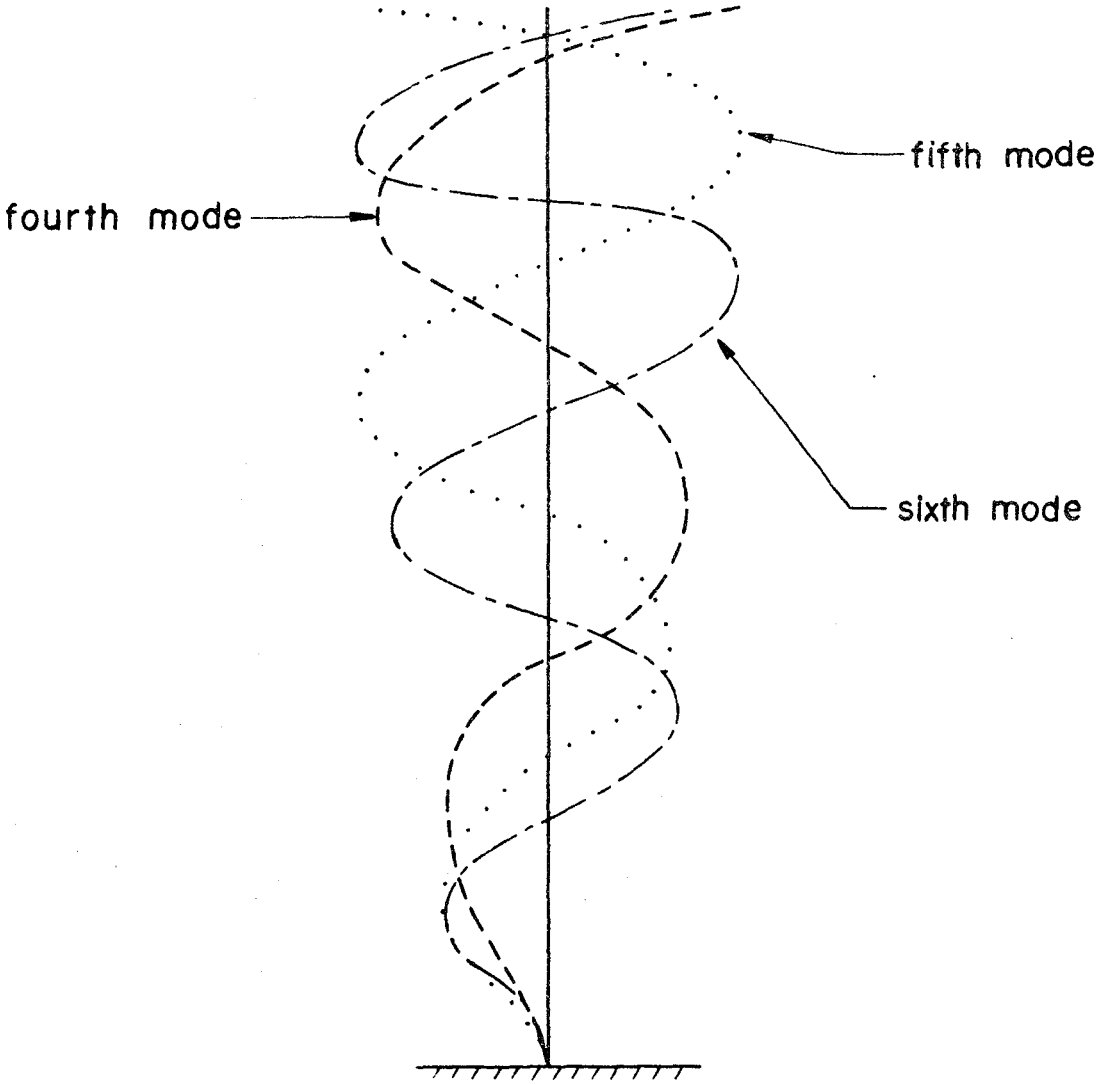

Fig. 5. The Fourth, Fifth, and Sixth Mode Shapes for the Chimney Outer Shell.

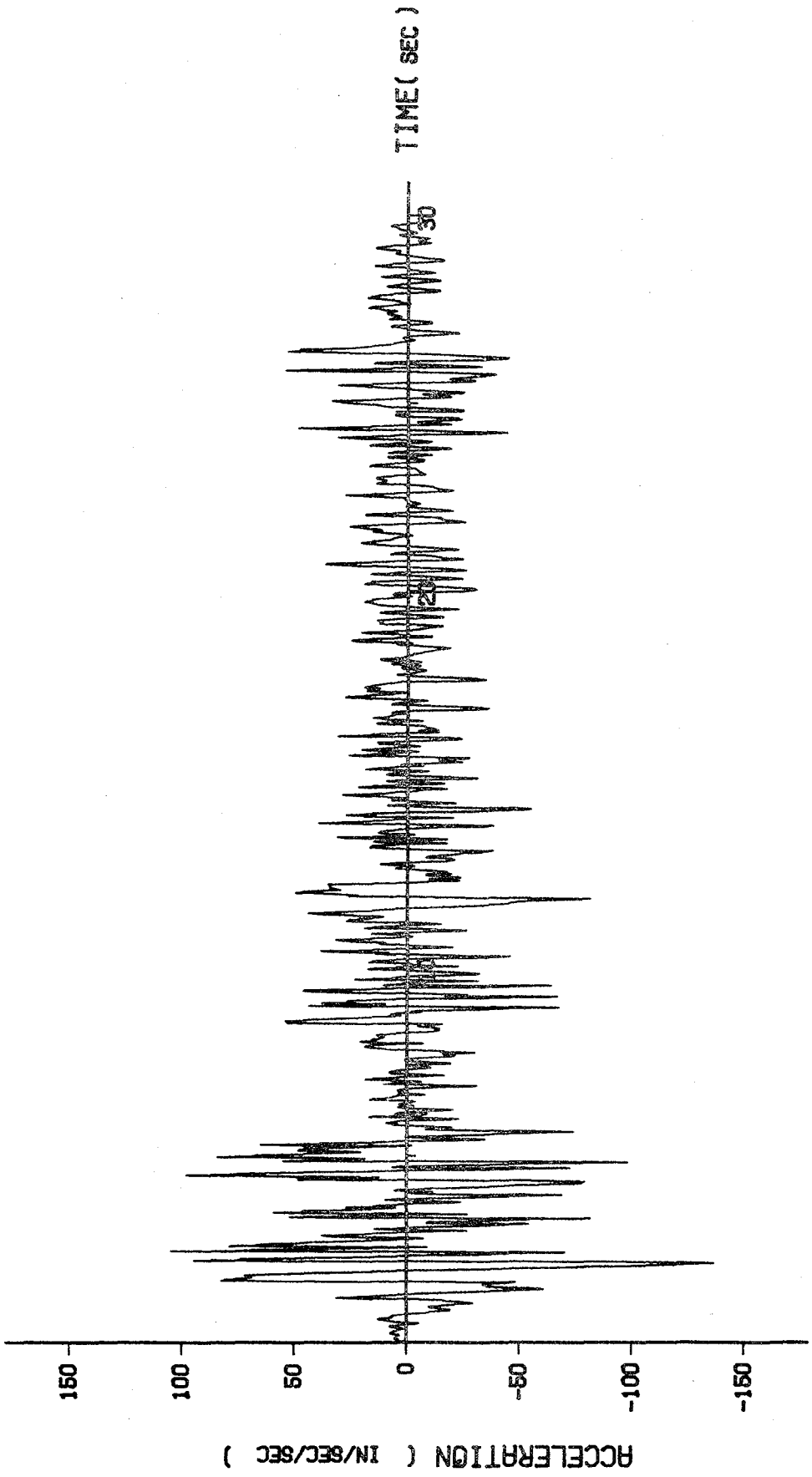

Fig. 6. The Record of the South-North Acceleration Component of the El Centro Earthquake on May 18, 1940.

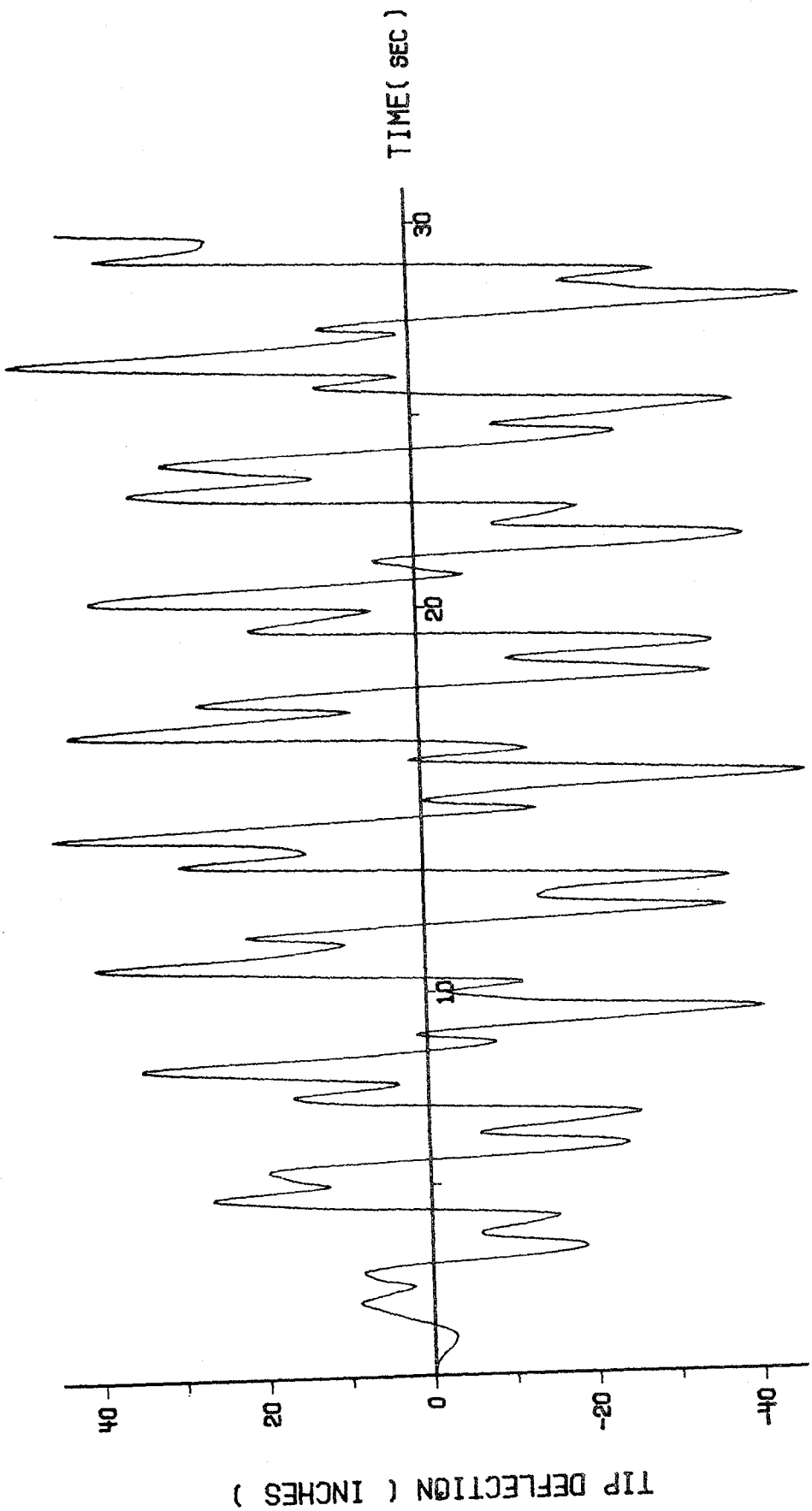

Fig. 7. Tip Deflection vs. Time Curve for Outer Shell Without Opening. (No Damp)

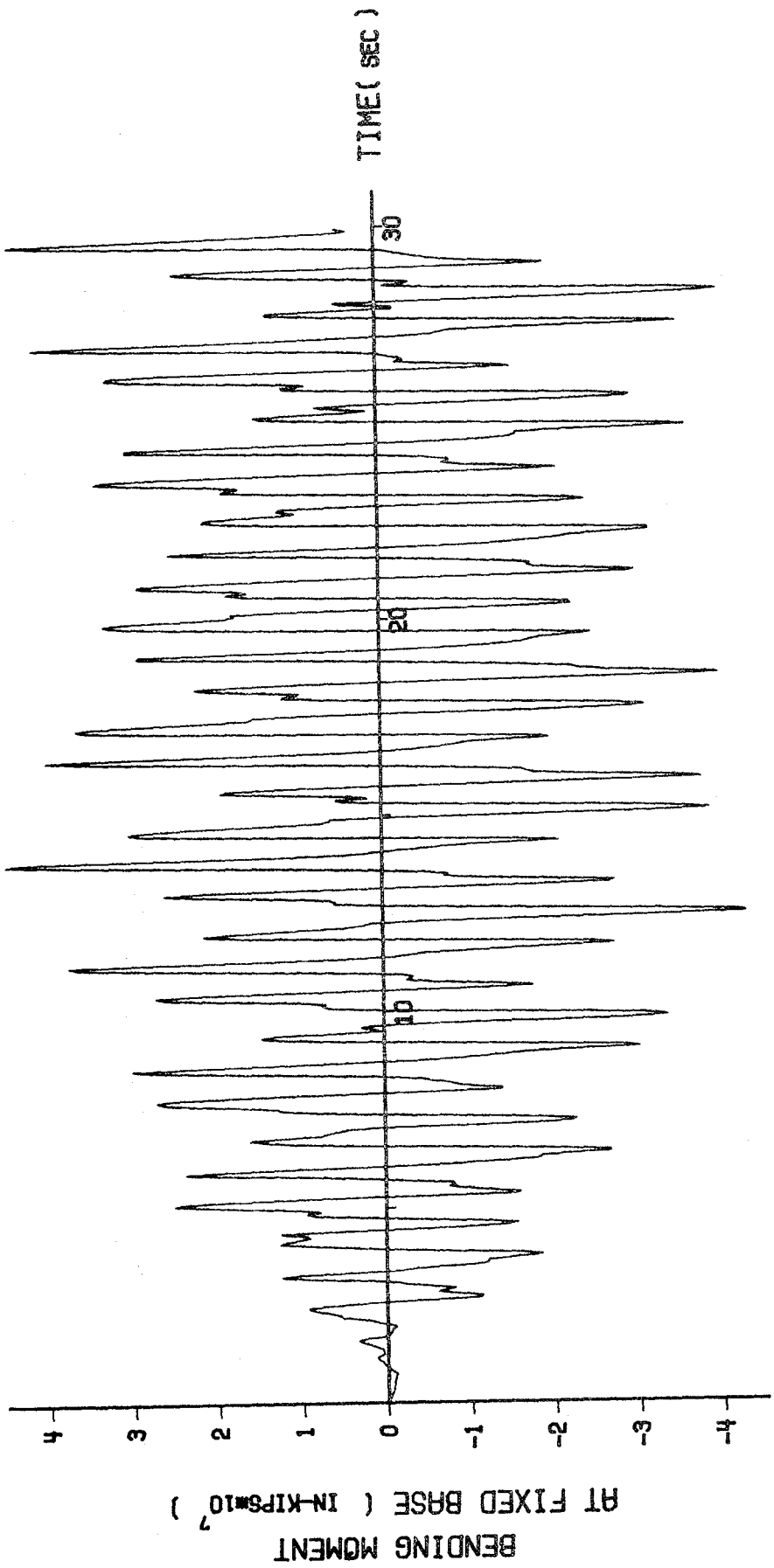

Fig. 8. Bending Moment at the Base vs. Time Curve for Outer Shell Without Opening.

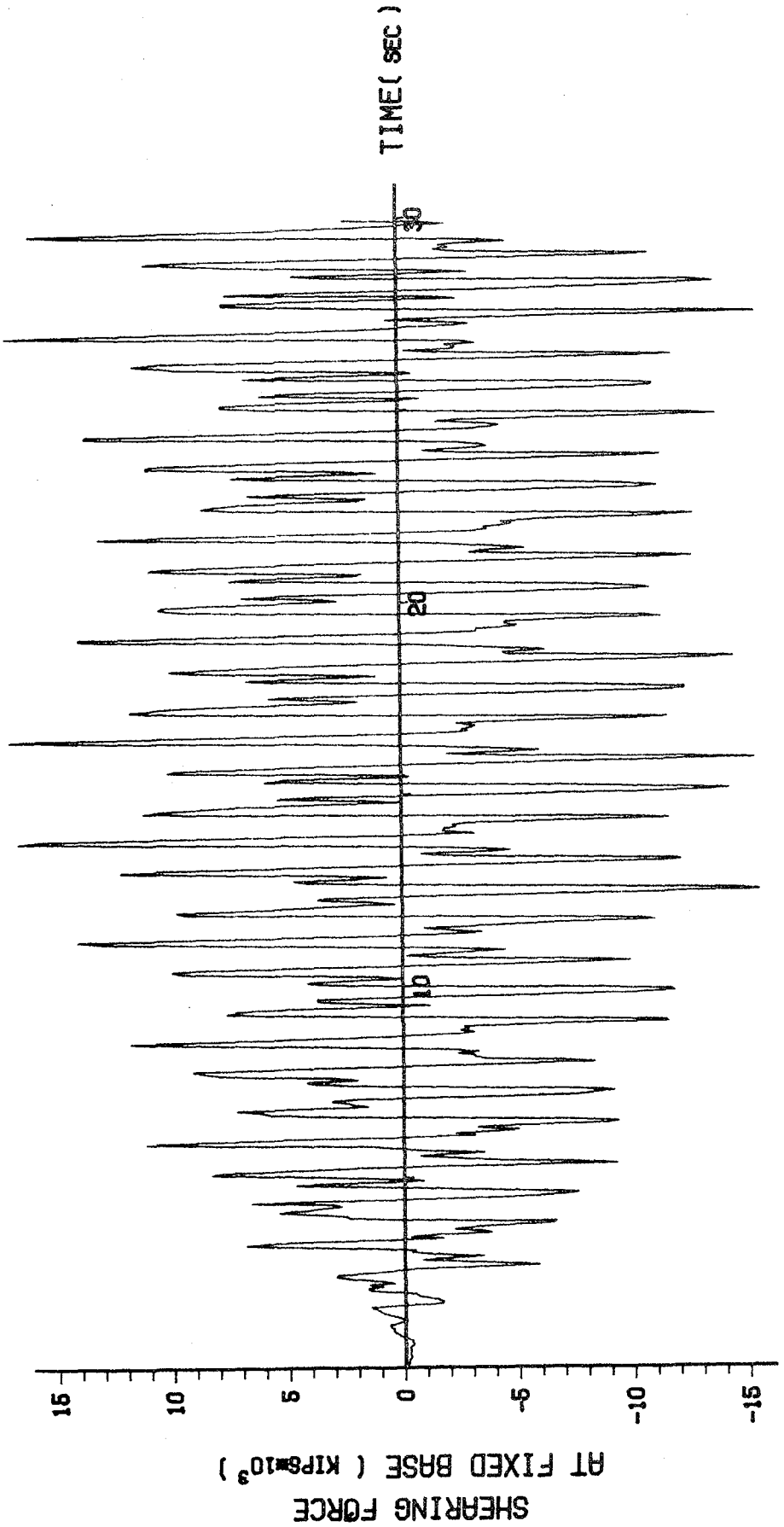

Fig. 9. Shearing Force at the Base vs. Time Curve for Outer Shell Without Opening.

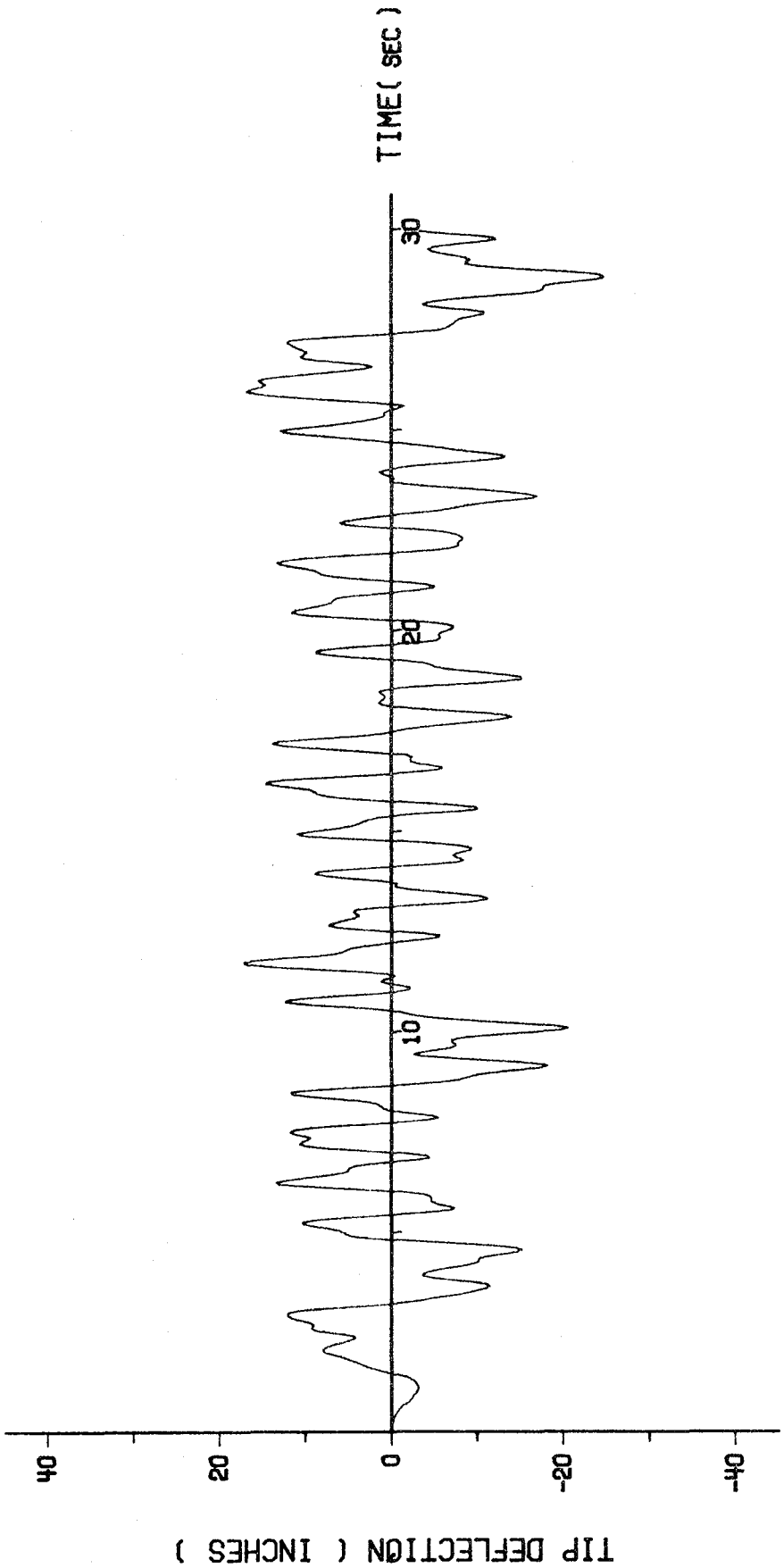

Fig. 10. Tip Deflection vs. Time Curve for Inner Shell Without Opening.

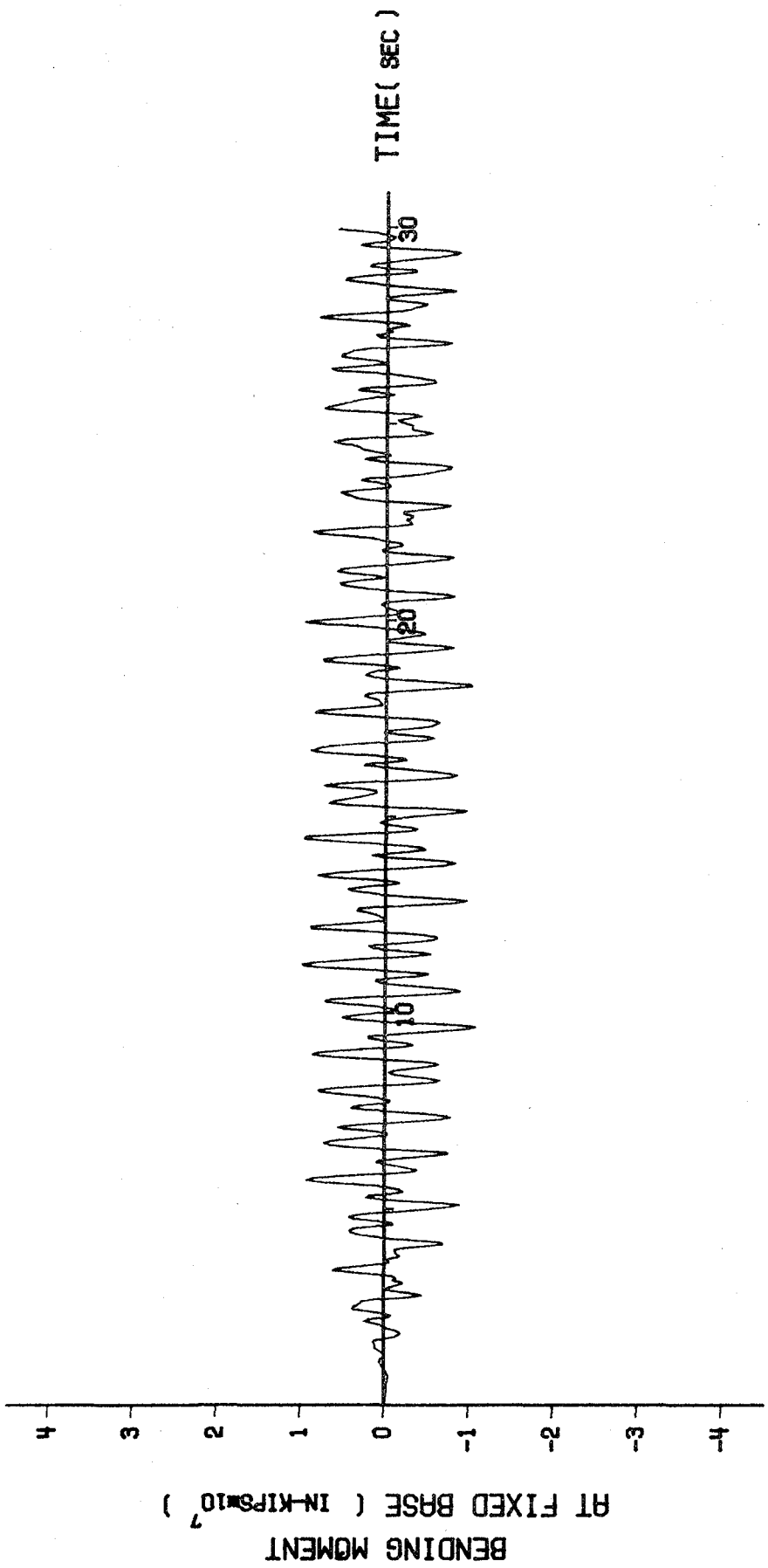

Fig. 11. Bending Moment at the Base vs. Time Curve for Inner Shell Without Opening.

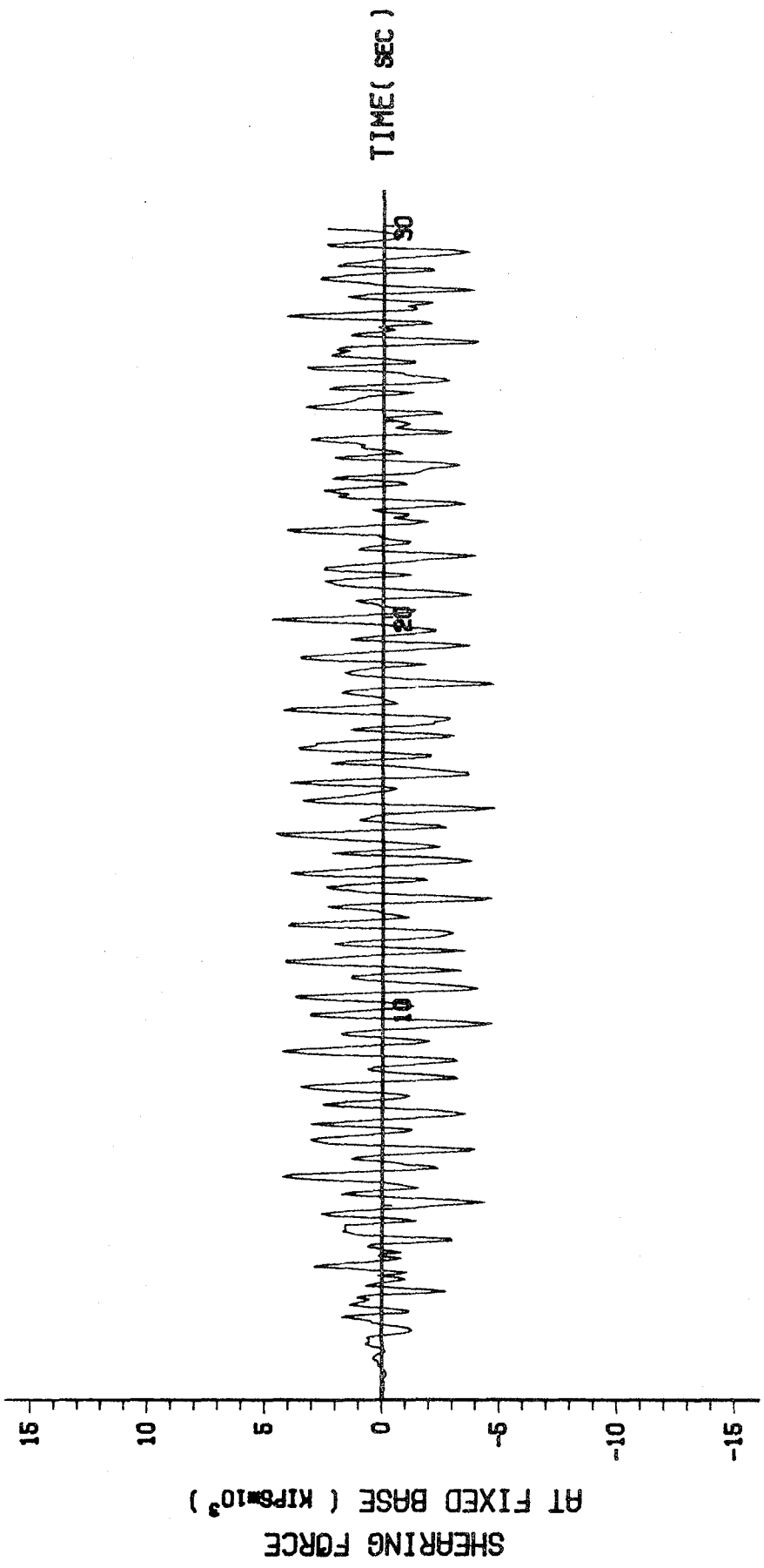

Fig. 12. Shearing Force at the Base vs. Time Curve for Inner Shell Without Opening.

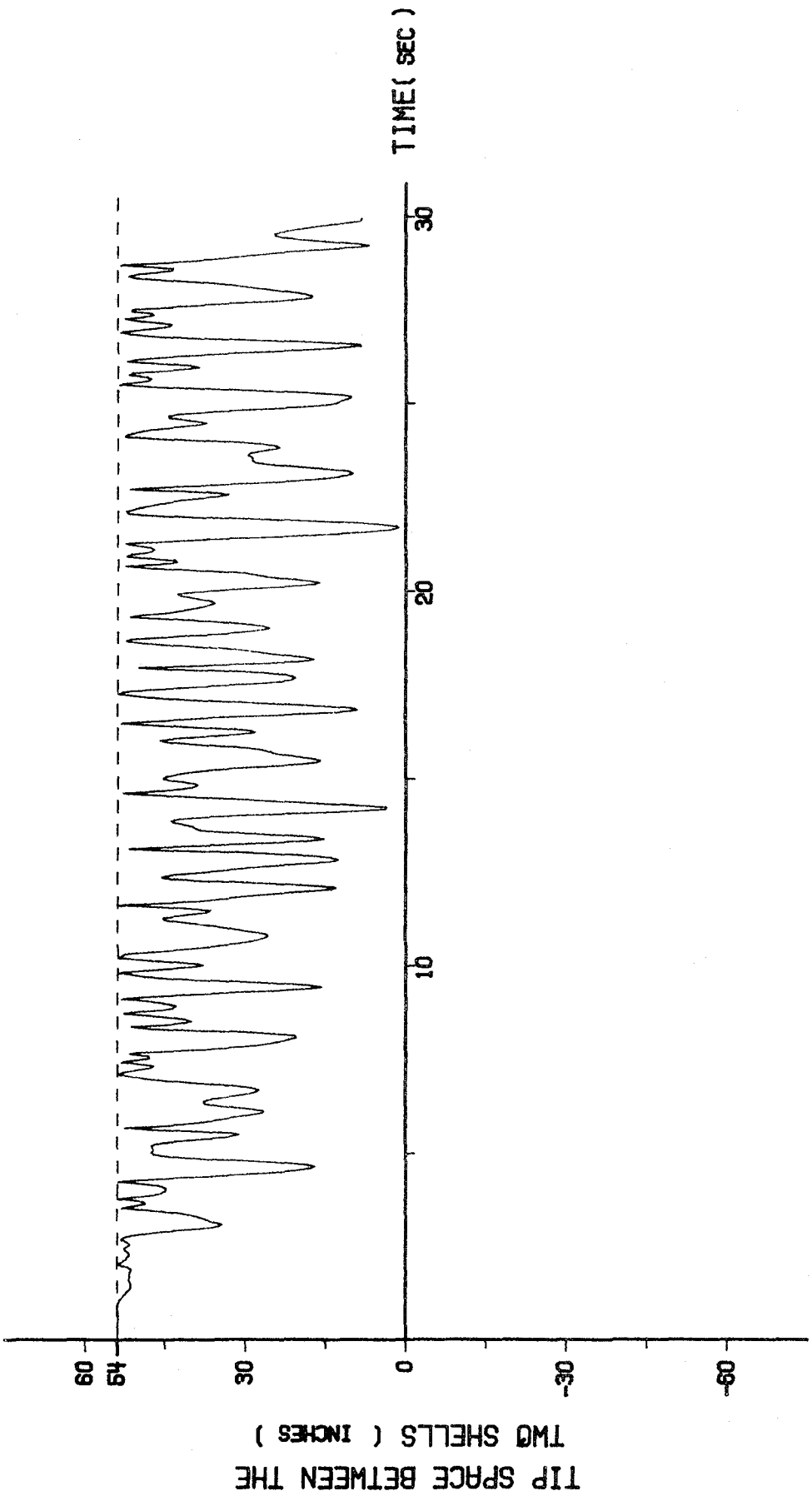

Fig. 13. Time History Curve for the Spacing Between the Tops of Outer and Inner Shells, Both Without Openings.

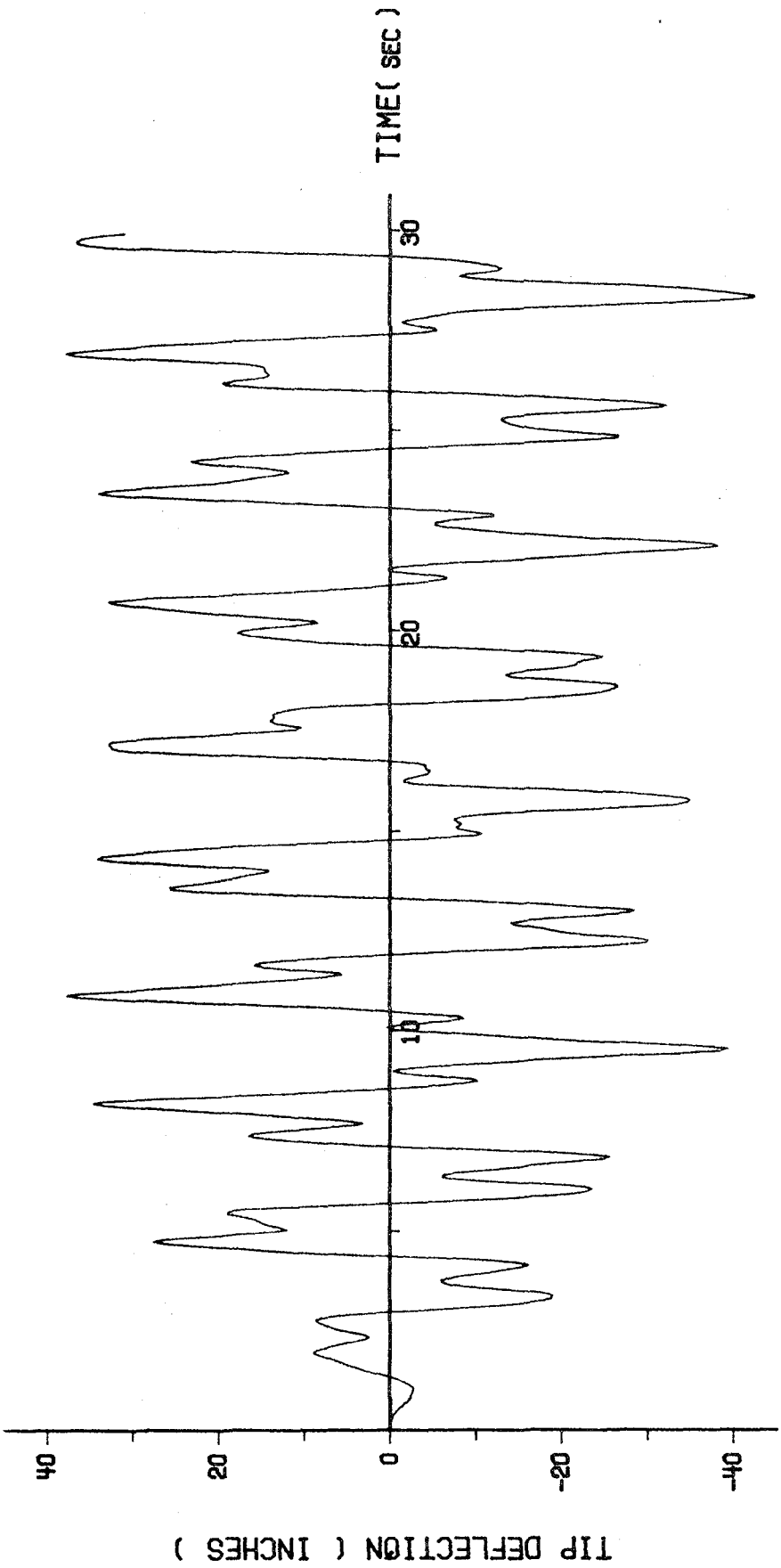

Fig. 14. Tip Deflection vs. Time Curve for Outer Shell with Two Openings.

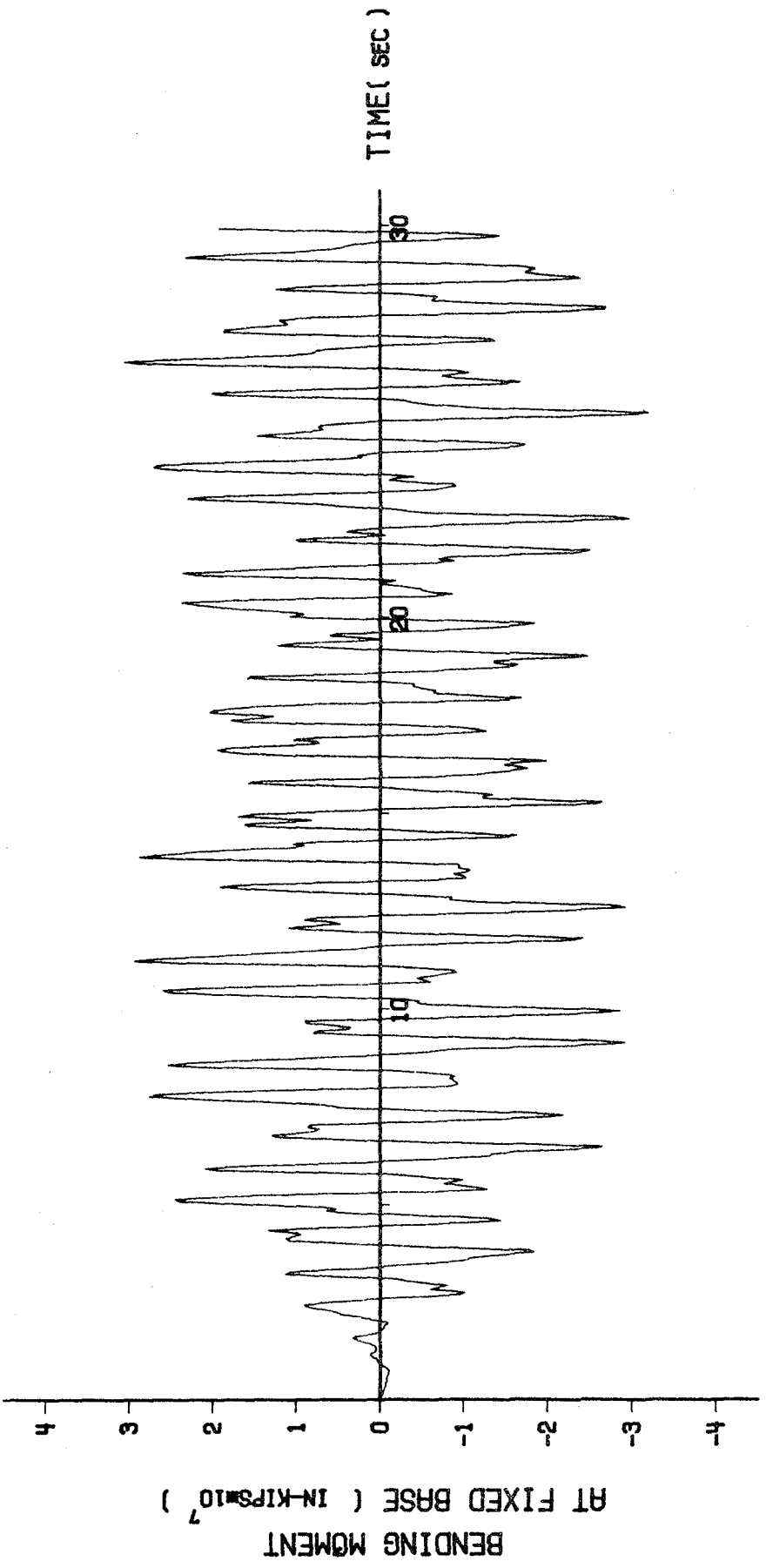

Fig. 15. Bending Moment at the Base vs. Time Curve for Outer Shell with Two Openings.

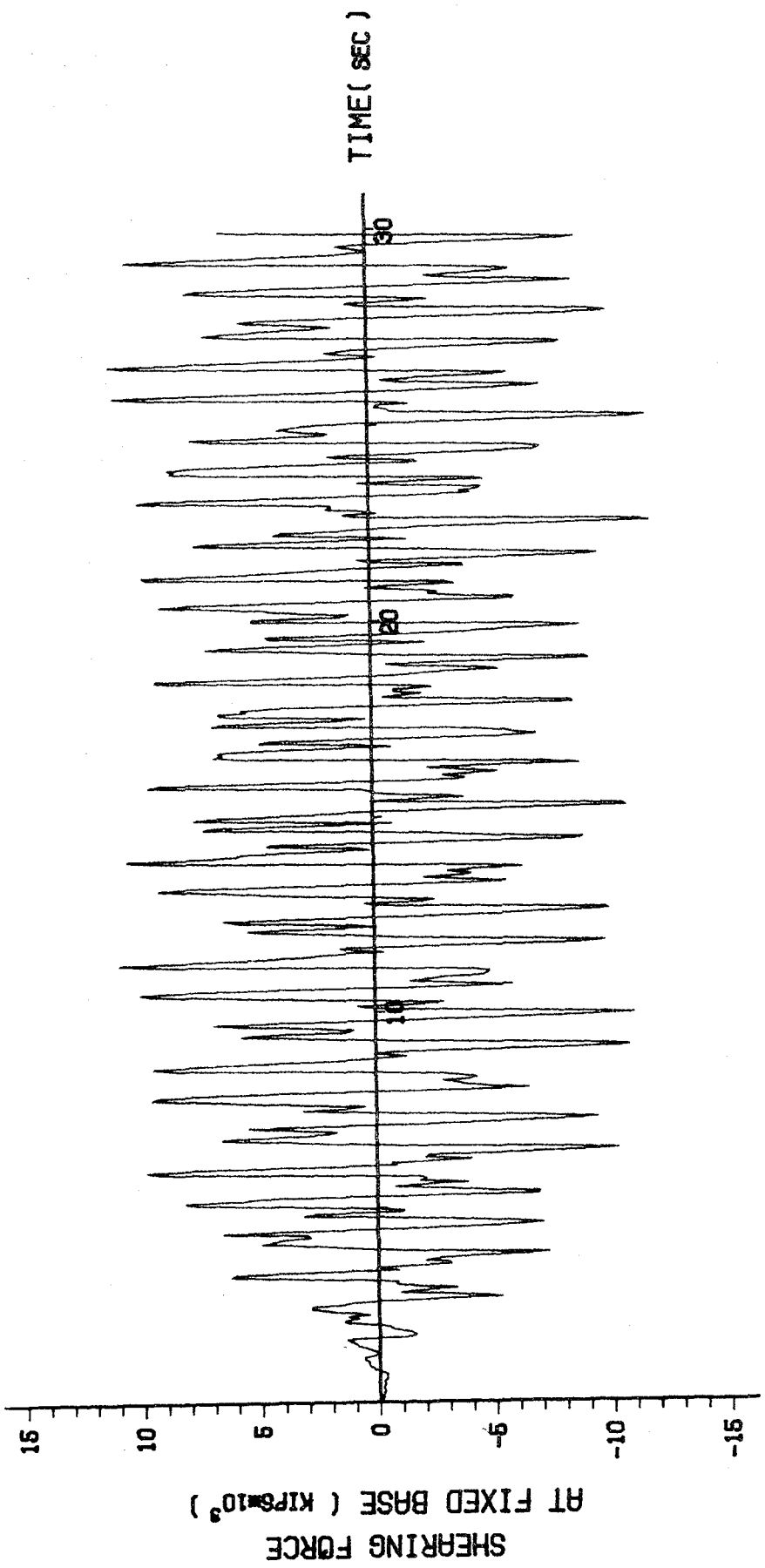

Fig. 16. Shearing Force at the Base vs. Time Curve for Outer Shell with Two Openings.

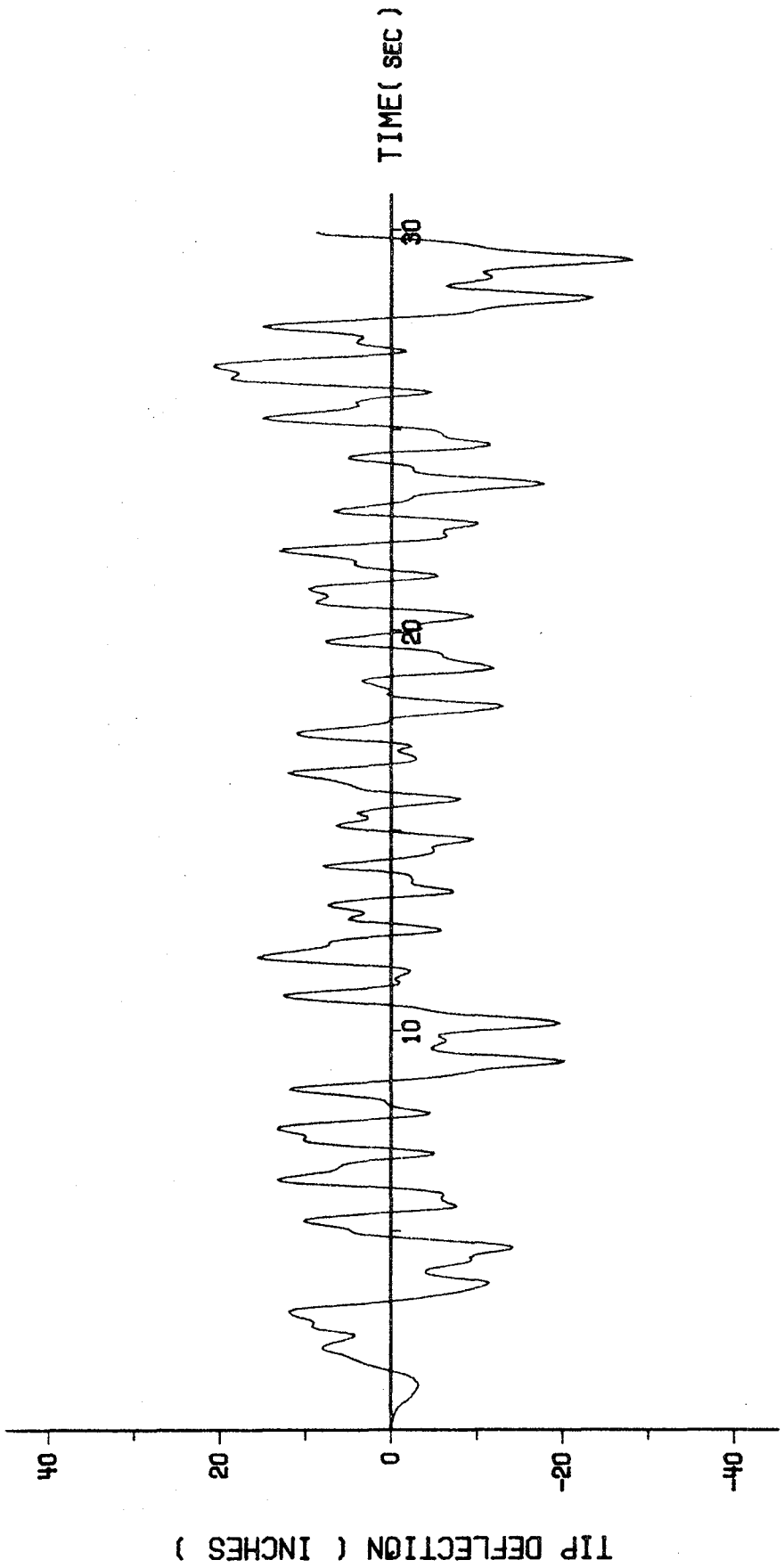

Fig. 17. Tip Deflection vs. Time Curve for Inner Shell with Two Openings.

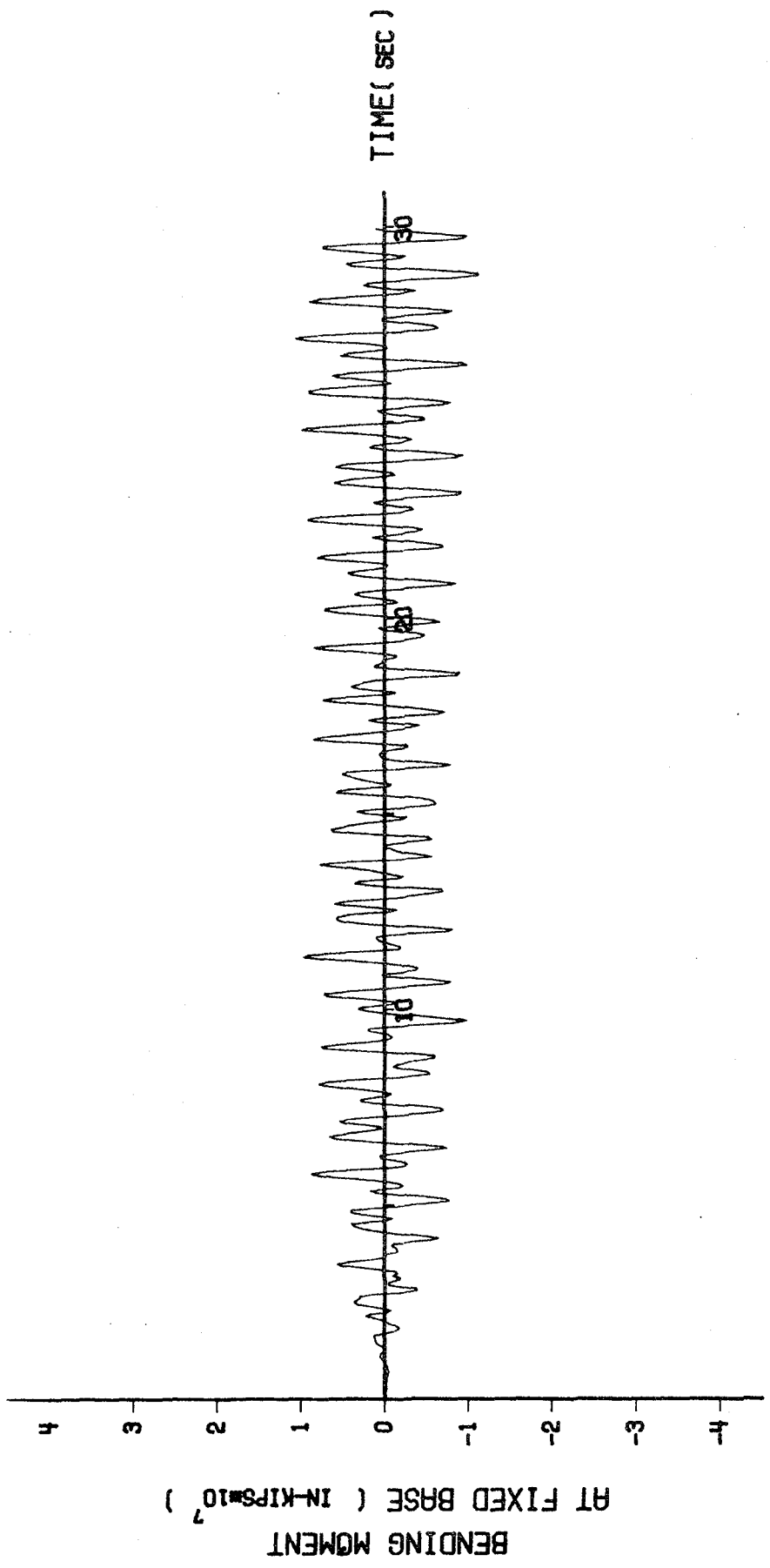

Fig. 18. Bending Moment at the Base vs. Time Curve for Inner Shell with Two Openings.

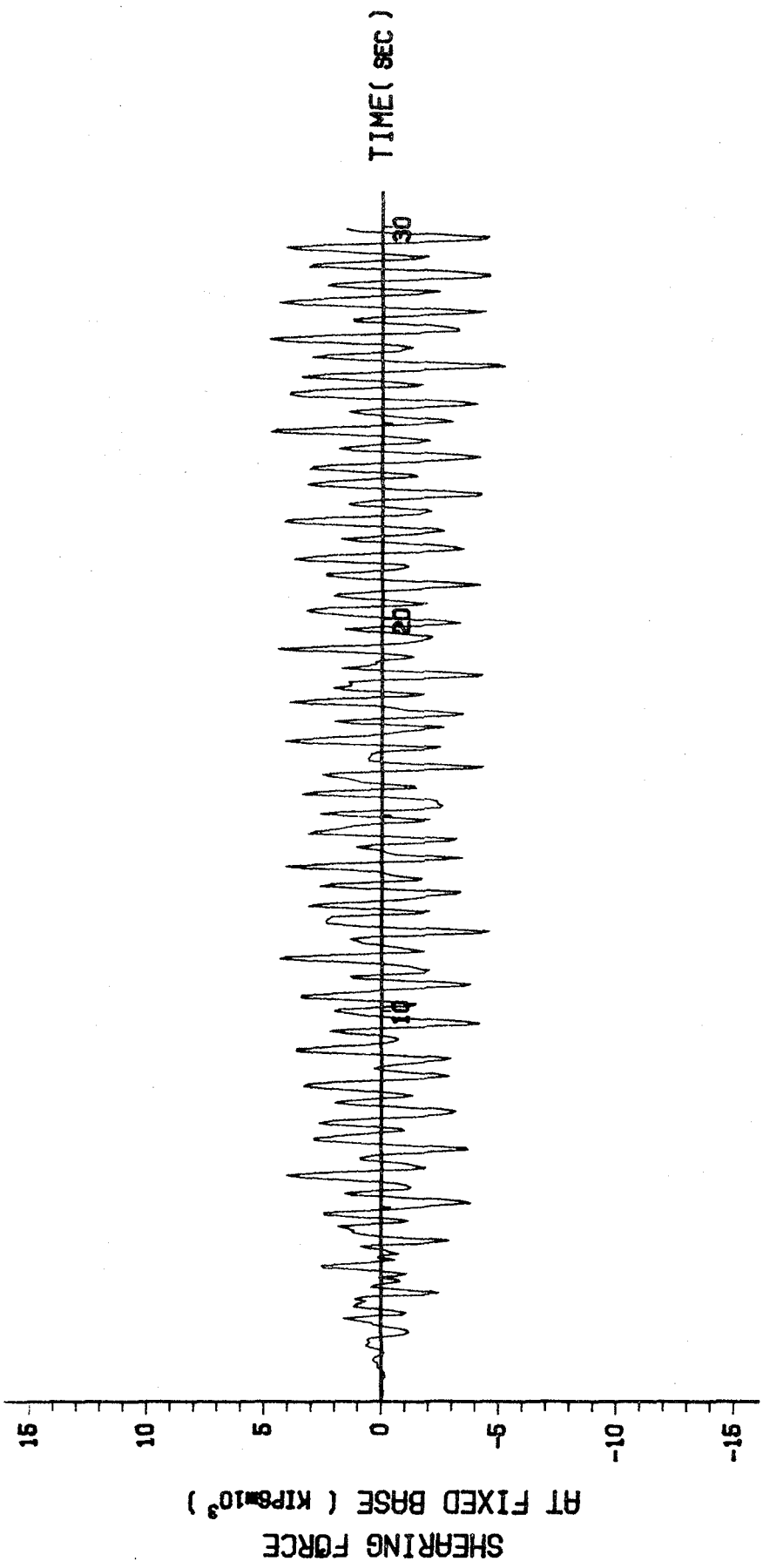

Fig. 19. Shearing Force at the Base vs. Time Curve for Inner Shell with Two Openings.

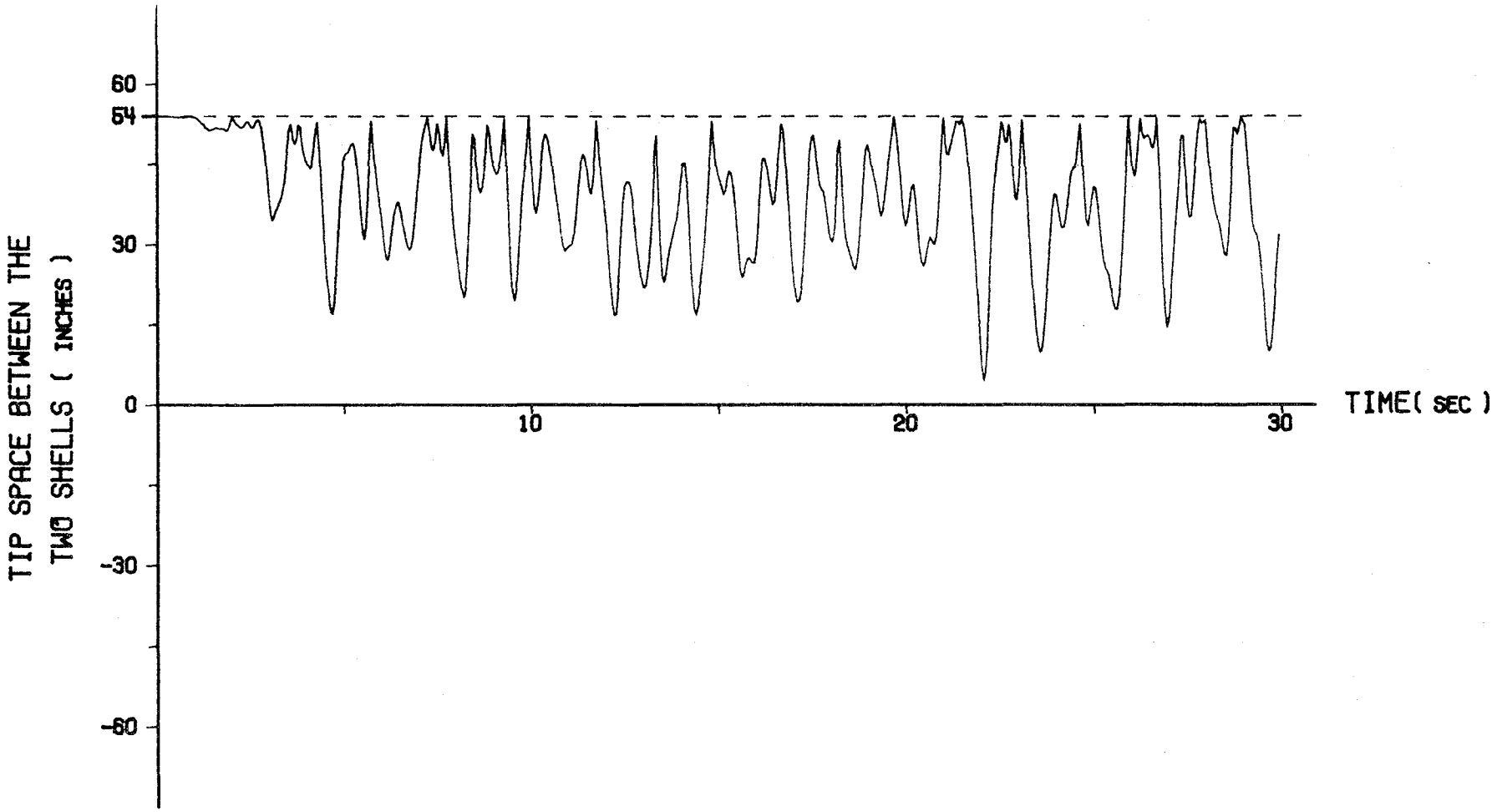

Fig. 20. Time History Curve for the Spacing Between the Tops of Outer and Inner Shells, Both with Two Openings.

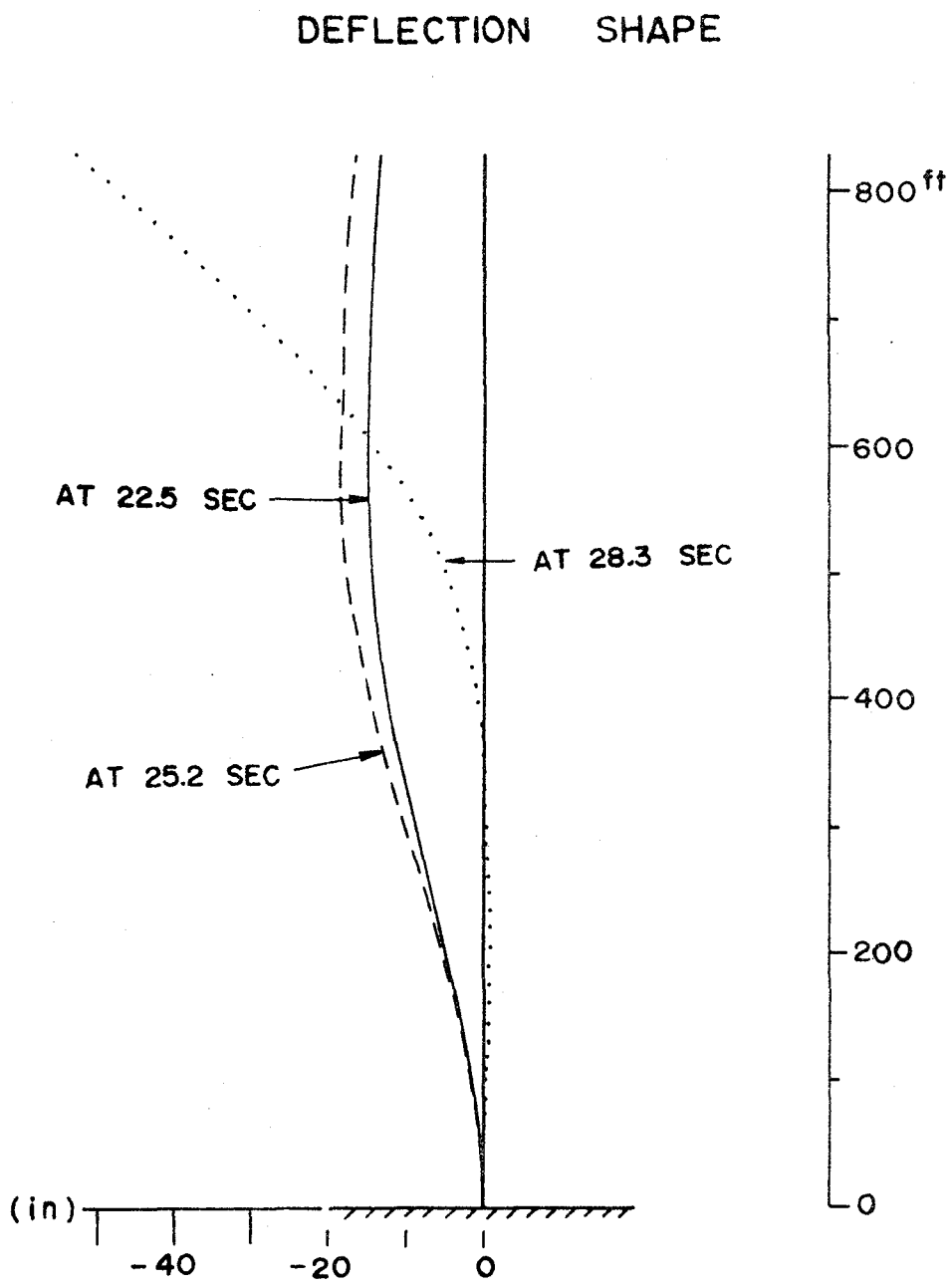

Fig. 21. The Deflection Shapes of the Outer Shell with Two Openings at Three Instances (Maximum Tip Deflection Occurs at 28.3 Seconds).

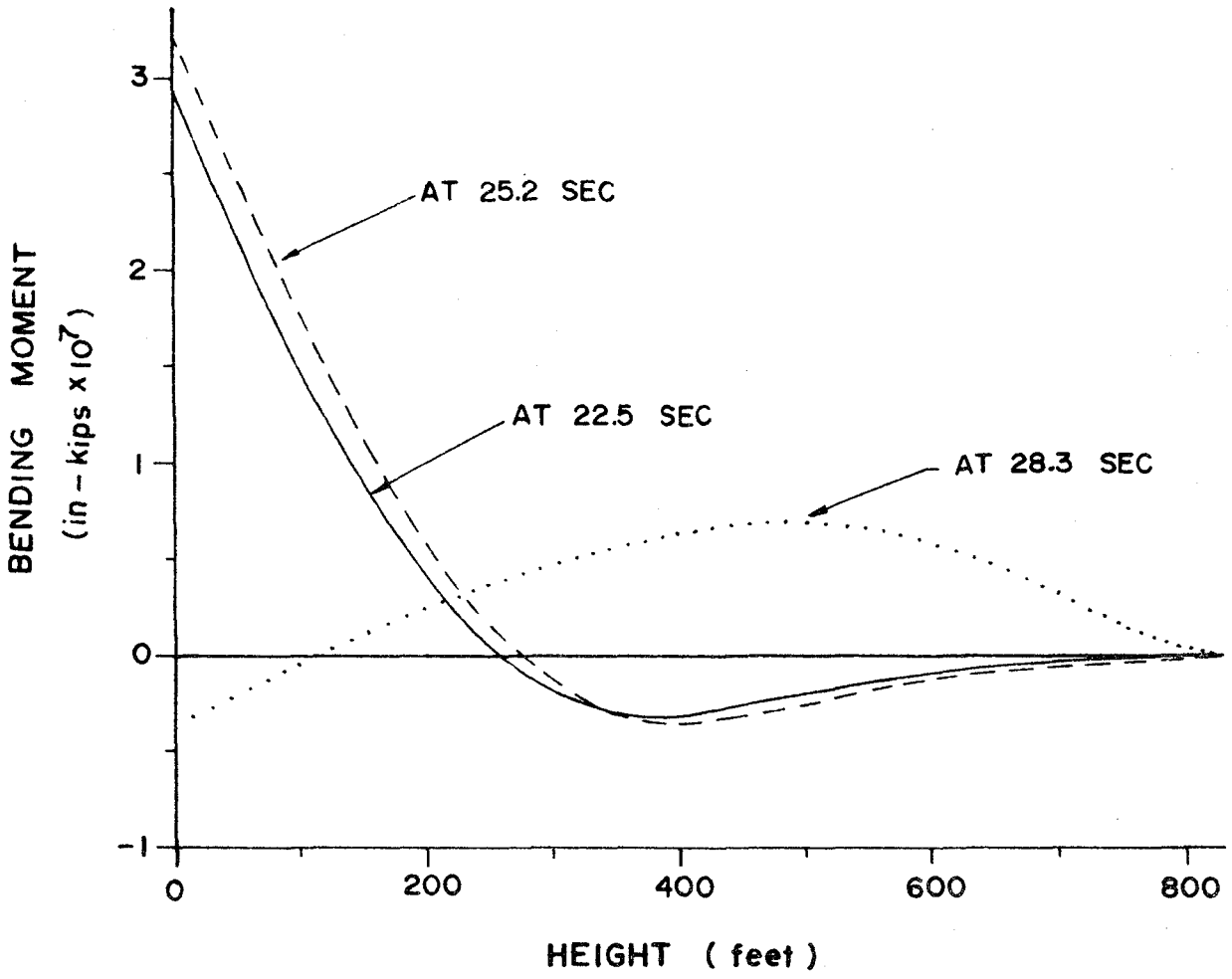

Fig. 22. The Distributions of Bending Moment for Outer Shell with Two Openings at Three Instances (Maximum Base Moment Occurs at 25.2 Seconds).

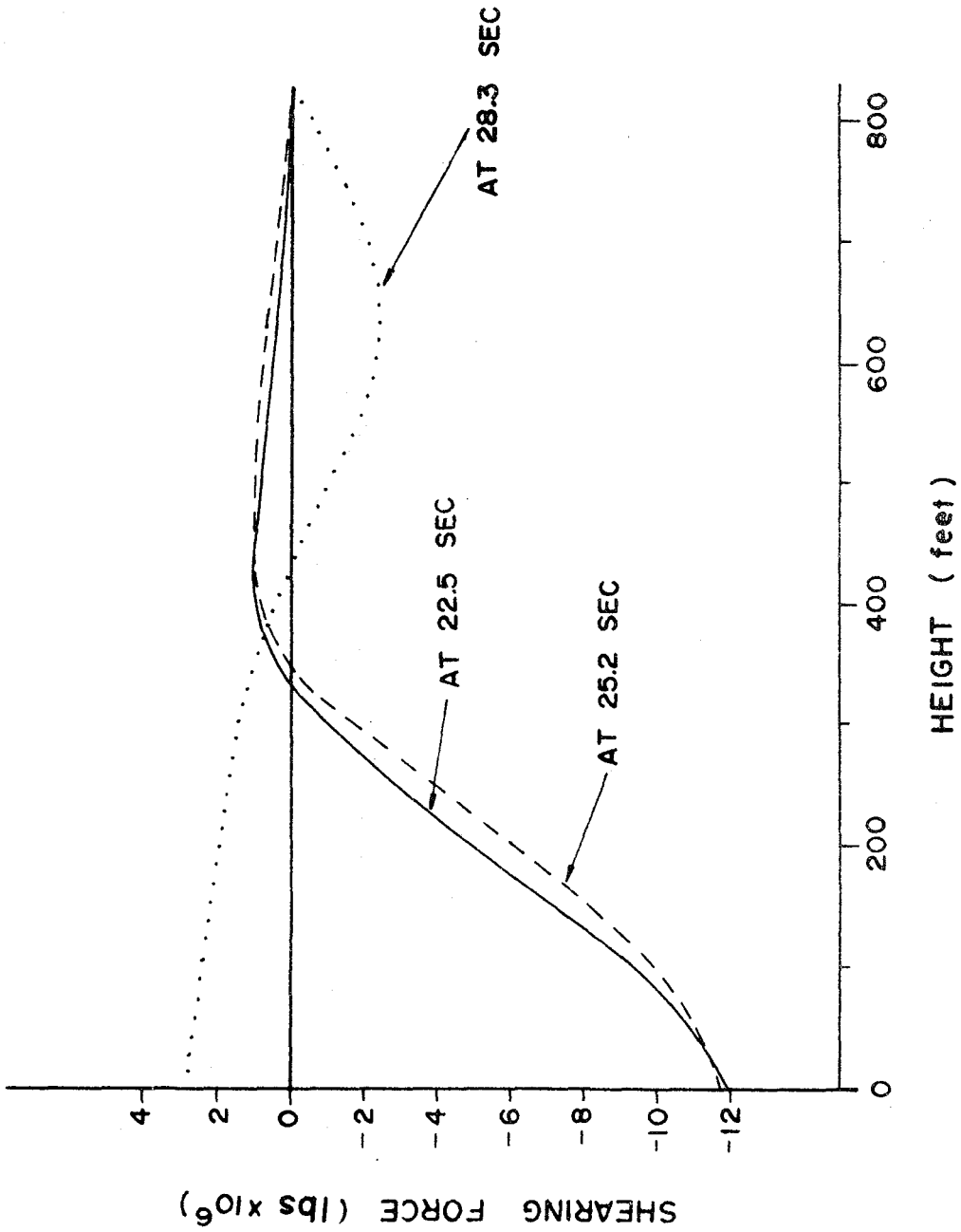

Fig. 23. The Distributions of Shearing Force for the Outer Shell with Two Openings at Three Instances (Maximum Base Shear Occurs at 22.5 Seconds).

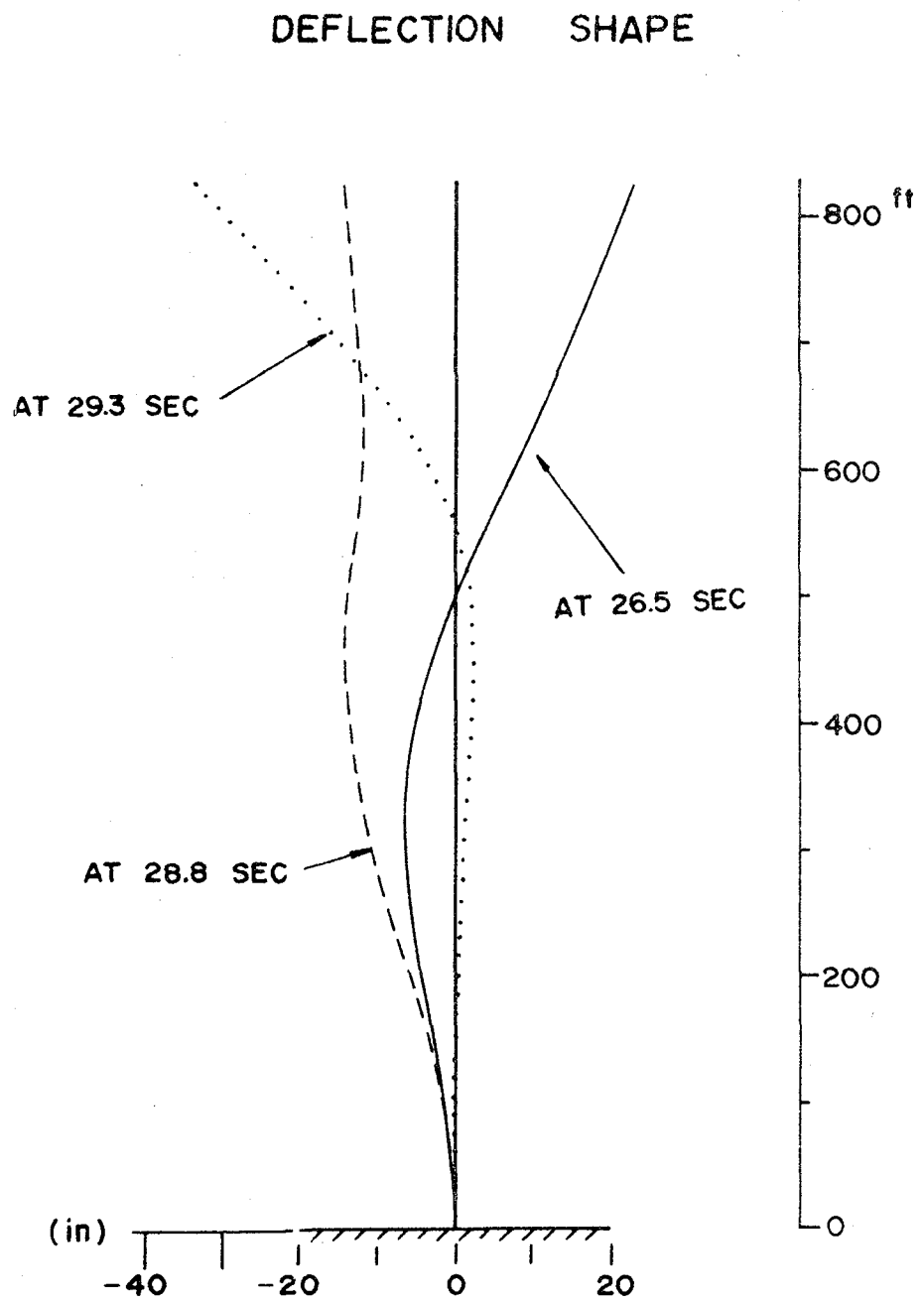

Fig. 24. The Deflection Shapes of the Inner Shell with Two Openings at Three Instances (Maximum Tip Deflection Occurs at 29.3 Seconds).

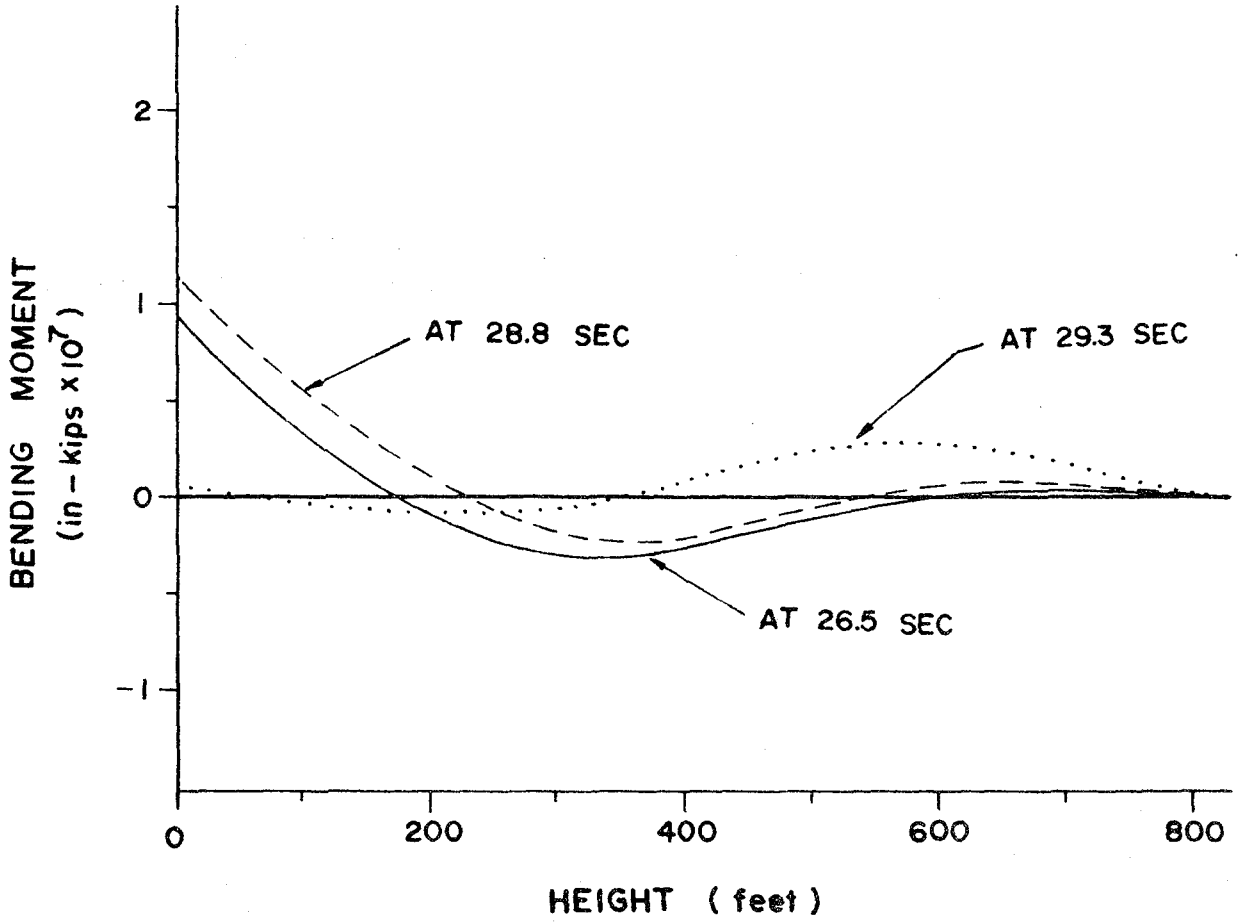

Fig. 25. The Distributions of Bending Moment for the Inner Shell with Two Openings at Three Instances (Maximum Base Moment Occurs at 28.8 Seconds).

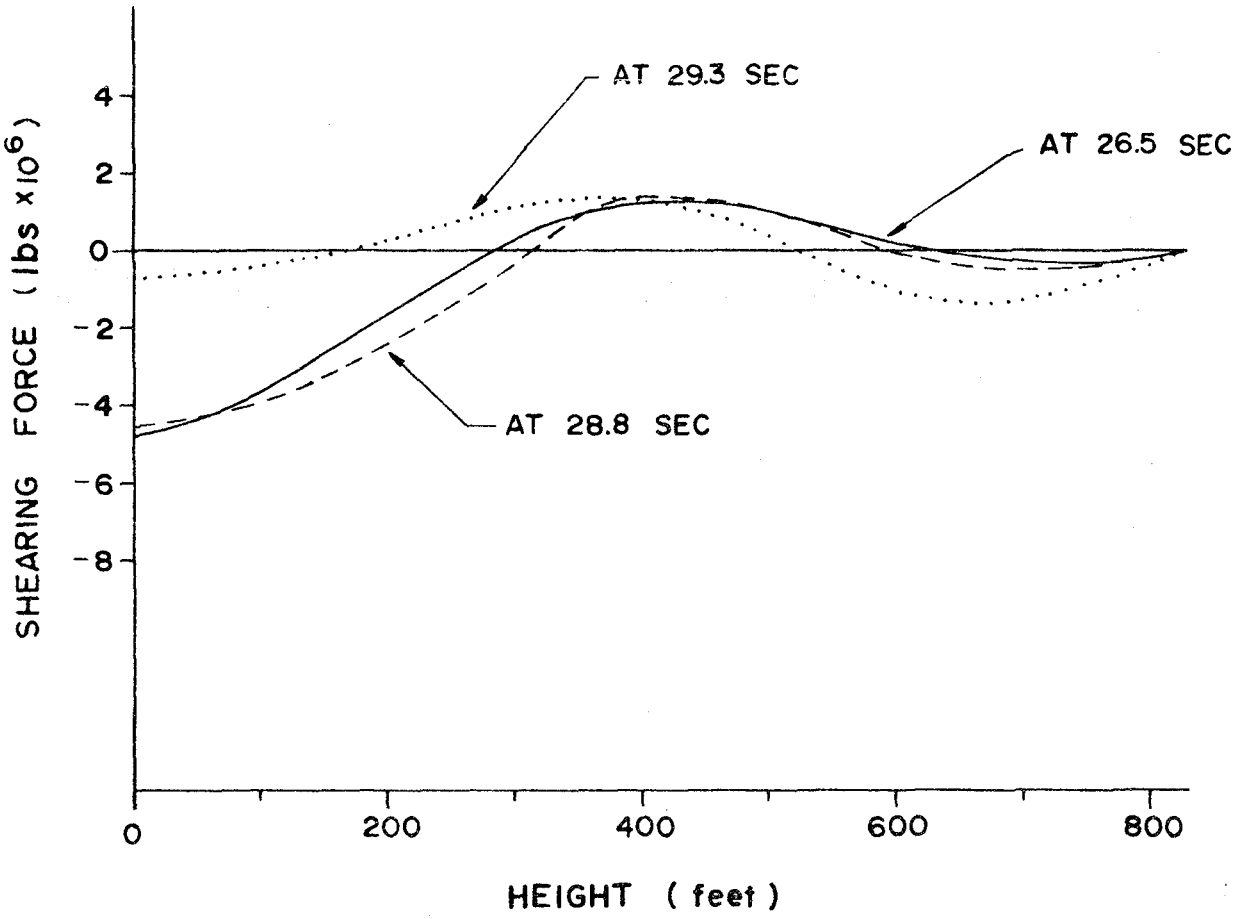

Fig. 26. The Distributions of Shearing Force for the Inner Shell with Two Openings at Three Instances (Maximum Base Shear Occurs at 26.5 Seconds).

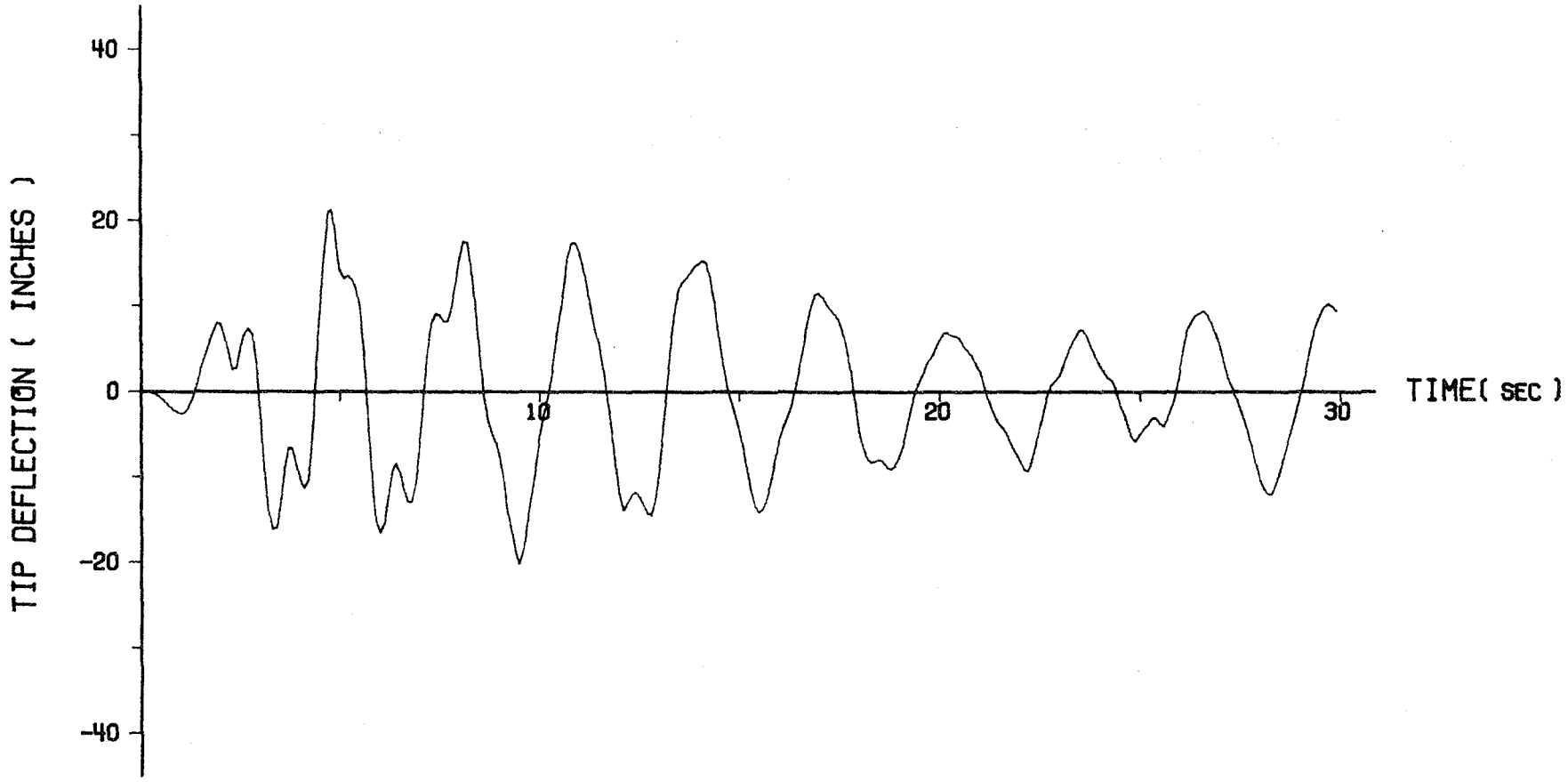

Fig. 27. Tip Deflection vs. Time Curve for the Outer Shell with Two Openings and with Damping Coefficient Equal to 4 Percent of its Critical Value.

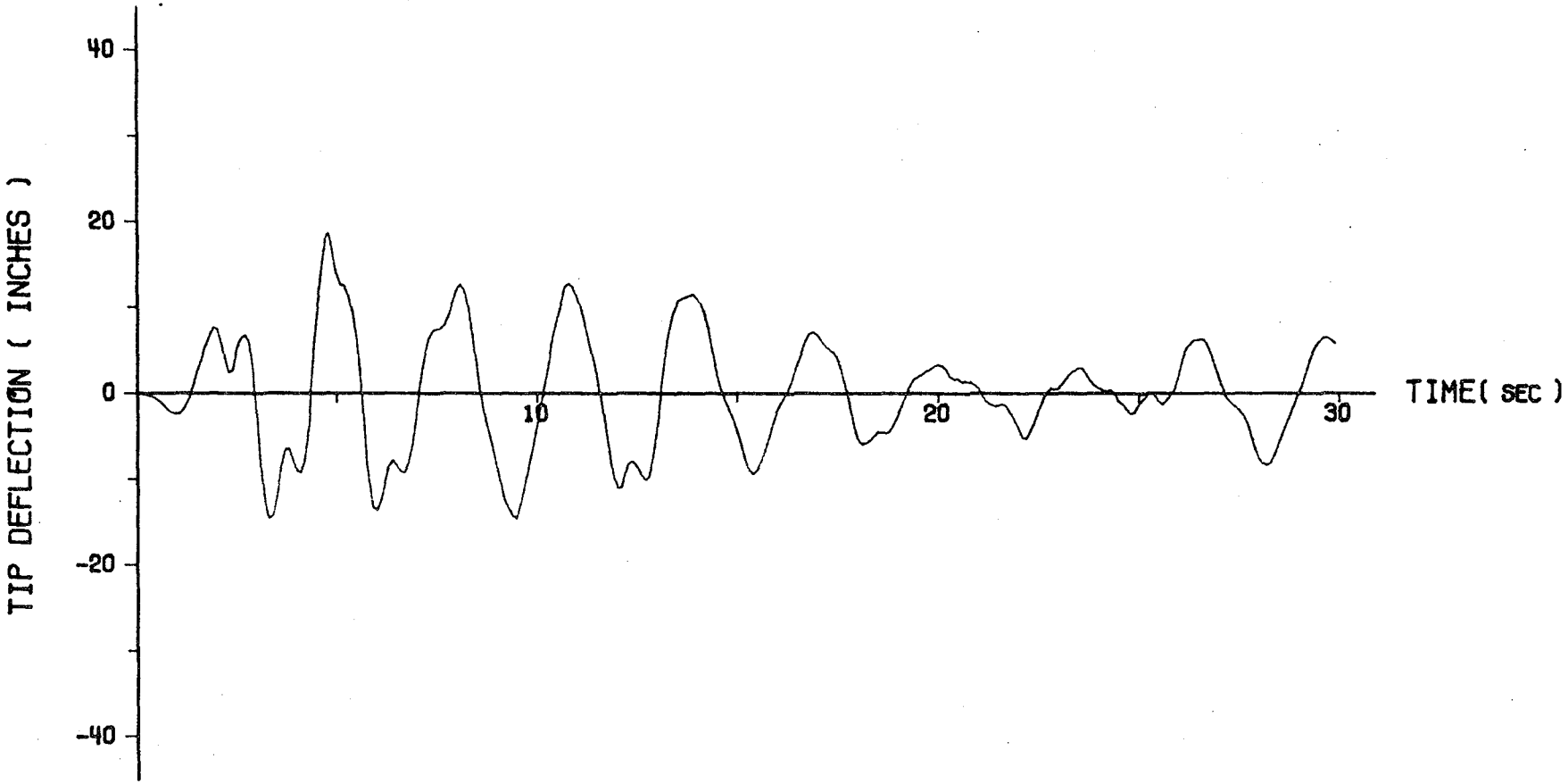

Fig. 28. Tip Deflection vs. Time Curve for the Outer Shell with Two Openings and with Damping Coefficient Equal to 7 Percent of its Critical Value.

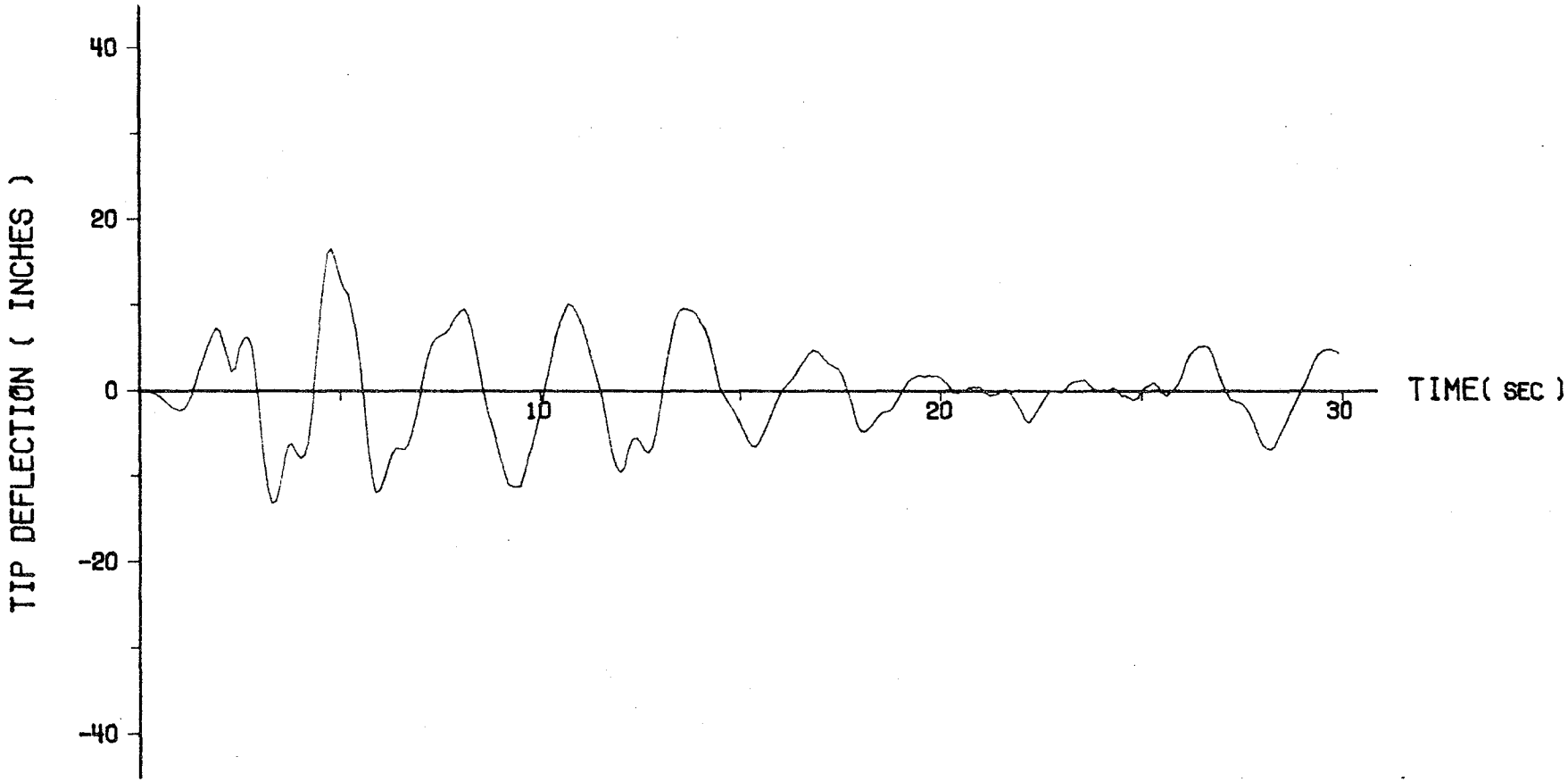

Fig. 29. Tip Deflection vs. Time Curve for the Outer Shell with Two Openings and with Damping Coefficient Equal to 10 Percent of its Critical Value.

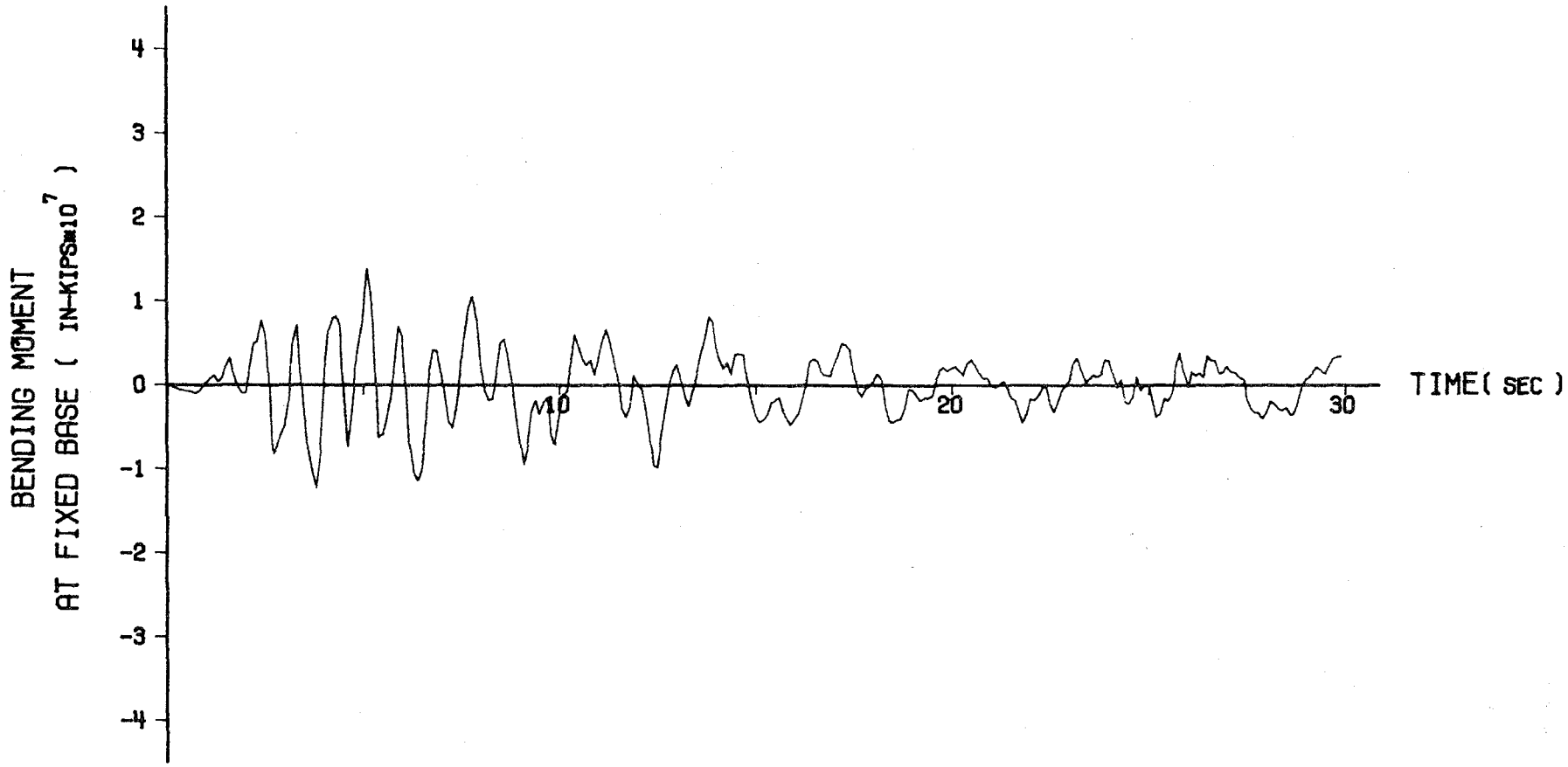

Fig. 30. Base Bending Moment vs. Time Curve for the Outer Shell with Two Openings and with Damping Coefficient Equal to 4 Percent of its Critical Value.

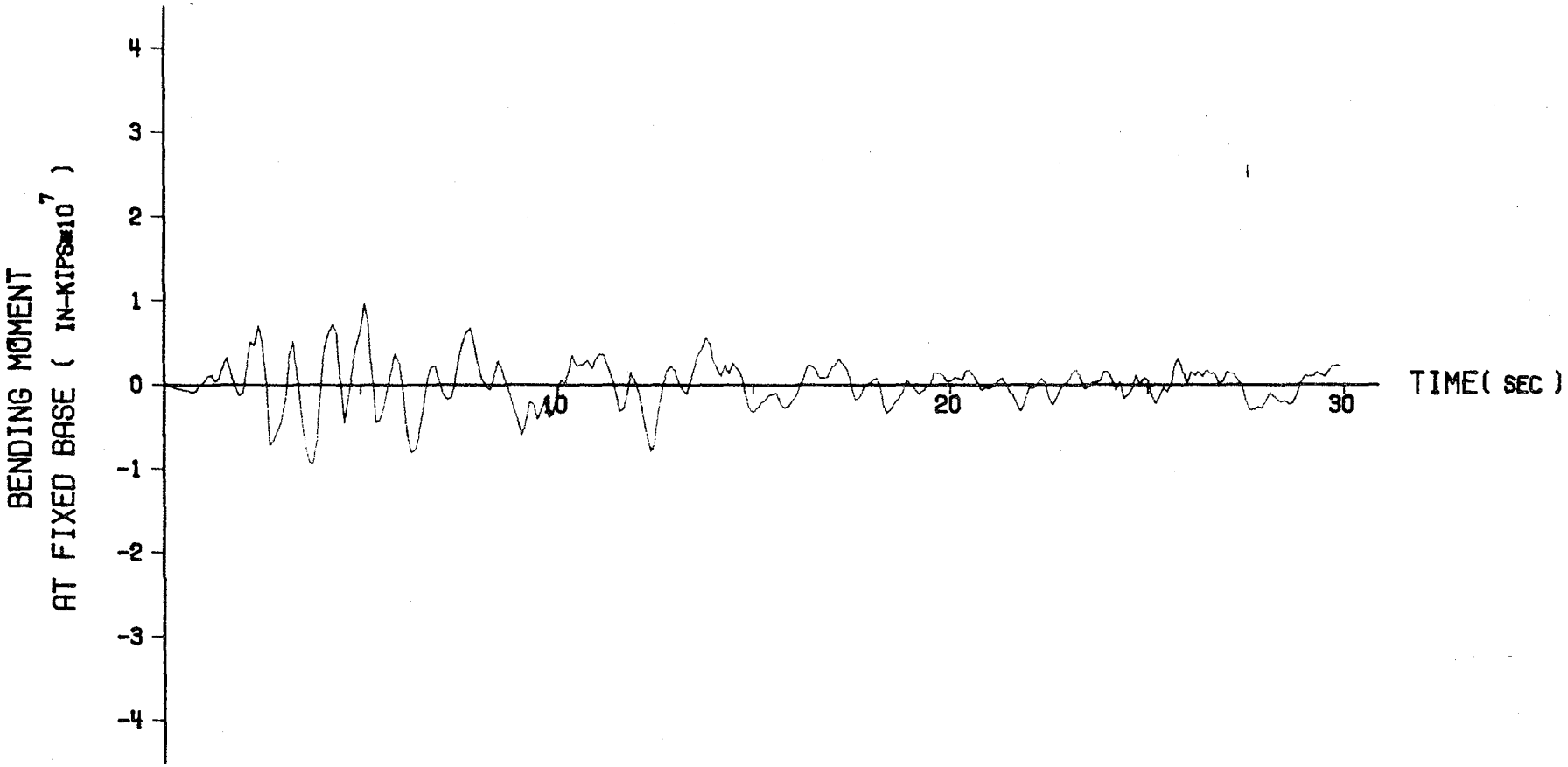

Fig. 31. Base Bending Moment vs. Time Curve for the Outer Shell with Two Openings and with Damping Coefficient Equal to 7 Percent of its Critical Value.

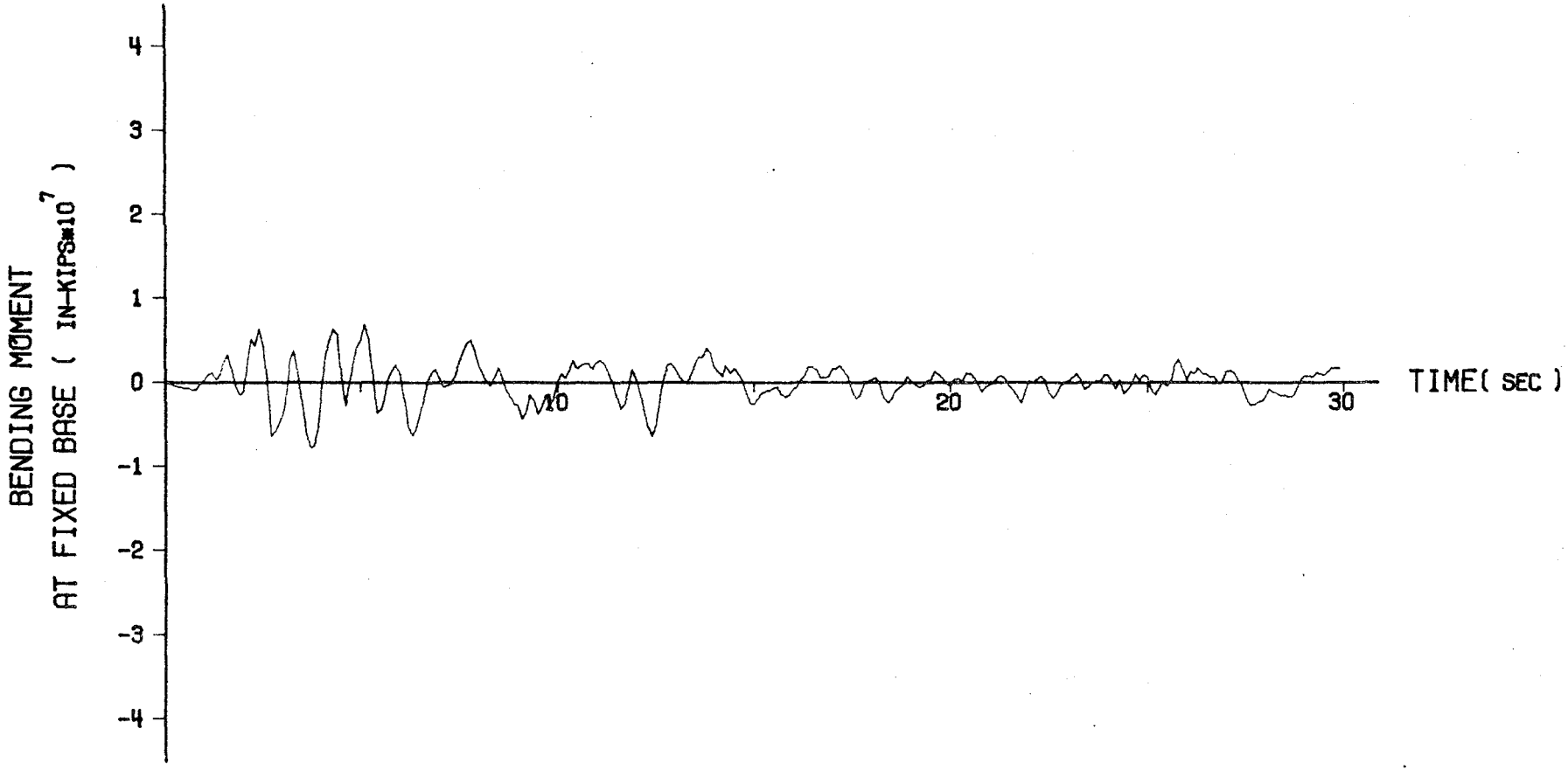

Fig. 32. Base Bending Moment vs. Time Curve for the Outer Shell with Two Openings and with Damping Coefficient Equal to 10 Percent of its Critical Value.

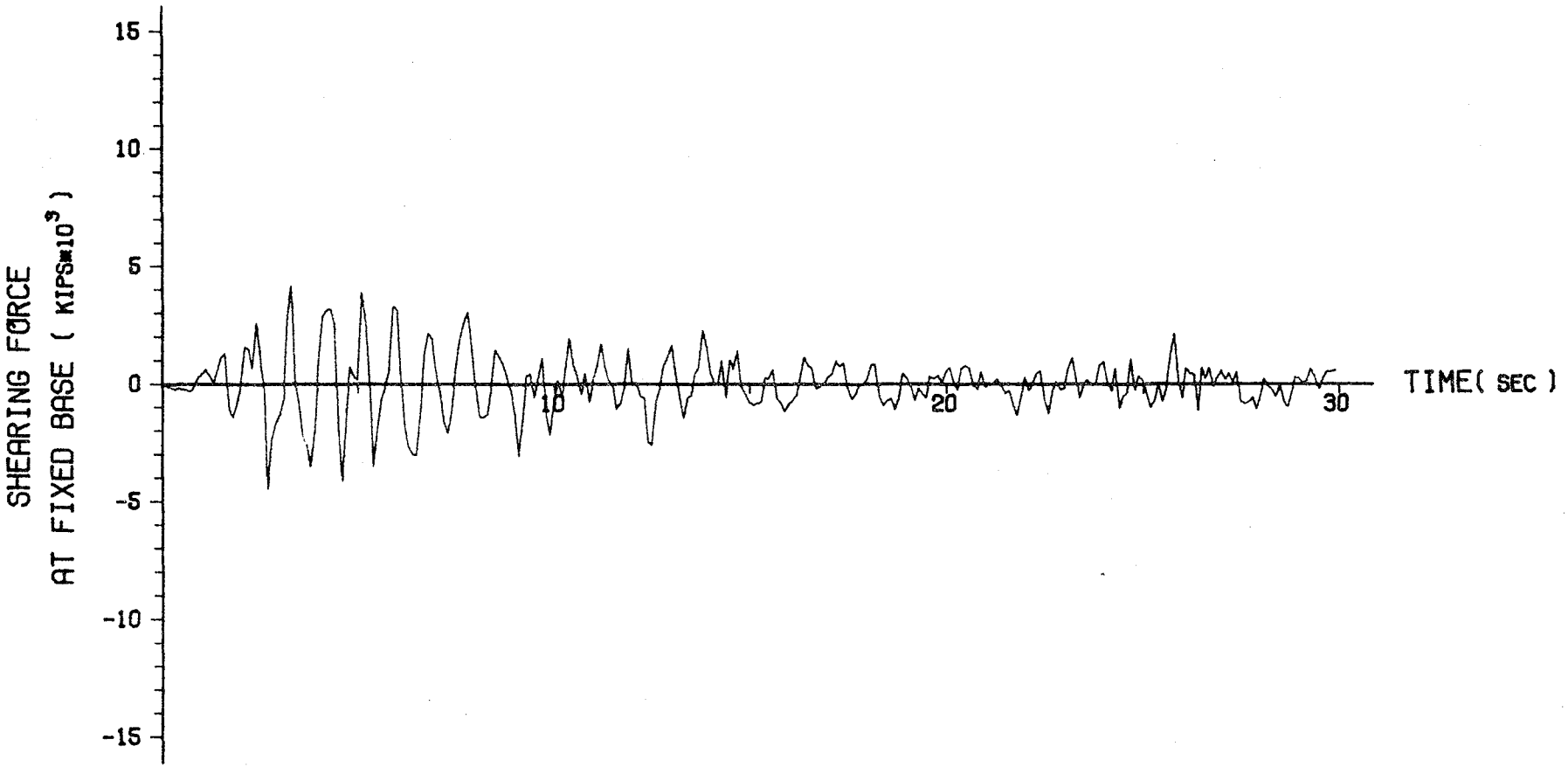

Fig. 33. Base Shearing Force vs. Time Curve for the Outer Shell with Two Openings and with Damping Coefficient Equal to 4 Percent of its Critical Value.

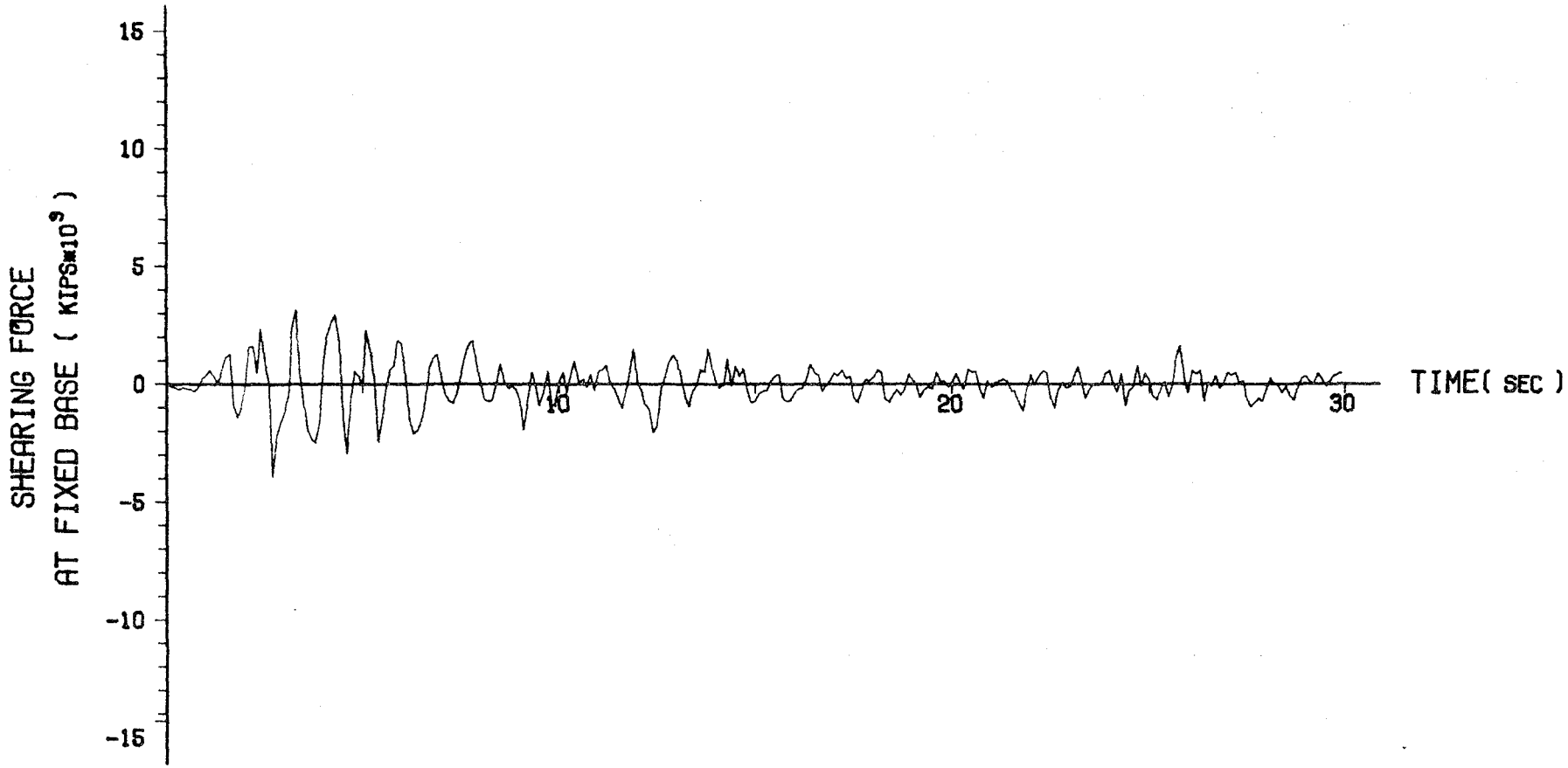

Fig. 34. Base Shearing Force vs. Time Curve for the Outer Shell with Two Openings and with Damping Coefficient Equal to 7 Percent of its Critical Value.

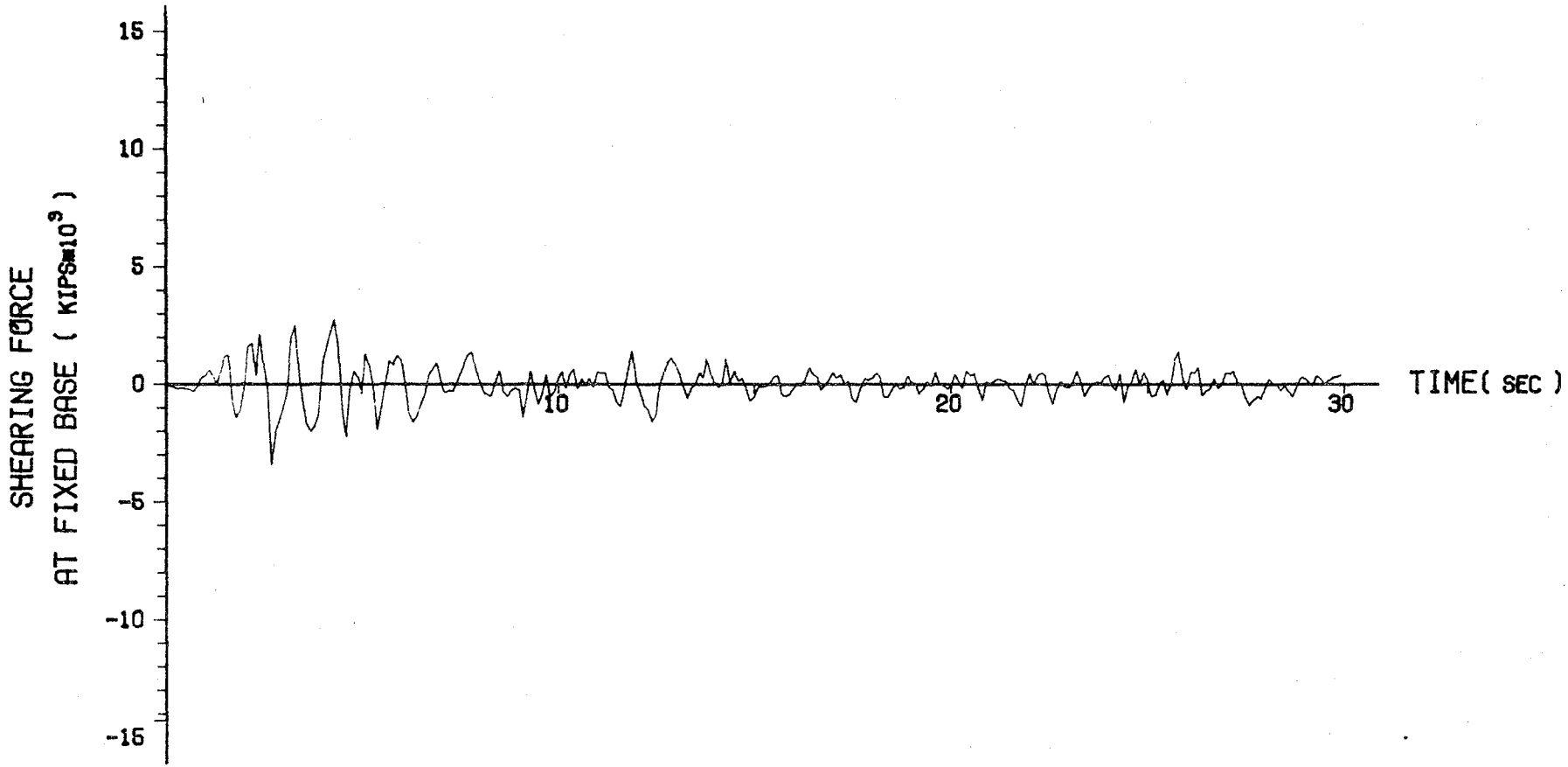

Fig. 35. Base Shearing Force vs. Time Curve for the Outer Shell with Two Openings and with Damping Coefficient Equal to 10 Percent of its Critical Value.

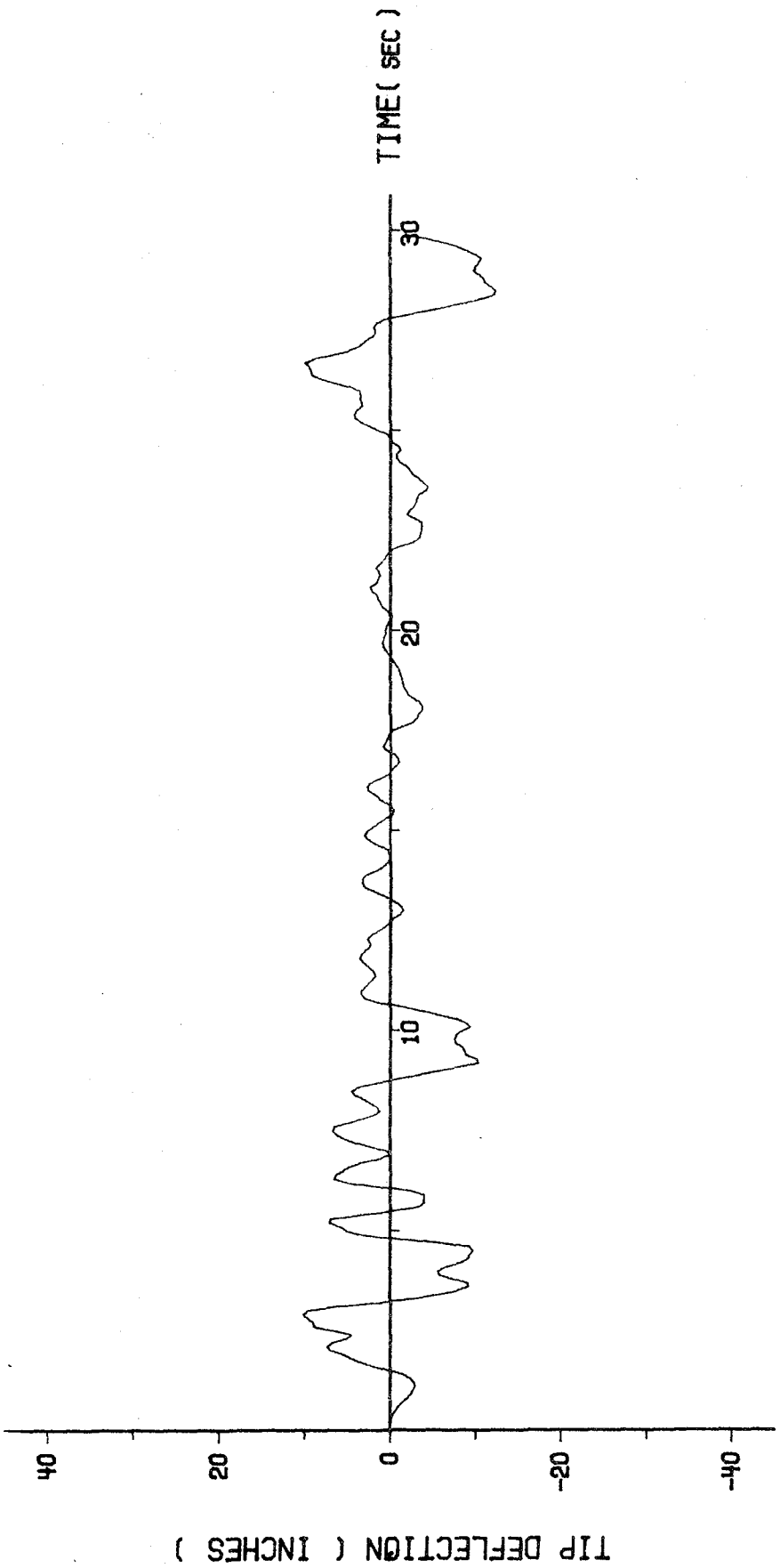

Fig. 36. Tip Deflection vs. Time Curve for the Inner Shell with Two Openings and with Damping Coefficient Equal to 4 Percent of its Critical Value.

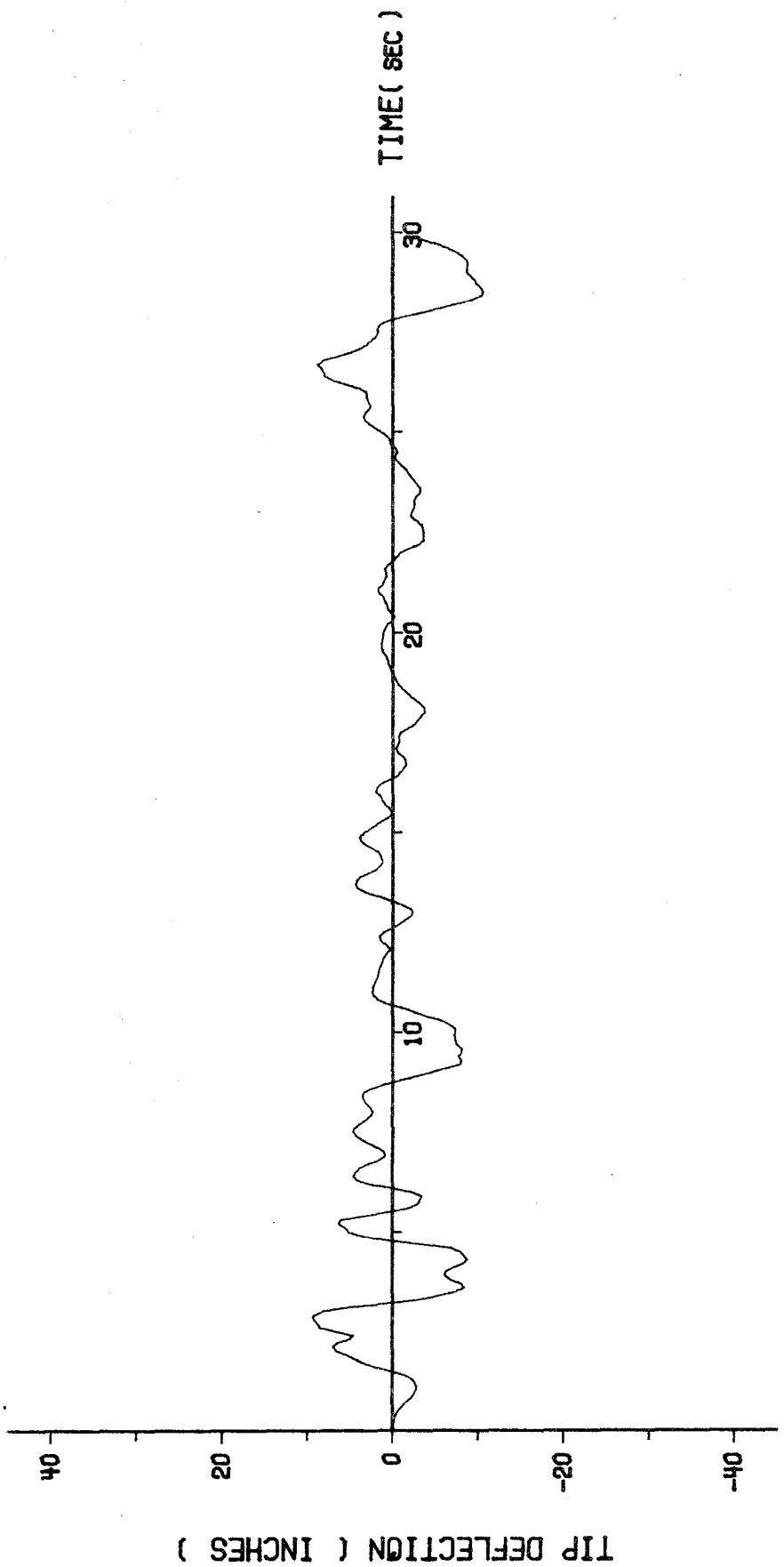

Fig. 37. Tip Deflection vs. Time Curve for the Inner Shell with Two Openings and with Damping Coefficient Equal to 7 Percent of its Critical Value.

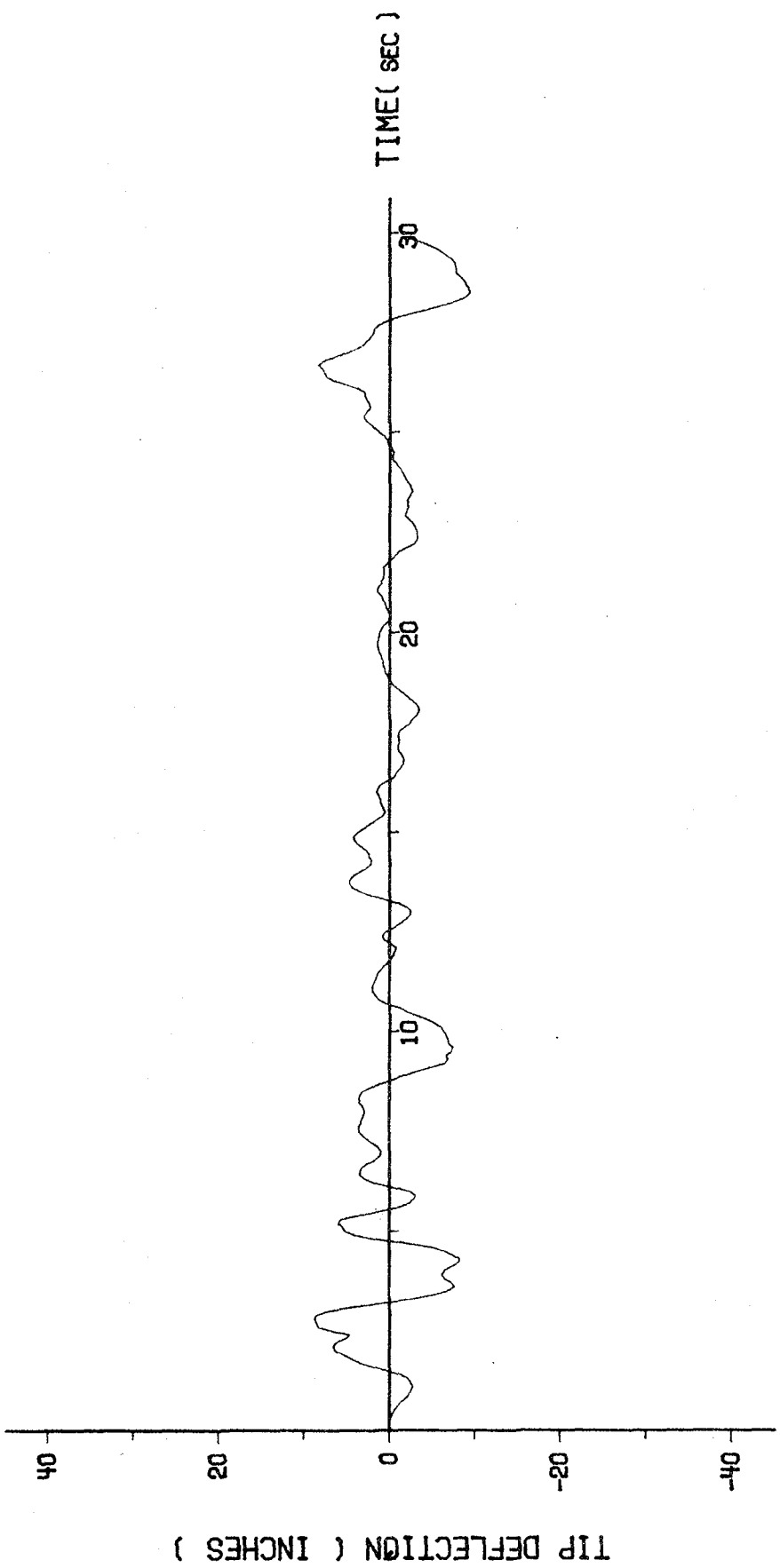

Fig. 38. Tip Deflection vs. Time Curve for the Inner Shell with Two Openings and with Damping Coefficient Equal to 10 Percent of its Critical Value.

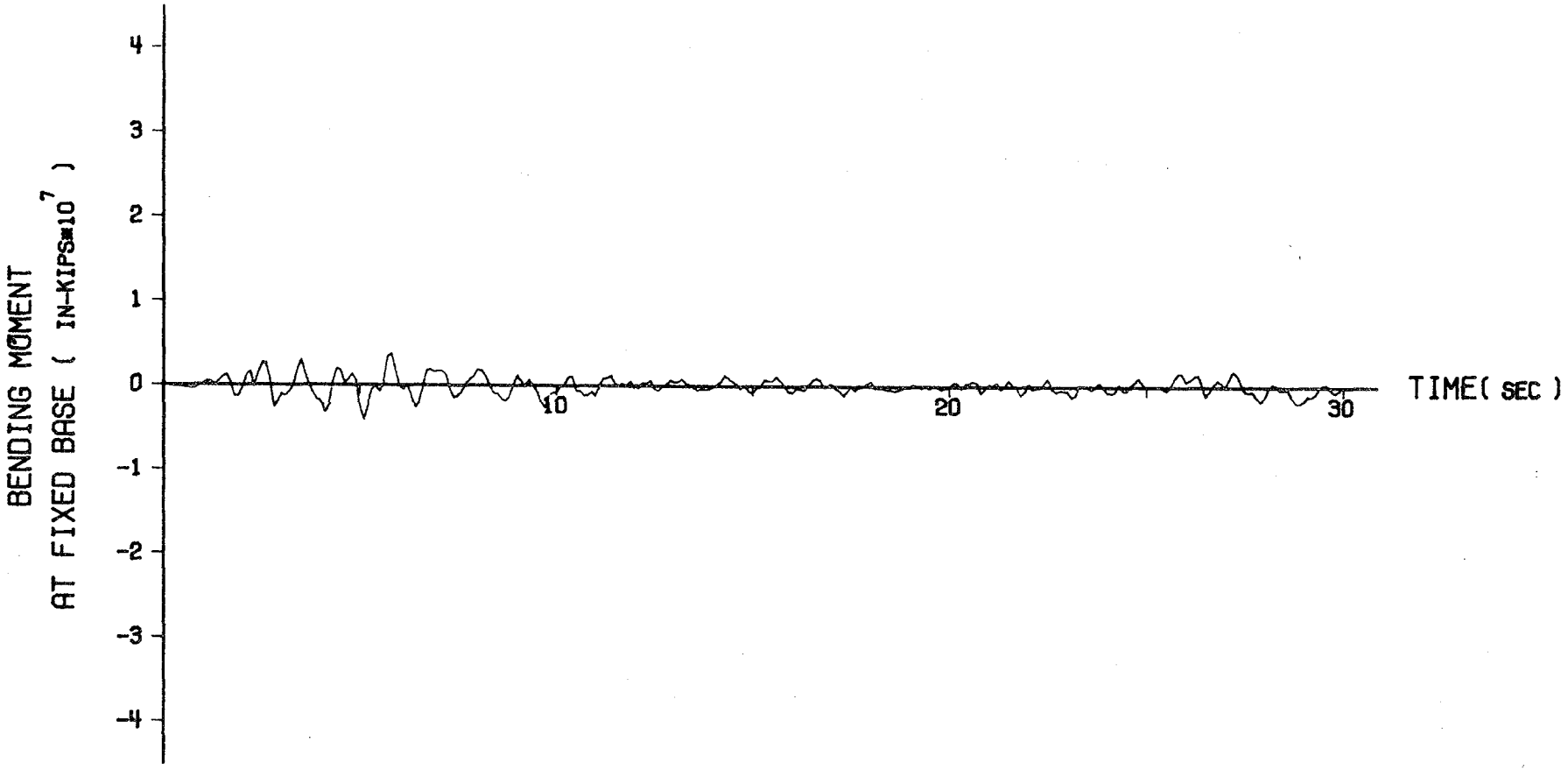

Fig. 39. Base Bending Moment vs. Time Curve for the Inner Shell with Two Openings and with Damping Coefficient Equal to 4 Percent of its Critical Value.

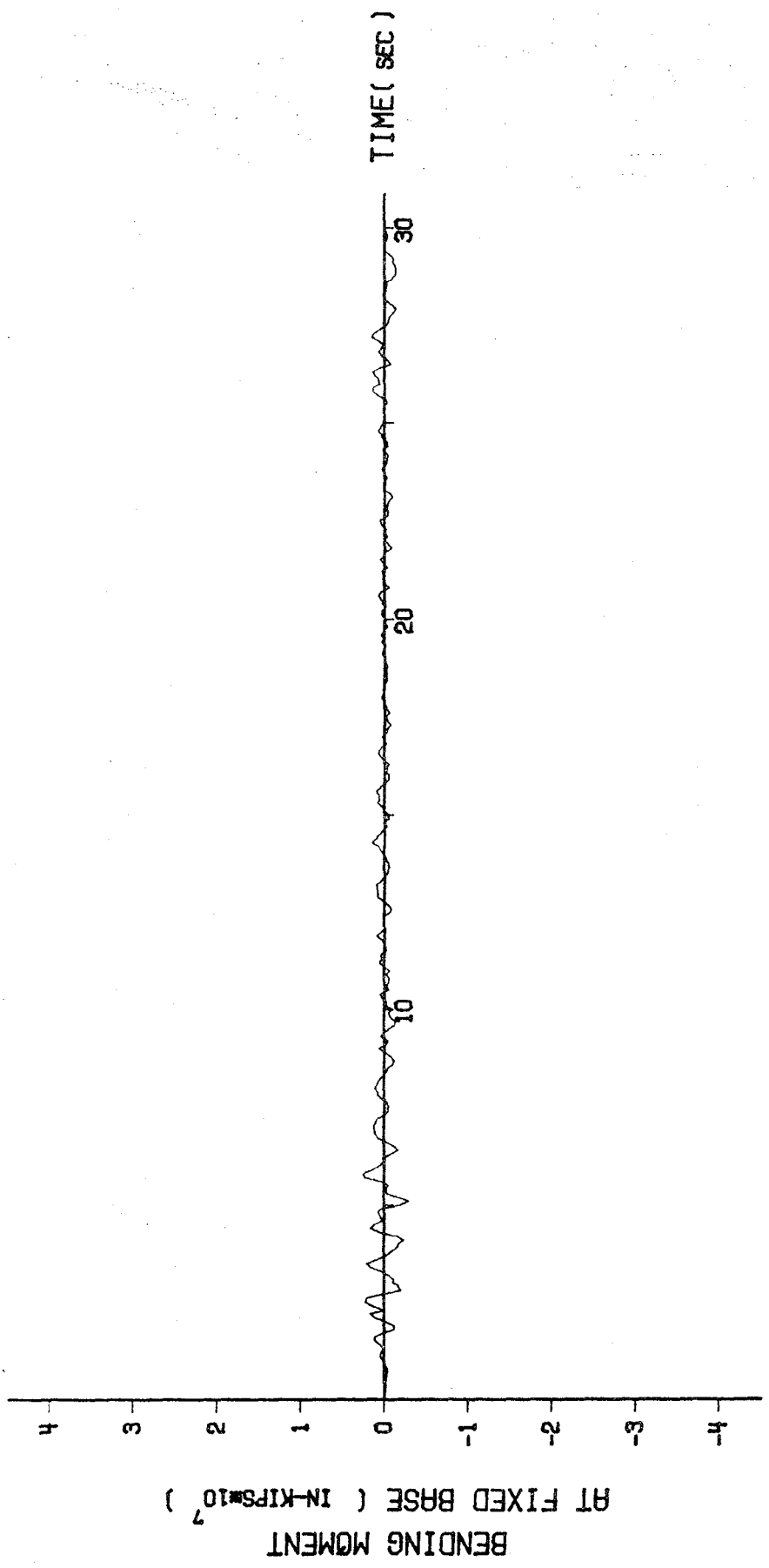

Fig. 40. Base Bending Moment vs. Time Curve for the Inner Shell with Two Openings and with Damping Coefficient Equal to 7 Percent of its Critical Value.

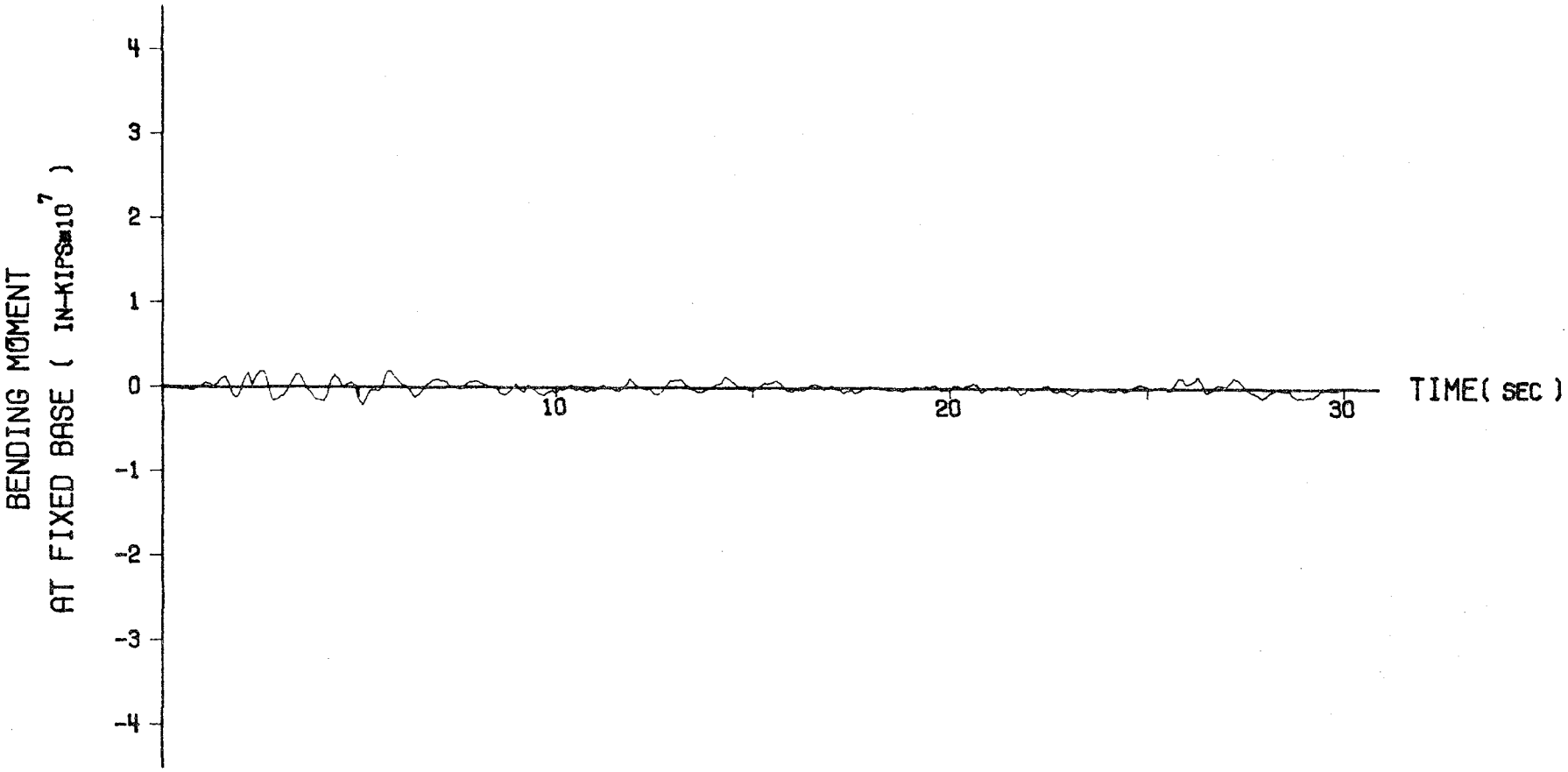

Fig. 41. Base Bending Moment vs. Time Curve for the Inner Shell with Two Openings and with Damping Coefficient Equal to 10 Percent of its Critical Value.

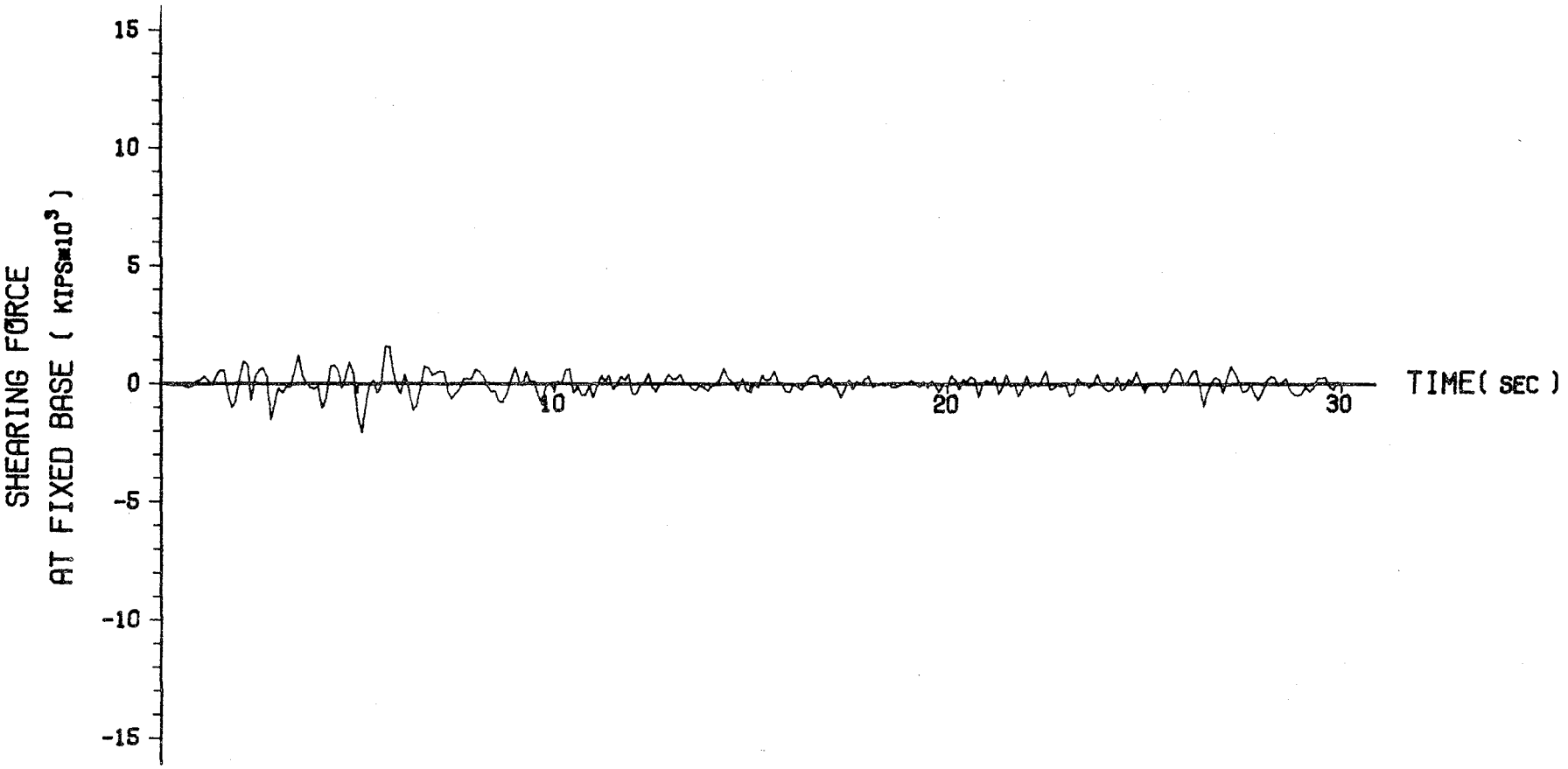

Fig. 42. Base Shearing Force vs. Time Curve for the Inner Shell with Two Openings and with Damping Coefficient Equal to 4 Percent of its Critical Value.

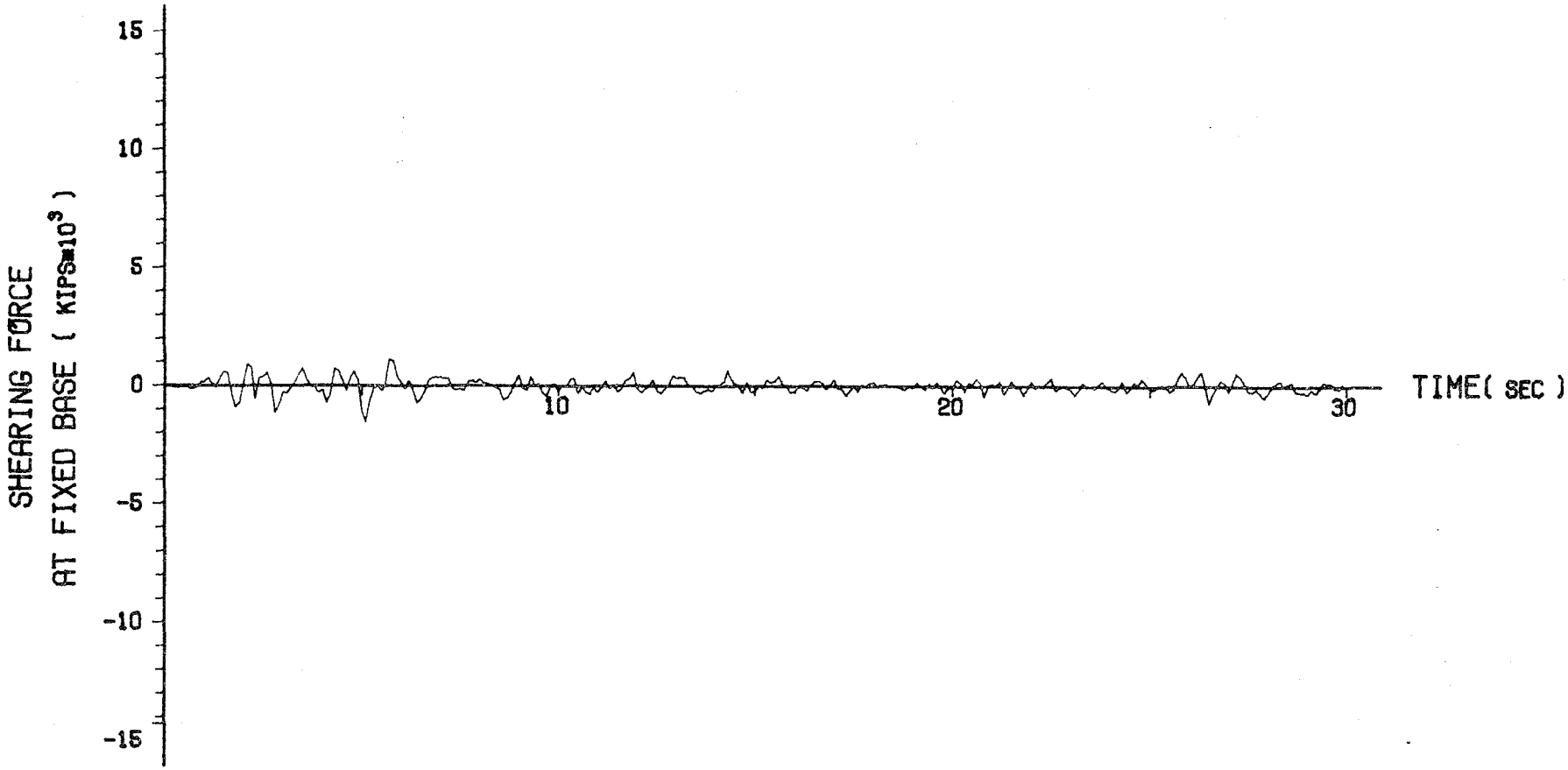

Fig. 43. Base Shearing Force vs. Time Curve for the Inner Shell with Two Openings and with Damping Coefficient Equal to 7 Percent of its Critical Value.

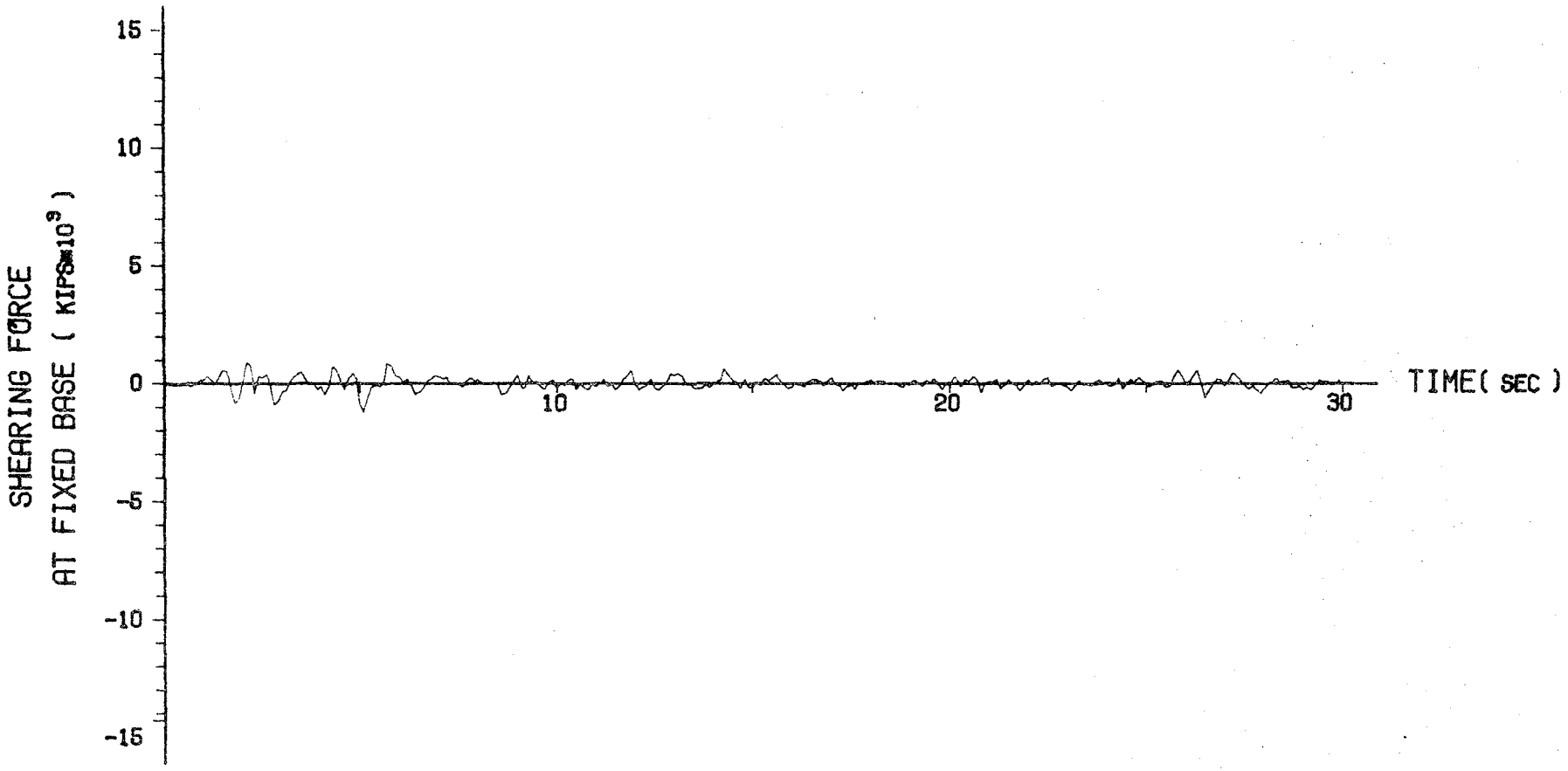

Fig. 44. Base Shearing Force vs. Time Curve for the Inner Shell with Two Openings and with Damping Coefficient Equal to 10 Percent of Its Critical Value.

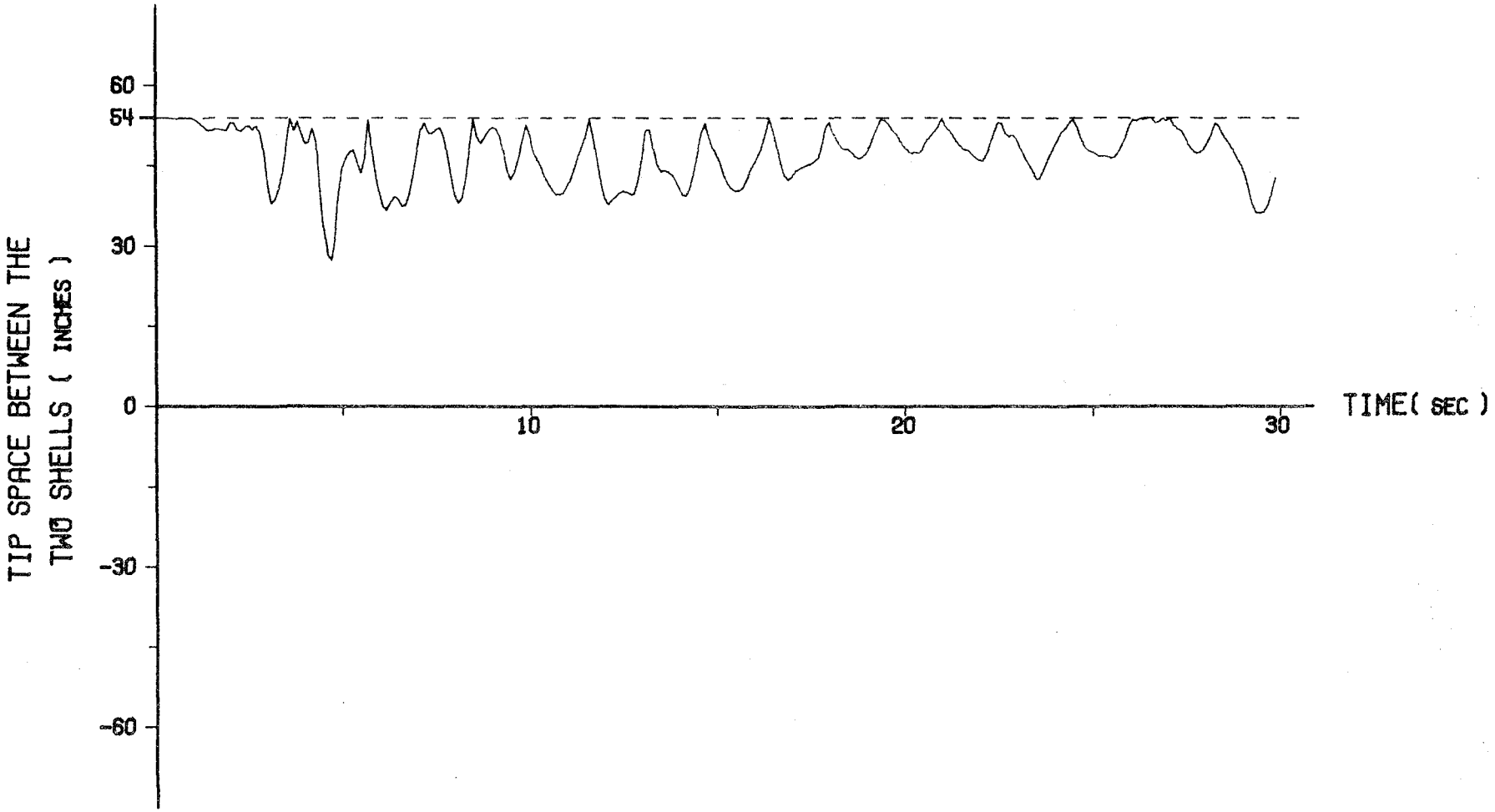

Fig. 45. Time History Curve for the Spacing Between the Tops of the Outer and Inner Shells with Openings and with Damping Coefficient Equal to 4 Percent of its Critical Value.

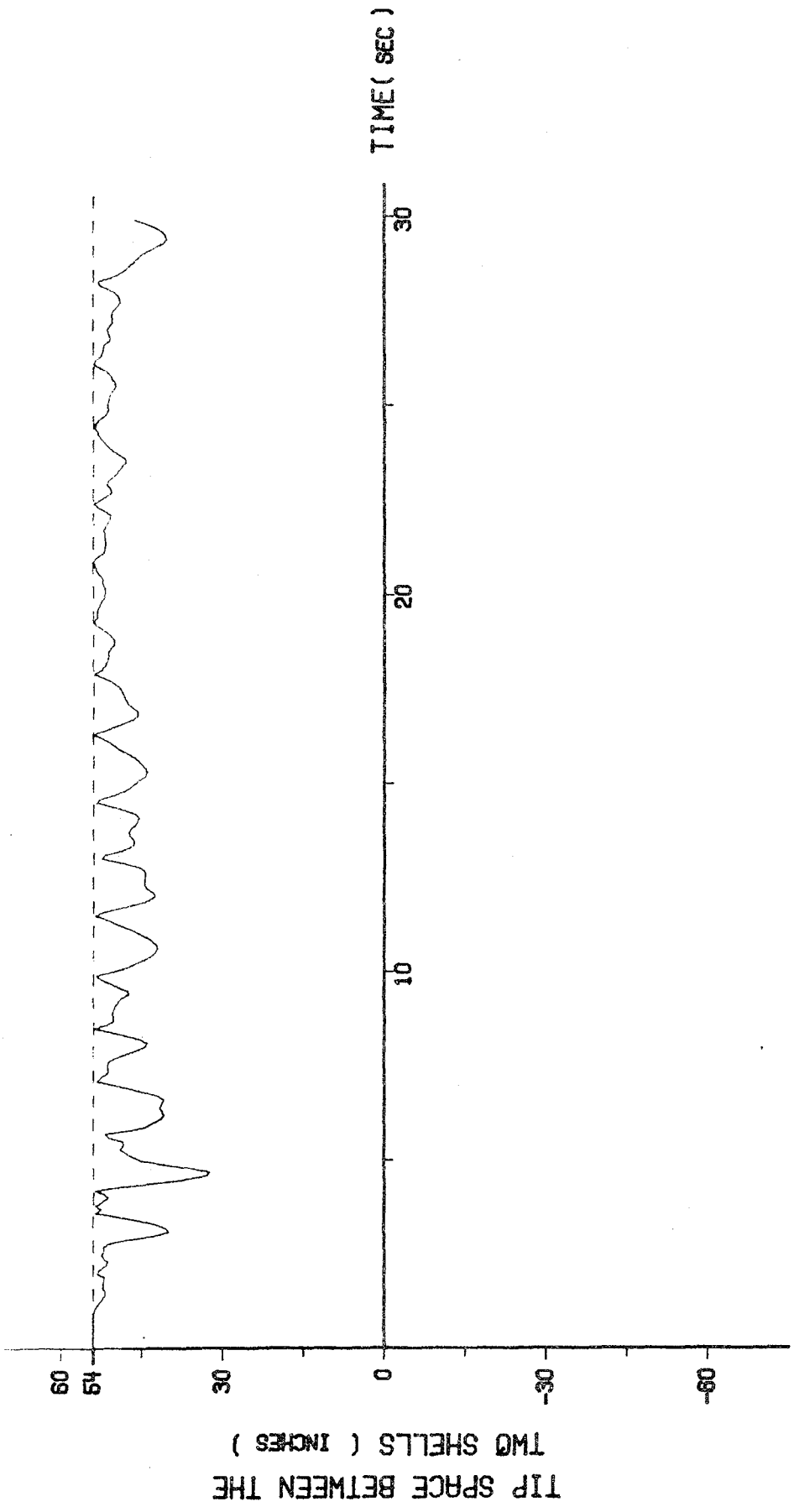

Fig. 46. Time History Curve for the Spacing Between the Tops of the Outer and Inner Shells with Openings and with Damping Coefficient Equal to 7 Percent of its Critical Value.

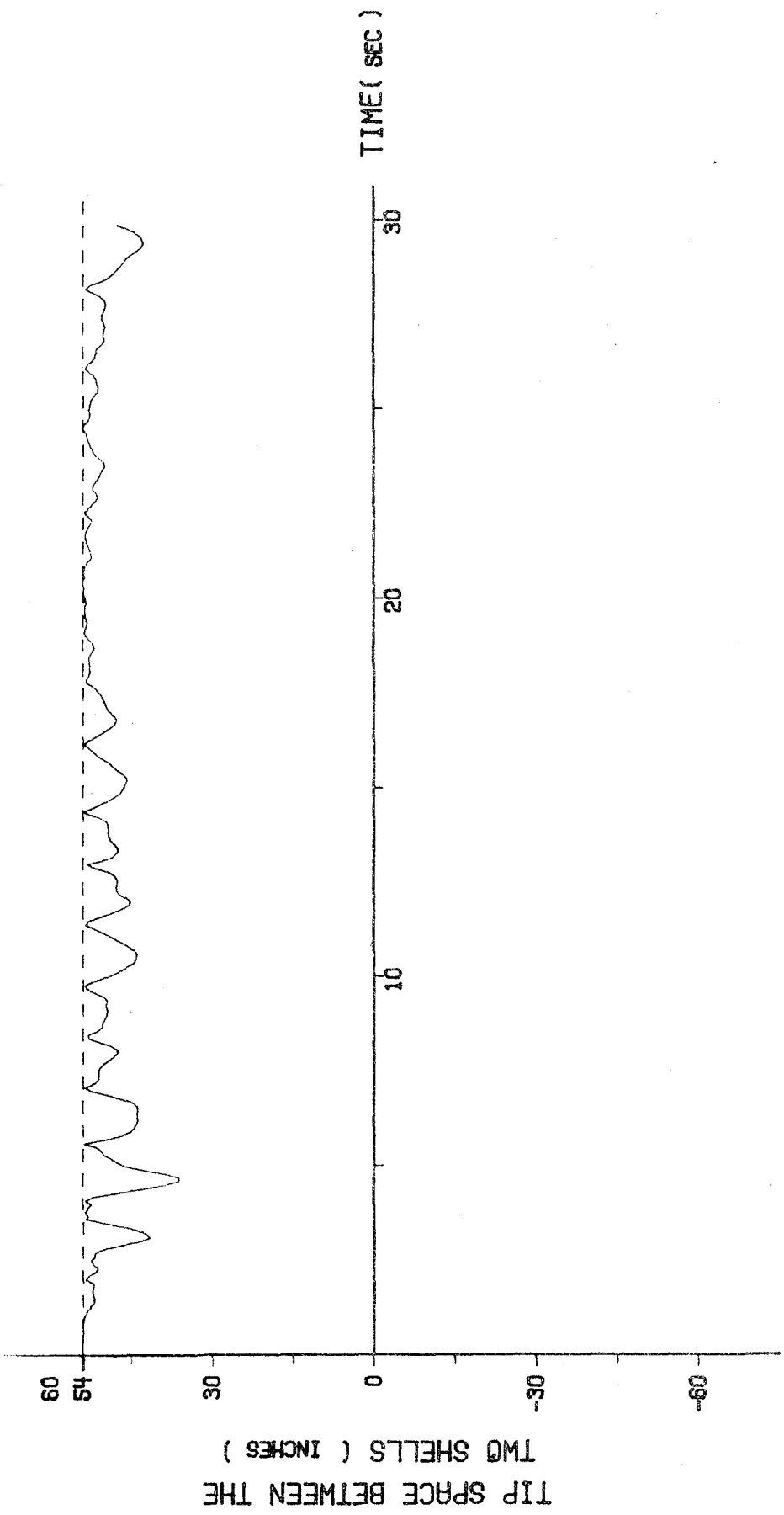

Fig. 47. Time History Curve for the Spacing Between the Tops of the Outer and Inner Shells with Openings and with Damping Coefficient Equal to 10 Percent of its Critical Value.

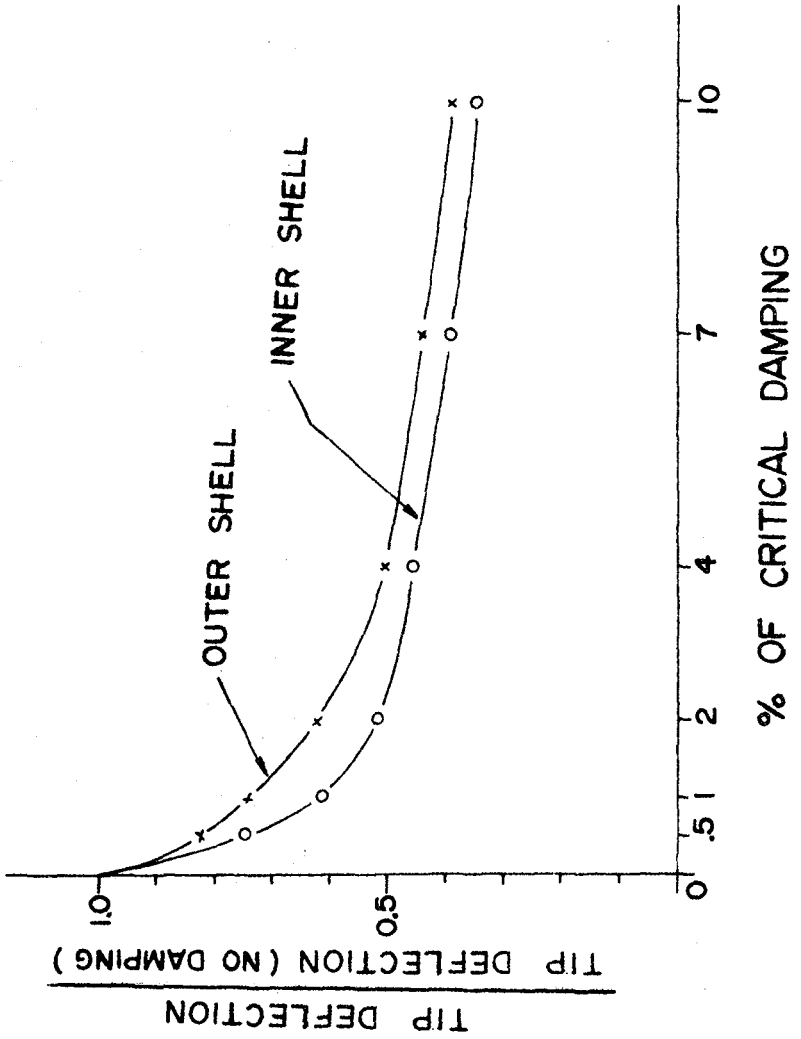

Fig. 48. Variation of Tip Deflection with Damping Coefficient for Both Shells with Openings.

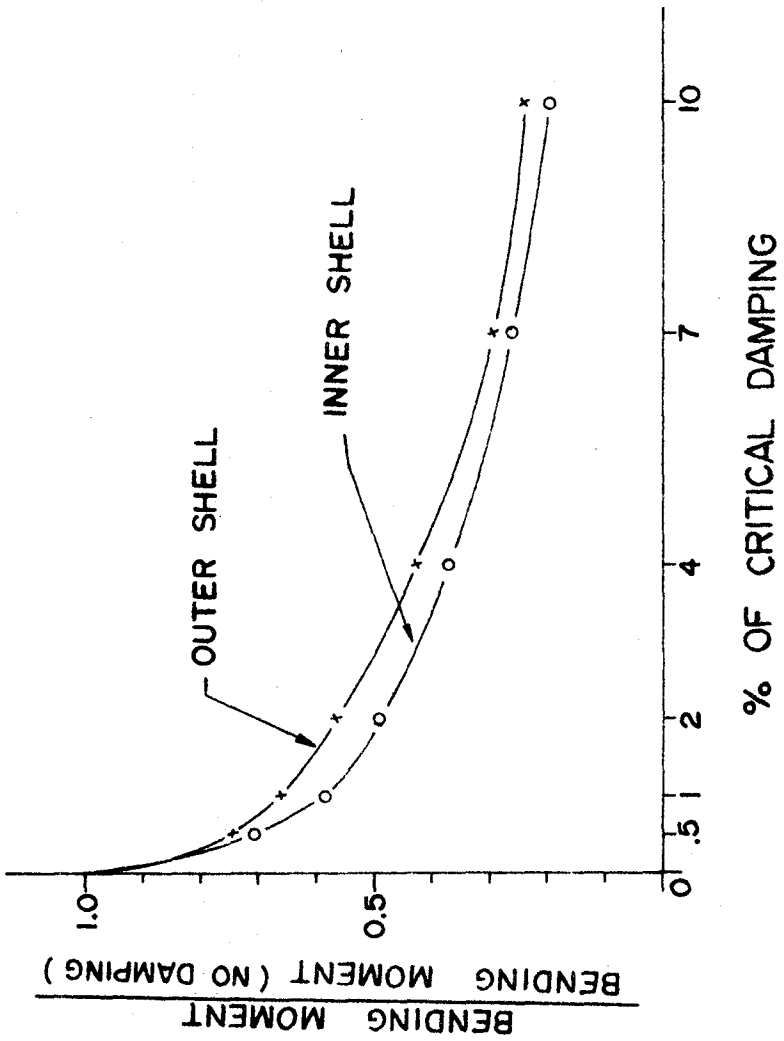

Fig. 49. Variation of Base Bending Moment with Damping Coefficient for Both Shells with Openings.

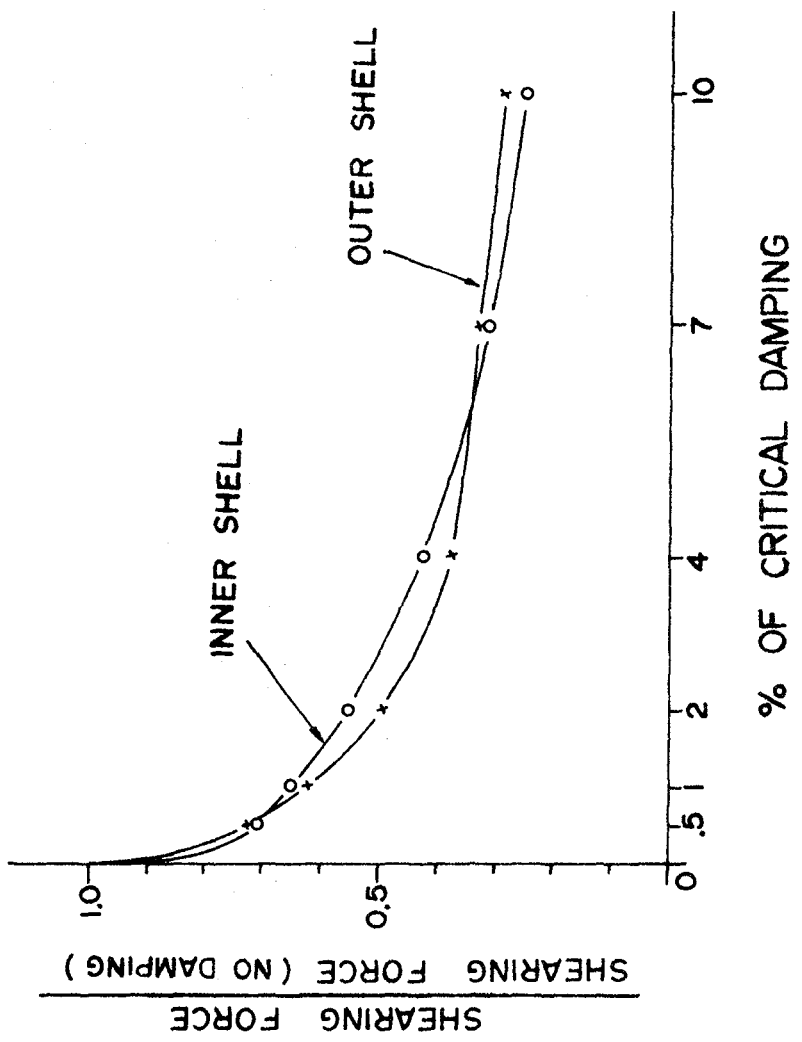

Fig. 50. Variation of Base Shearing Force with Damping Coefficient for Both Shells with Openings.

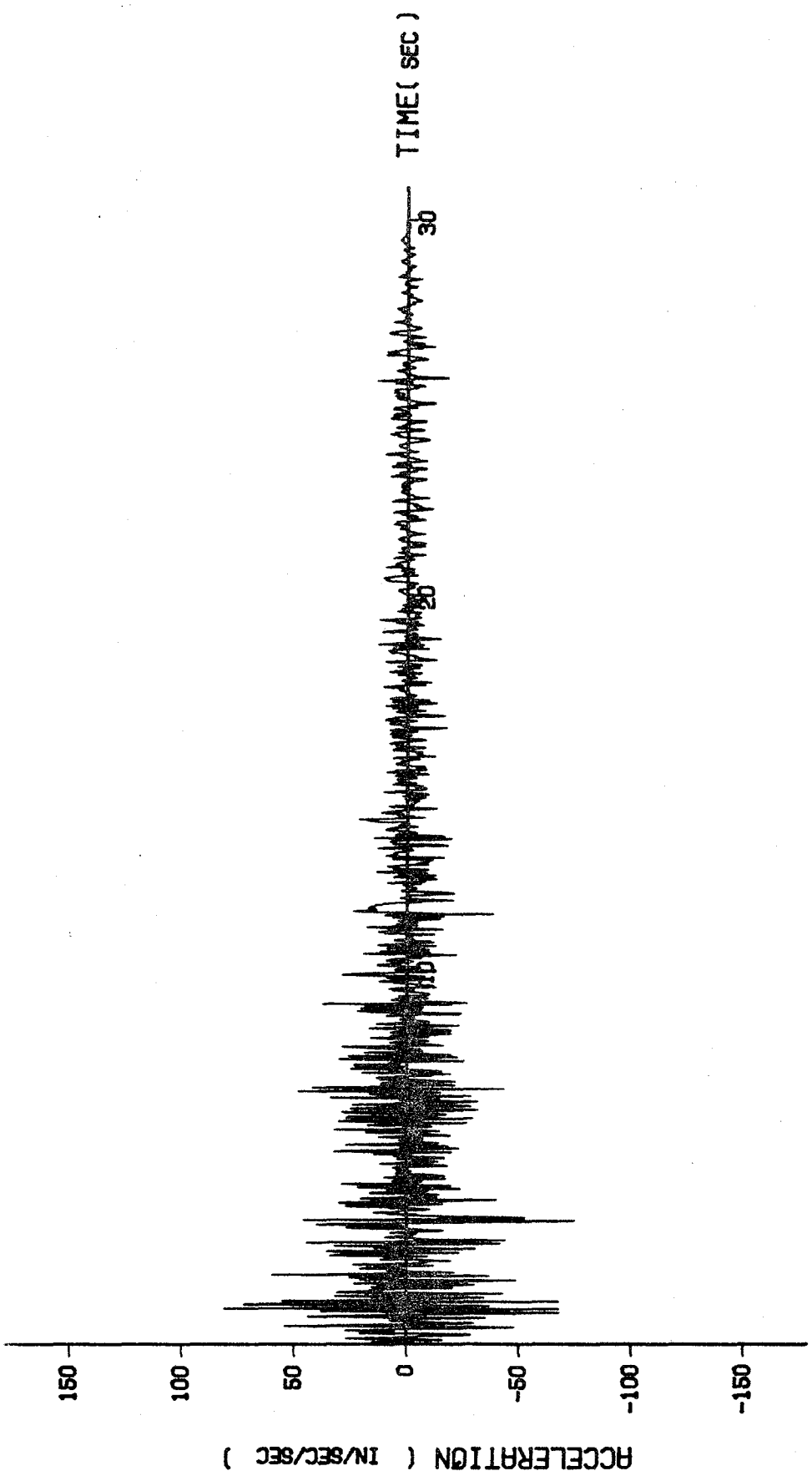

Fig. 51. The Record of the Vertical Acceleration Component of the El Centro Earthquake on May 18, 1940.

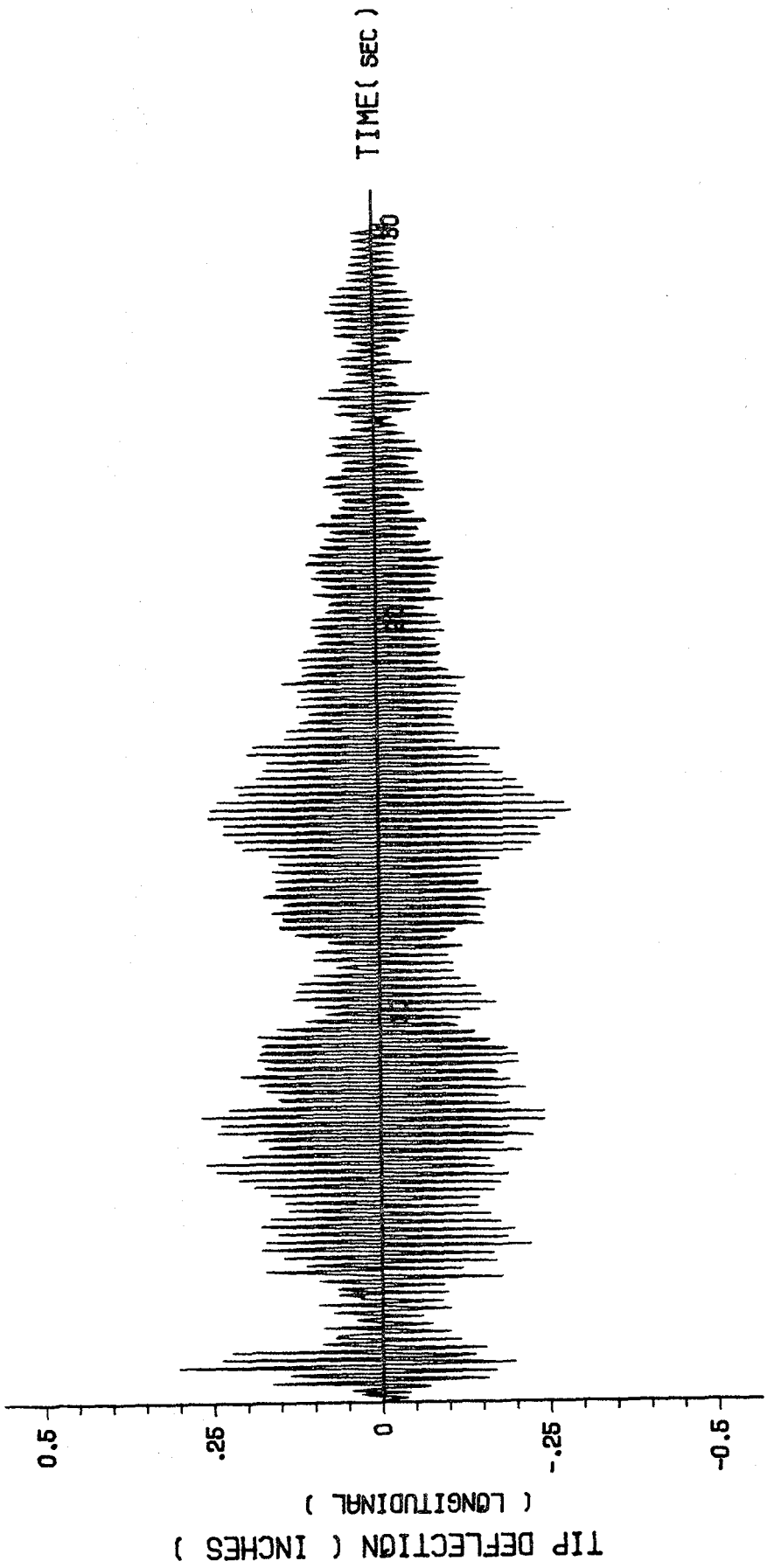

Fig. 52. Vertical Tip Displacement vs. Time Curve for Outer Shell Without Opening.

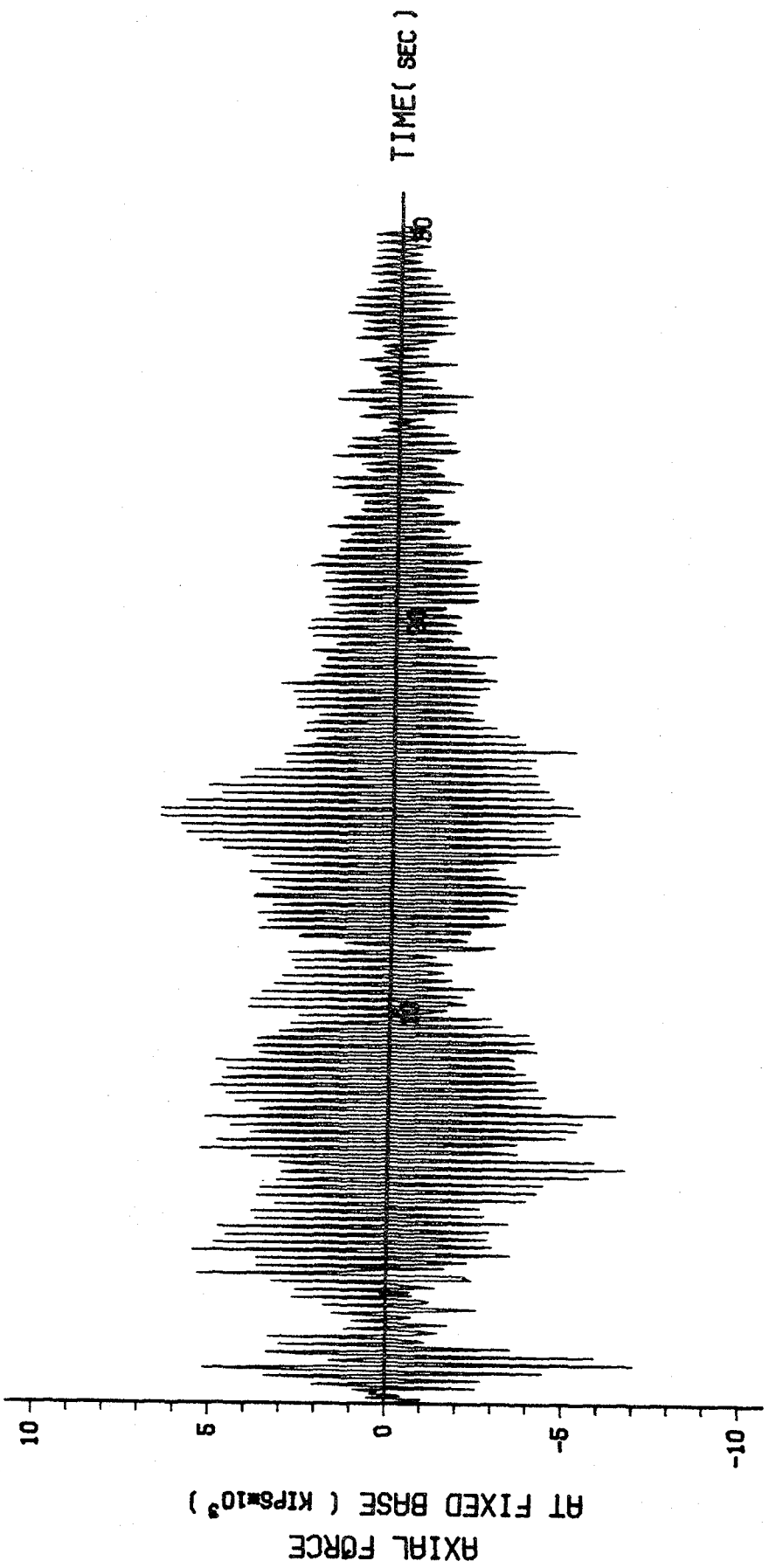

Fig. 53. Axial Force at Base vs. Time Curve for Outer Shell Without Opening.

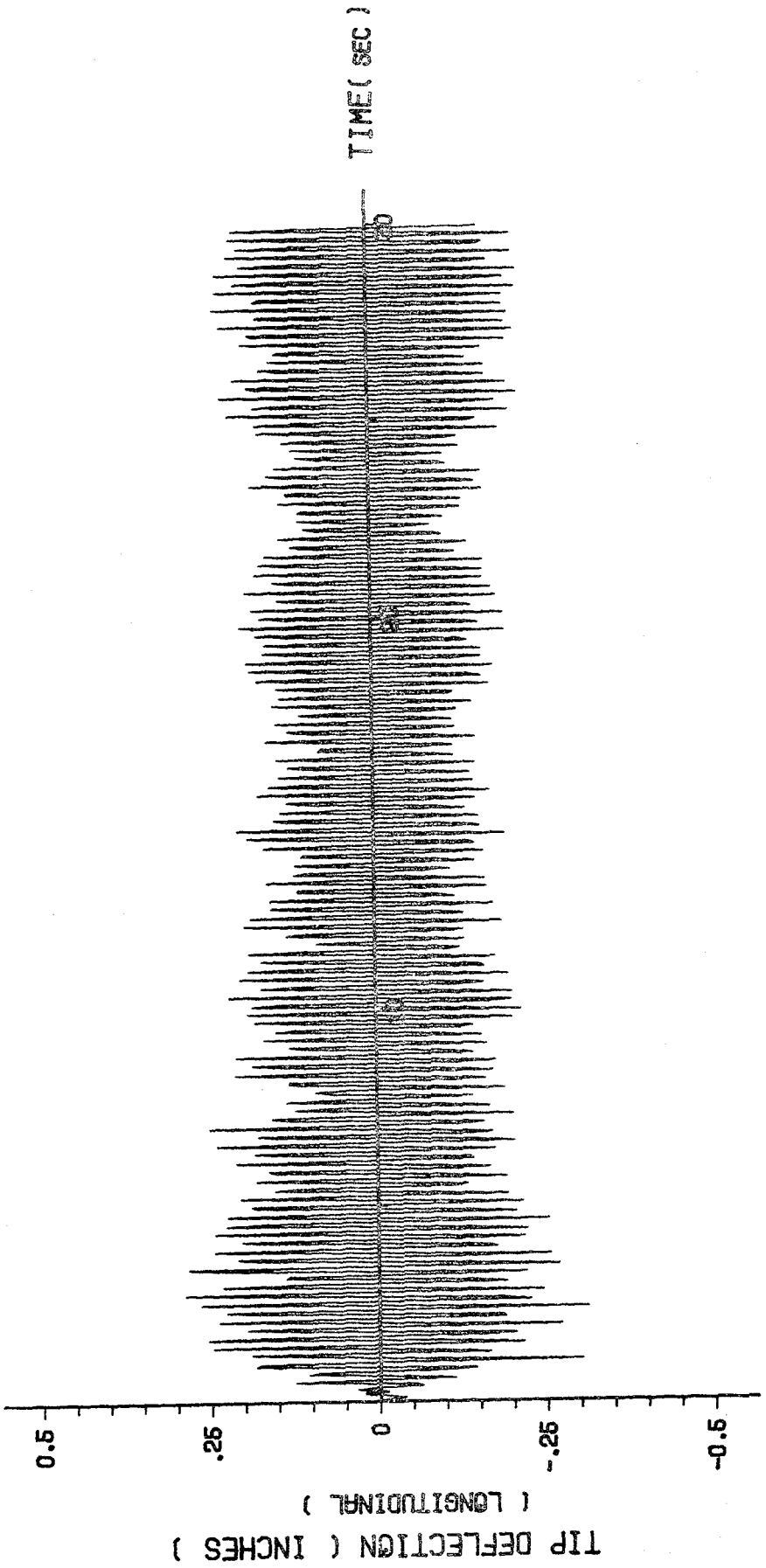

Fig. 54. Vertical Tip Displacement vs. Time Curve for Inner Shell Without Opening.

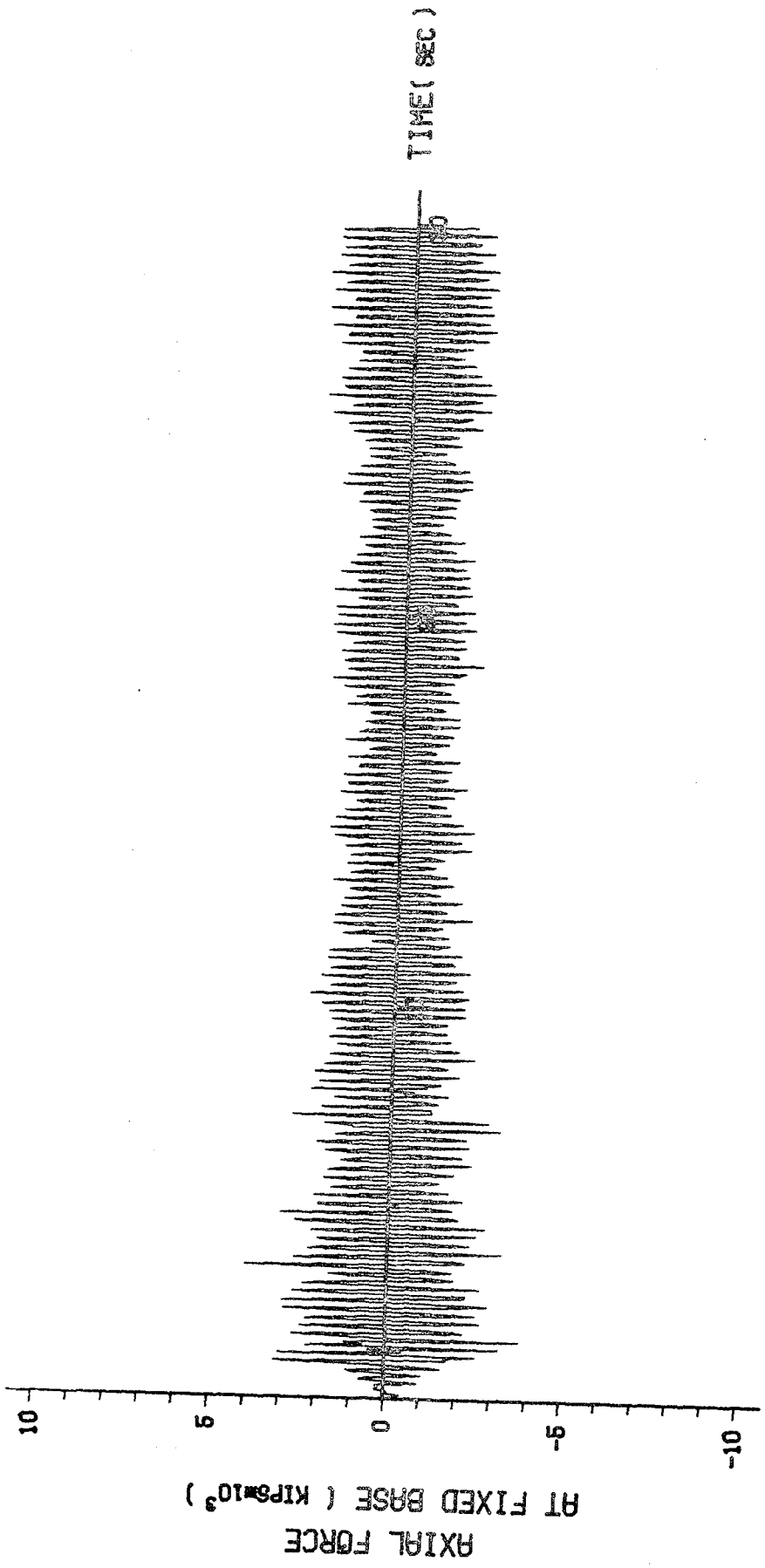

Fig. 55. Axial Force at Base vs. Time Curve for Inner Shell Without Opening.

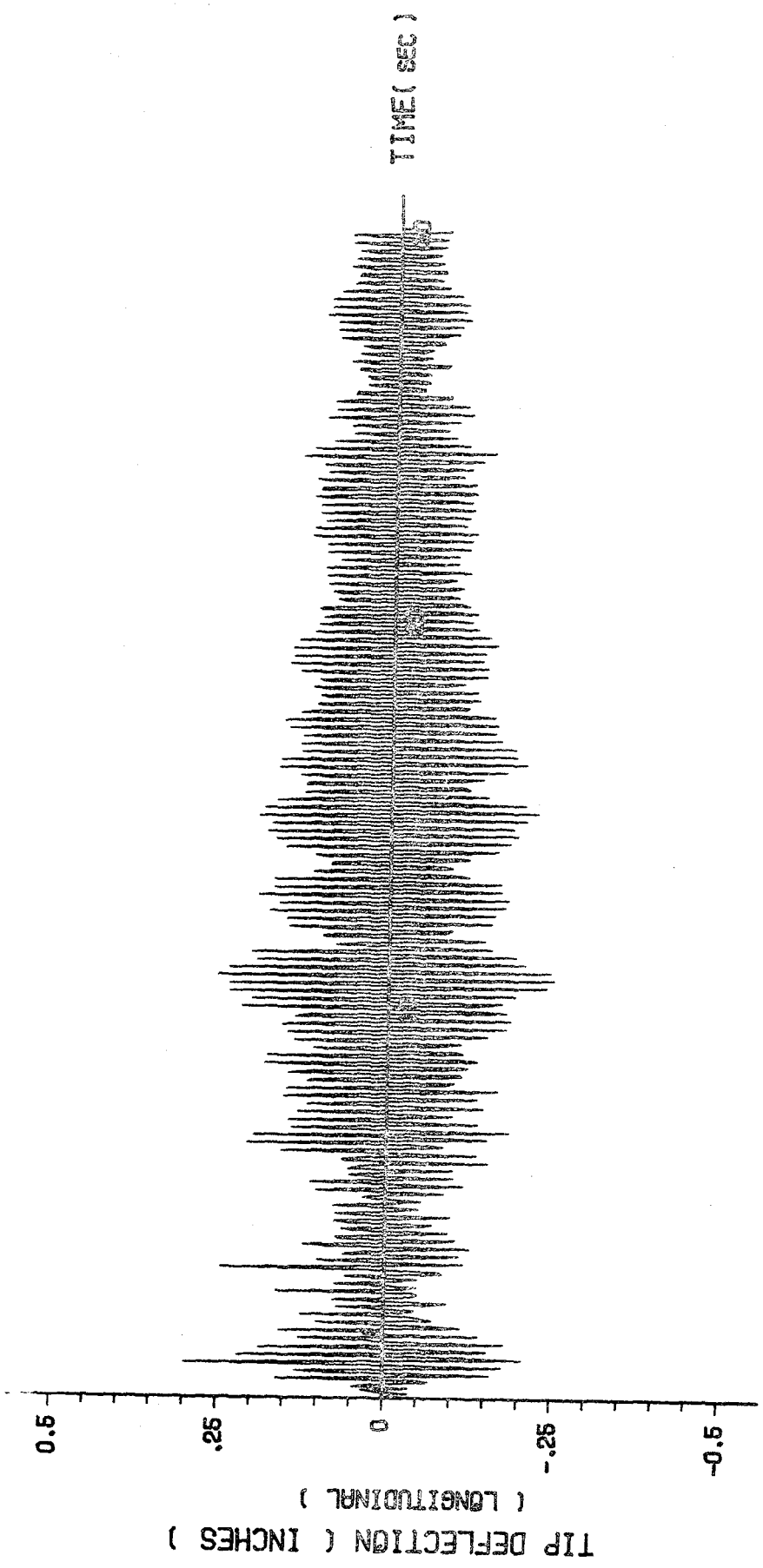

Fig. 56. Vertical Tip Displacement vs. Time Curve for Outer Shell with Two Openings.

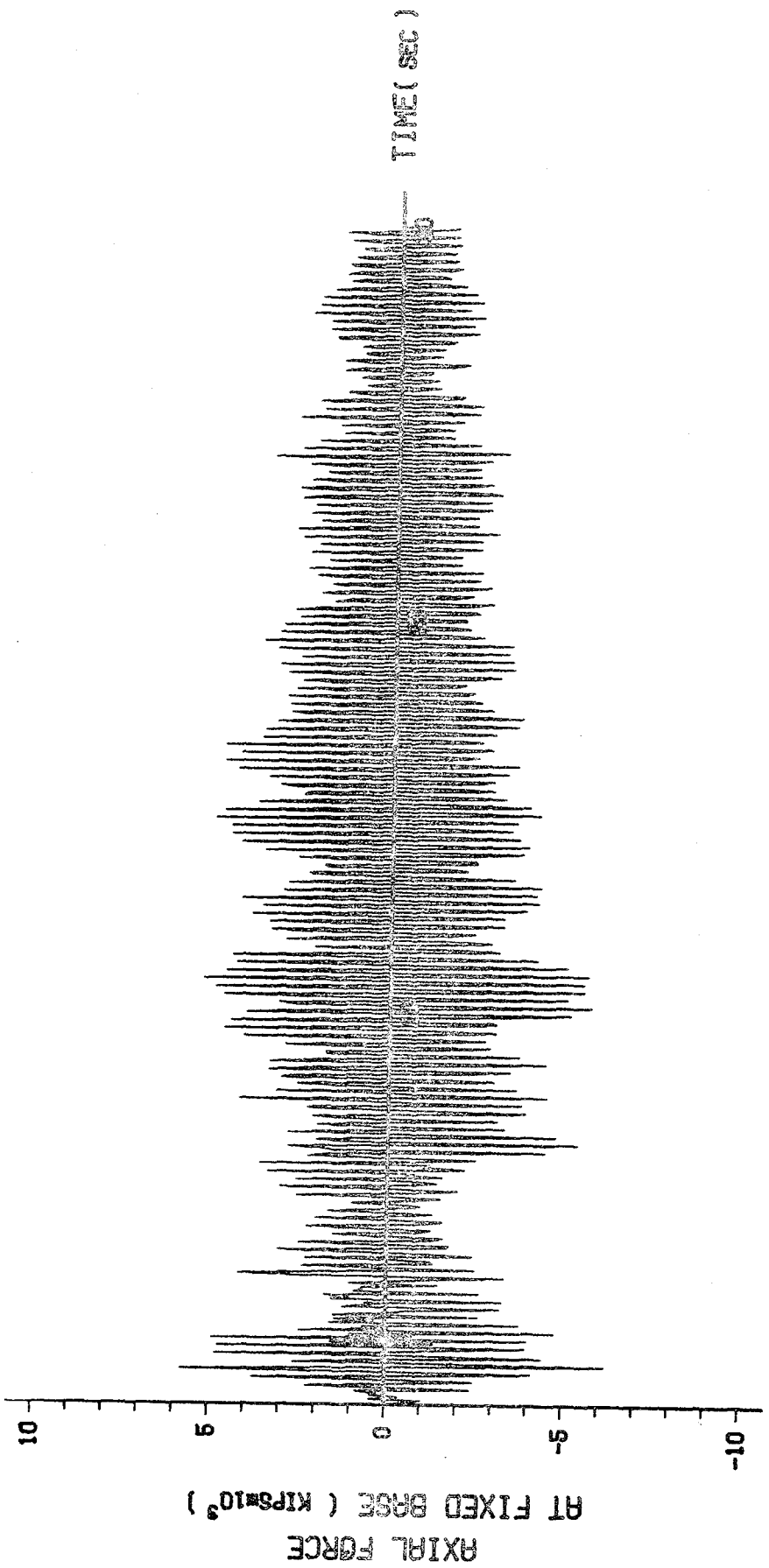

Fig. 57. Axial Force at Base vs. Time Curve for Outer Shell with Two Openings.

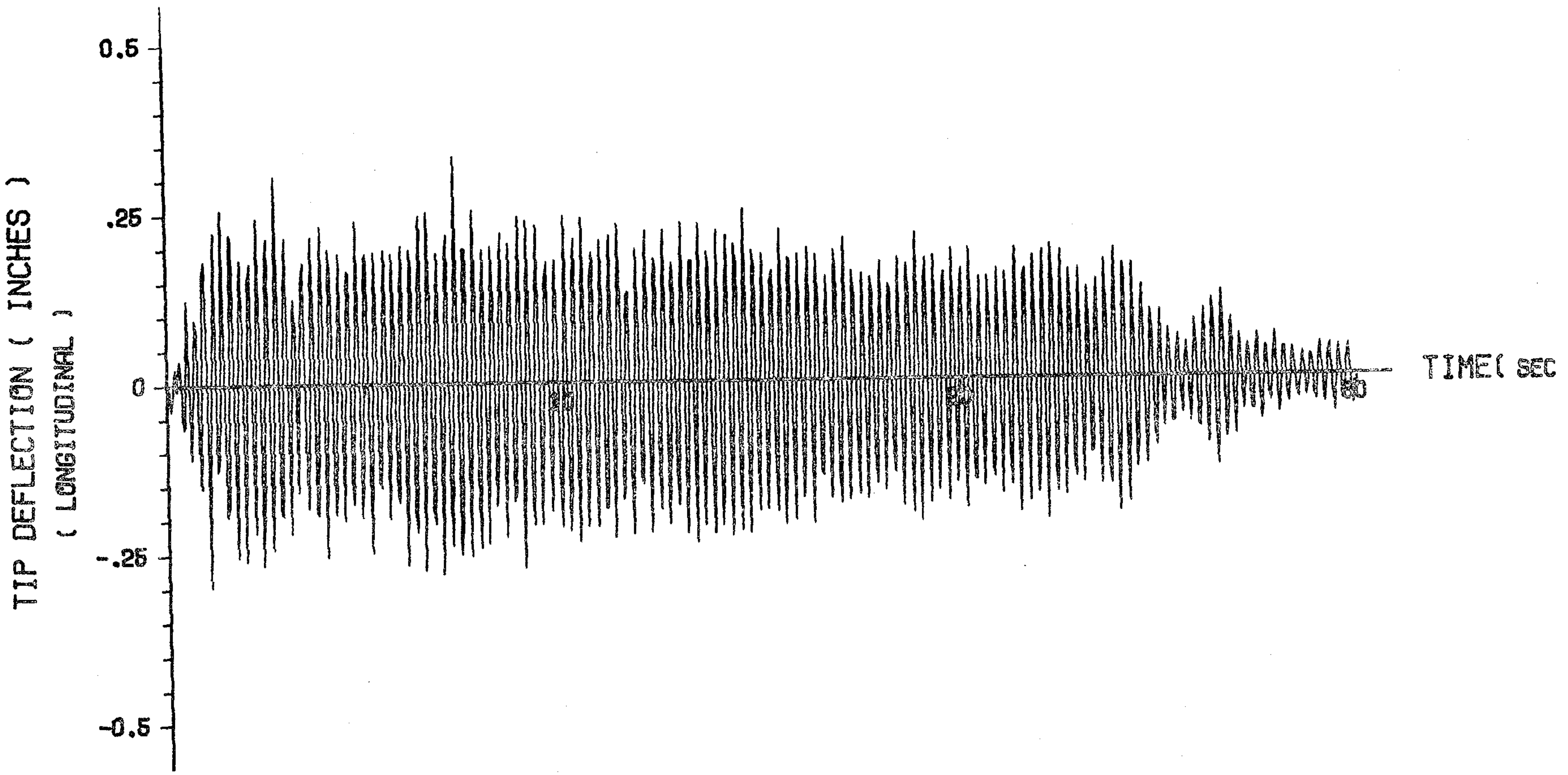

Fig. 58. Vertical Tip Displacement vs. Time Curve for Inner Shell with Two Openings.

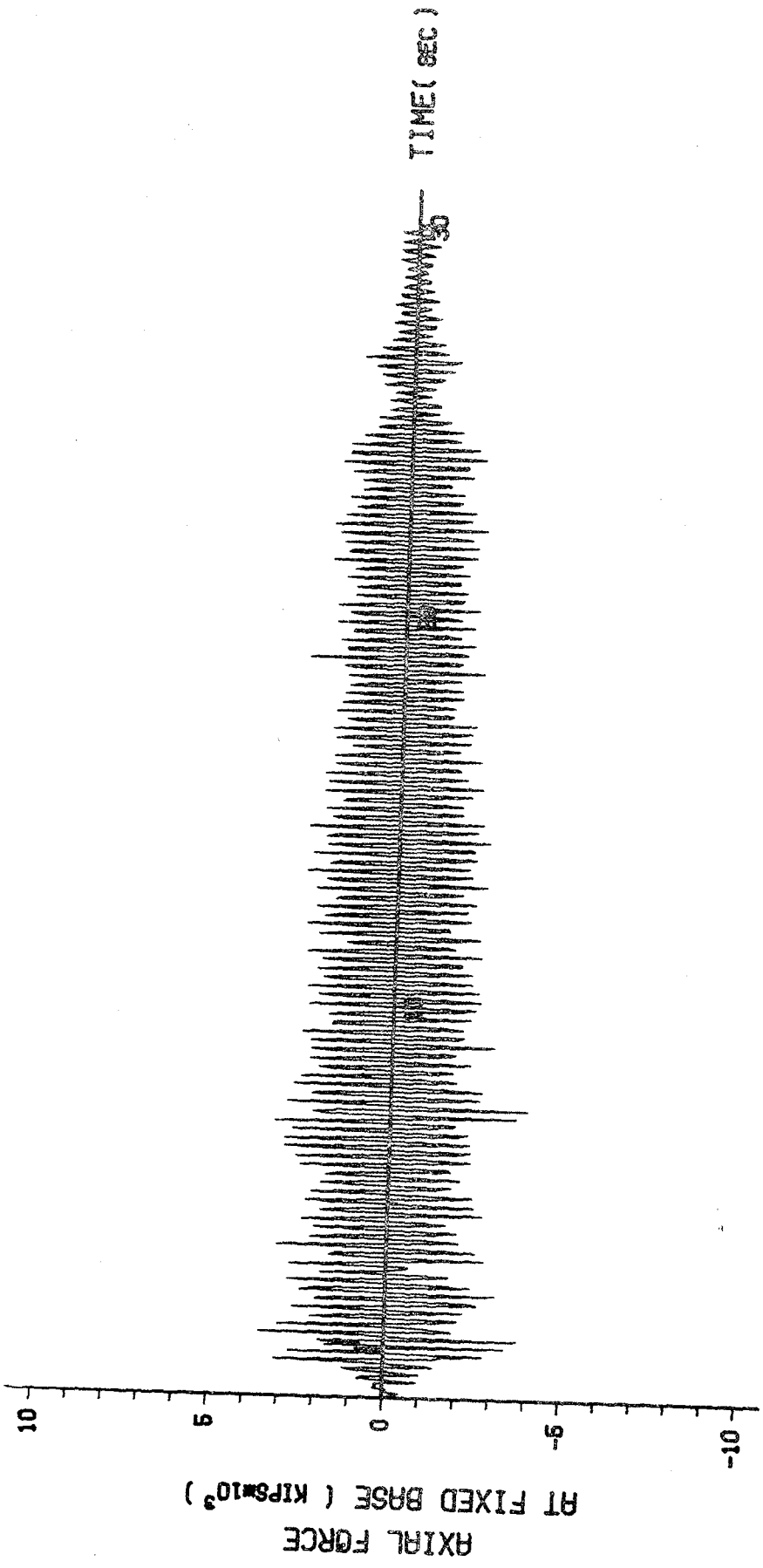

Fig. 59. Axial Force at Base vs. Time Curve for Inner Shell with Two Openings.

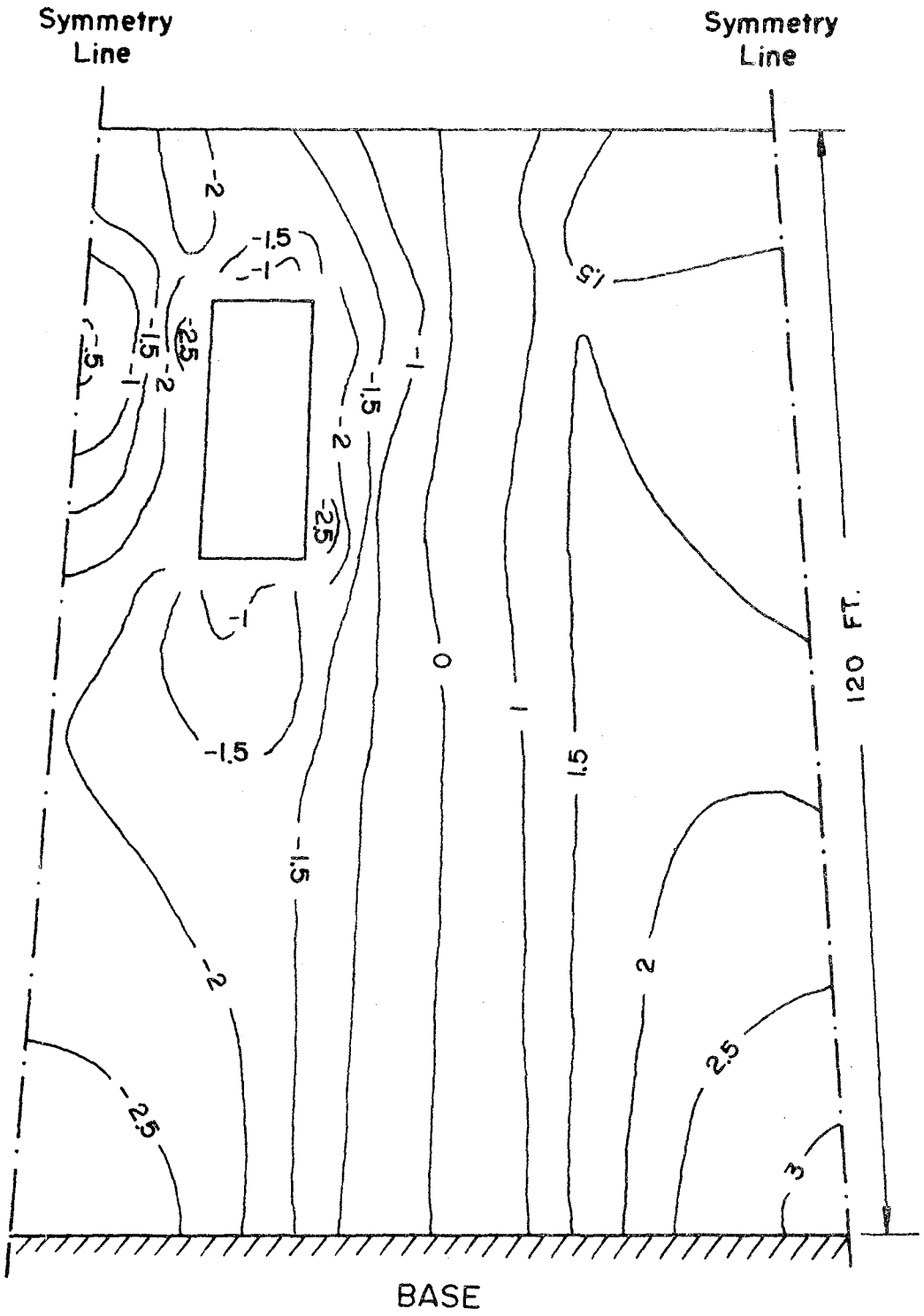

Fig. 60. Contour Plot of the Axial Stress (ksi) in the Outer Surface of the Outer Shell Around one Flue Opening at the Most Critical Time (25.2 Seconds) with Bending Moment = 32.048×10^9 in-lbs; Shearing Force = 11.81×10^6 lbs; and Axial Compression = 21.77×10^4 lbs at the Base.

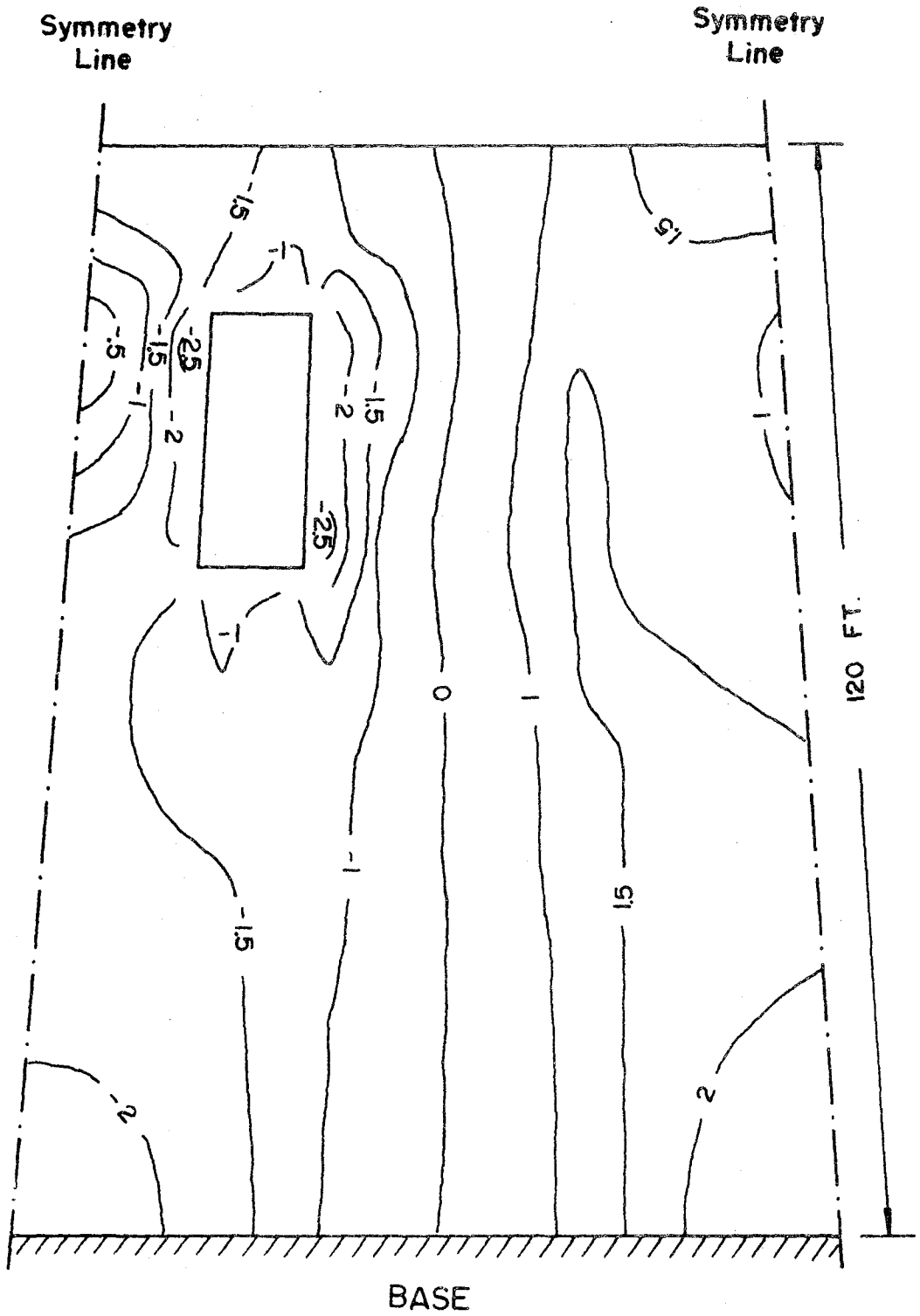

Fig. 61. Contour Plot of the Axial Stress (ksi) in the Outer Surface of the Inner Shell Around One Flue Opening at the Most Critical Time (28.8 Seconds) with Bending Moment = 11.28×10^9 in-lbs; Shearing Force = 45.57×10^5 lbs; and Axial Tension = 15.05×10^4 lbs at the Base.